UNIVERSITY OF CALIFORNIA
RIVERSIDE

Development of Technologies for RNG Utilization

A Dissertation submitted in partial satisfaction
of the requirements for the degree of

Doctor of Philosophy

in

Chemical and Environmental Engineering

by

Partho Sarothi Roy

December 2018

Dissertation Committee:
Dr. Nosang Myung, Co-Chairperson
Dr. Chan Seung Park, Co-Chairperson
Dr. Charles Wyman

The Dissertation of Partho Sarothi Roy is approved:

_____

_____

Committee Co-Chairperson

_____

Committee Co-Chairperson

University of California, Riverside

ACKNOWLEDGEMENTS

I express my gratitude to the Department of Chemical and Environmental Engineering in Bourns College of Engineering at the University of California Riverside for giving me the opportunity to carry out graduate study towards a Doctor of Philosophy in Chemical and Environmental Engineering. In addition, I would like to thank Center for Environmental Research and Technology (CE-CERT).

I would like to thank Dr. Chan Seung Park for his advice and guidance during this research. I am also thankful to Dr. Arun SK Raju, Dr. Kiseok Kim for additional guidance and feedback. This work was assisted by fellow students Annie Chang, Vincent Van, Kyle Hunter, Richard Rangel and Gustavo Salazar.

I would like to express my gratitude to my committee members, Dr. Nosang Myung, Dr. Chan Seung Park and Dr. Charles Wyman.

I would like to thank Dr. Kent Johnson and Sean Franco for their support during my studies.

I would like to thank my friends Niluthpol Chowdhury Mithun, Mohammad Atiqul Islam, Tonmoy Bhowmick, Dipankar Ranjan Baisya, Ashraful Arefeen and Pritom Ahmed for all the supports.

Parts of this doctoral work have been previously published in the following journals:

Chapter 2 (Journal of CO2 Utilization, 25 (2018), 275-282)

Chapter 3 (Journal of industrial and engineering chemistry, 62(2018), 120-129)

Chapter 5 (Fuel, 224 (2018), 121-127)

DEDICATIONS

To my parents

ABSTRACT OF THE DISSERTATION

Development of Technologies for RNG Utilization

by

Partho Sarothi Roy

Doctor of Philosophy, Graduate Program in Chemical and Environmental Engineering
University of California, Riverside, December 2018
Dr. Nosang Myung, Co-Chairperson
Dr. Chan Seung Park, Co-Chairperson

Renewable energy production processes have achieved significant technological and commercial maturity over the past two decades. Most carbon based renewable fuel gases contain significant quantities of CO_2. Converting the CO_2 along with methane into syngas is an attractive option since it can potentially increase utilization of distributed renewable carbon resources while creating additional revenue streams.

An integrated renewable power generation system where the SBR process was coupled with a Solid Oxide Fuel Cell (SOFC) was studied using the Aspen Plus model. The steam-biogas reforming (SBR) process performed over a Pd-Rh catalyst was compared with equilibrium values predicted by Aspen Plus. At steam to carbon ratio of 1.50 and temperature of 1073 K or above, positive CO_2 conversion was obtained. Coke formation

was significantly reduced during reforming reaction performed experimentally over the Pd-Rh compared to literature data. SBR integrated with combustion process works with an efficiency of 40% or higher. The variation of the catalytic support material composition helps to adjust H_2/CO ratio and H_2/CH_4 yield. $CeZrO_2$ addition suppressed coke formation, for improved oxygen storage and oxide reducibility. Pd-Rh catalysts exhibit stable performance for 200 h, although sintering occurred regardless the catalyst composition used.

A life cycle assessment was performed for methanol production pathway using syngas produced via bi-reforming pathway from CO_2, H_2O reforming with methane. GHG emission is about 203 kilograms of CO_2e per metric tonne of methanol produced using the proposed bi-reforming pathway. GHG emission reduction is 0.29 kg/ CO_2e/kg of CH_3OH compared to the commercial scale production. With NG price $3.50/GJ and methanol price $400/tonne IRR is 57% with 5 years payback period.

A database for Wobbe Index, Methane Number, thermal conductivity, sound velocity of biogas, anaerobic digester gas and natural gas mixture was built. A prediction model for WI and MN of a gaseous fuel mixture was developed that uses thermal conductivity and sonic velocity. The model can predict the Wobbe Index with an average error of ±2.76% and Methane Number with an average error of ±1.65%. The prediction model coupled with a thermal conductivity sensor and sonic velocity measurement sensor enables the combustion of gas efficiently.

TABLE OF CONTENTS

LIST OF FIGURES

LIST OF TABLES

Abbreviations

ANL	Argonne National Laboratory
ATR	Autothermal Reforming
BET	Brunauer-Emmett-Teller
CCS	Carbon Capture and Storage/ CO_2 capture and sequestration
CWI	Cummins Westport Inc.
DCF	Discounted Cash Flow
DME	Di-Methyl Ether
DR	Dry Reforming
DRM	CO_2 or Dry Reforming of Methane
EDX	Energy-dispersive X-ray spectroscopy
EGR	Exhaust Gas Recirculation
GC	Gas Chromatograph
GHG	Green House Gas
GHGenious	GHGenious lifecycle analysis (LCA) model
GHSV	Gas Hourly Space Velocity
GREET	Greenhouse Gases, Regulated Emissions, and Energy Use in Transportation
GWP	Global Warming Potential
HEP	Heat Exchanger Platform
HHV	Higher Heating Value
ICP	Inductively-Coupled Plasma
IOU's	Investor Owned Utilities
IPCC	Intergovernmental Panel on Climate Change
ktoe	kilotonne of oil equivalent
LCA	Life Cycle Analysis/Assessment
LFG	landfill gas

LPG	Liquefied Petroleum Gas
LHV	Lower Heating Value
MCF	Thouans Cubic Feet
MN	Methane Number
NGV	Natural Gas Vehicle
NPV	Net Positive Value
PM	Particulate Matters
POX	Partial Oxidation
PSFM	Power Systems Financial Model
S/C	Steam to Methane ratio
SBR	Steam Biogas Reforming
Sccm	Standard Cubic Centimeter per Minute
SEM	Scanning Electron Microscope
SLCP	Short Lived Climate Pollutant
SMR	Steam Methane Reforming
SNG	Synthetic Natural Gas
SOFC	Solid Oxide Fuel Cell
Syngas	Synthesis Gas (H_2 + CO)
RGA	Residual Gas Analyzer
RMS	Root Mean Square
RNG	Renewable Natural Gas
RPS	Renewables Portfolio Standard
RWGS	Reverse Water Gas Shift
TCD	Thermal Conductivity Detector
TEM	Transmission Electron Microscopy
TPD	Tonne per day
TTW	Tank to Wheel

TWC	Three Way Catalyst
VNGV	Variable Natural Gas Vehicle
WGS	Water Gas Shift
WI	Wobbe Index
WTT	Well to Tank
WTW	Well to Wheel
XPS	X-ray Photoelectron Spectroscopy

CHAPTER 1 INTRODUCTION

The secure and adequate supply of energy is a critical for modern economies, and fear of supply interruptions have caused serious concerns around the globe [1]. The transportation sector is one of the biggest energy consumers and carbon emitters. Global climate change by large quantity of fossil fuel usage is an urgent issue. The fossil fuel usage emits greenhouse gases (GHG) such as CO_2, CH_4 and N_2O are expressed in term of CO_2equivalent and the global CO_2 emission is presented in Figure 1-1. Average global temperature is rising due to emission of GHG and the rise should not be more than 2 °C than the pre-industrial time and throughout the current century [2–5]. Sustainable fuels, produced from renewable resources, are widely accepted as the solution that can avoid a potential energy crisis in all major sectors including commercial, residential, and transportation and any irrevocable impairment to the climate by global warming potential reduction [5–9].

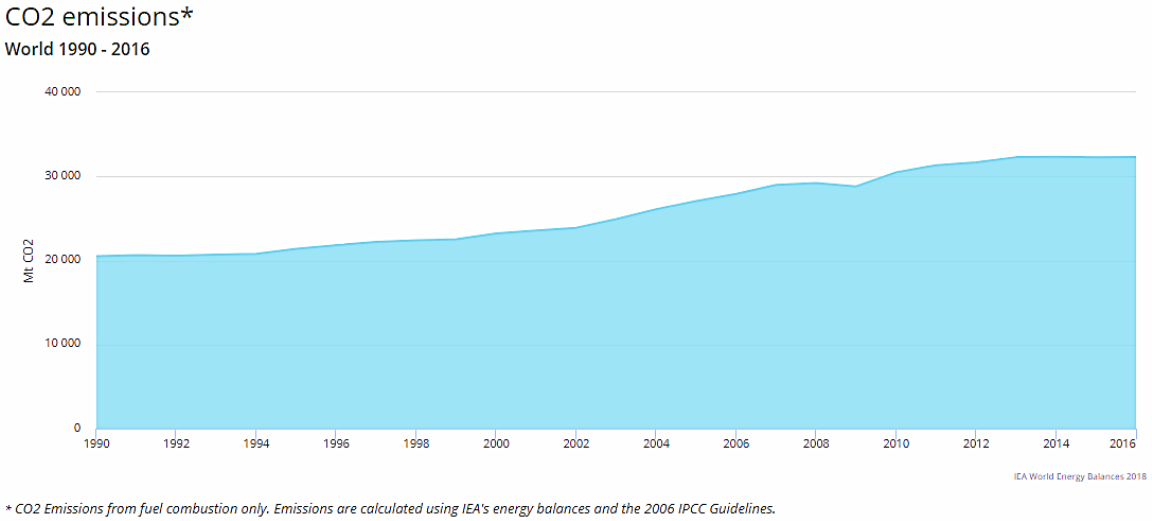

Figure 1-1: World CO_2 emission from fuel combustion over the year of 1990-2016 [10].

World energy consumption at present, however, is dominated by fossil fuels, as shown in Figure 1-2 and electricity generation as shown in Figure 1-3. More than 80% of the primary energy consumption is derived from fossil fuels, and approximately 67% of the world electricity is generated from fossil sources [10]. The State of California's Renewables Portfolio Standard (RPS) requires investor-owned utilities (IOUs), electric service providers, and community choice aggregators to increase renewable energy resources to 33% of total procurement by 2020 [11]. California is not the only place where the change is happening. During the past years, global energy supply sources have not significantly improved with renewable sources, however, a substantial amount of electricity generated from solar and wind sources [10].

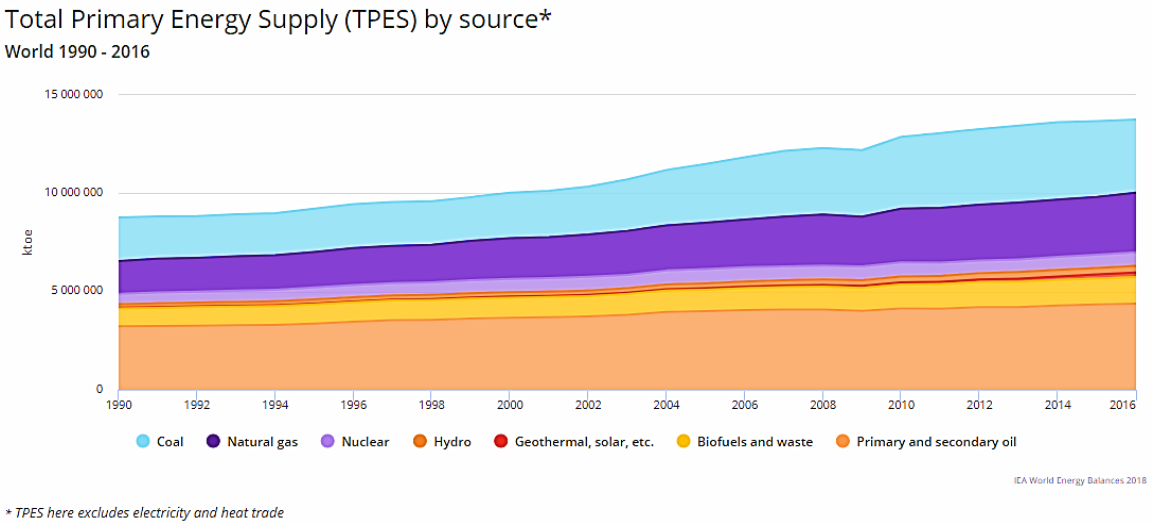

Figure 1-2: World Total Primary Energy Supply (TPES) by source (1990-2016) [10].

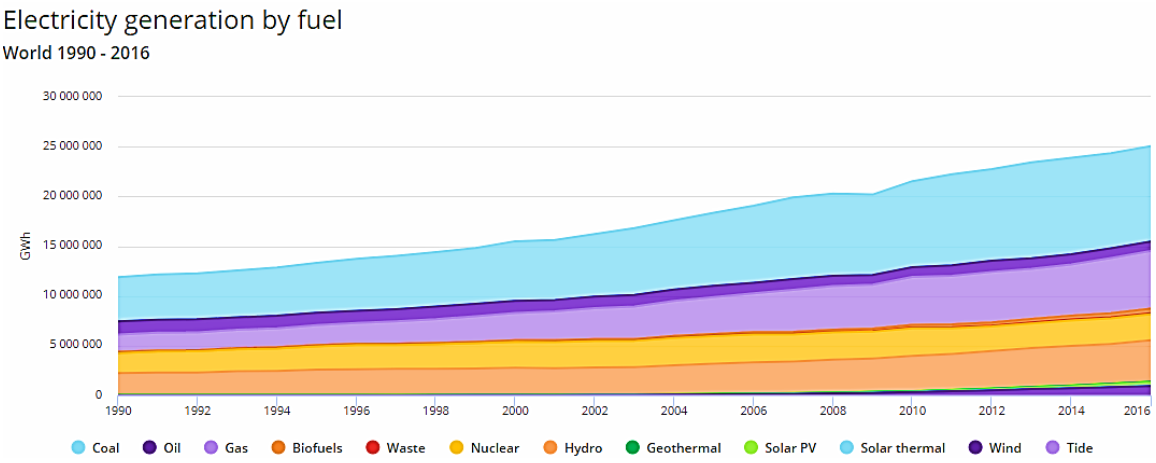

Figure 1-3: World's electricity generation by different types of fuel (1990-2016) [10].

Solar, wind, hydropower, geothermal energy and some carbonaceous components are the major forms of renewable energy. The use of renewable energy reduces the GHG emissions and criteria pollutants (O_3, PM, CO, Pb, SO_x, NO_x) related to energy production. Renewable electricity generated from renewable sources which restore with time and do not diminish very easily. Utilization of renewable energy also enables the reducing dependence on imported fuels by diversifying the fuel supply source [12]. However, the cost of renewable energy process and generation is still not competitive comparing the fossil fuel generation. Renewable resources located in remote areas that are not ready or not cost-effectively accessible for transportation to a central processing facility requires additional cost for utilization. Therefore, it is hard to implement clear utility regulations that enable investments in small-scale renewable energy projects where a portion of the cost is reimbursable from government level and leading slow development of utility-scale renewable projects in their territory. However, with the recent technological advancement,

the costs for renewables even without subsidies are approaching levels competitive with new natural gas plants [13].

The renewable energy utilization across the world varies depending on the goals of the government, resource potential or technology availability. In the United States California, New Jersey, Arizona, Massachusetts, New York, Nevada, Texas, Pennsylvania are top eight ranked states by their installed solar generation capacity produces 99.5 percent of United States solar PV installations, whereas the states are ranked as Arizona, California, Colorado, Hawaii, New Mexico, Nevada, Texas, Utah, Wyoming based on their solar generation potential [12].

Finding the proper technology is an important step of alternative fuel production that can help the State to meet the RPS objectives is necessary. Renewable energy technologies are mature for direct electricity generation while fuel synthesis (ex. syngas) is still under development [14,15]. Fuel can be produced from carbonaceous and renewable feedstocks through a number of technologies including anaerobic digestion, landfill waste decomposition, gasification, and pyrolysis. The technologies available for carbonaceous feedstock conversion to fuel/chemicals are often inefficient and the production cost is inferior to fossil fuel synthesis.

1.1 Biomass

Biomass has always considered as one of the major energy sources for the world. Biomass can be defined as plant materials and animal waste, although broader definitions that

include other forms of carbonaceous waste are used in the renewable energy context. Earth's primary source of biomass is the plant matter that grows through photosynthesis. The carbon stored in the biomass is from the carbon dioxide consumed during photosynthesis and is ultimately converted back to carbon dioxide during any energy generation processes. As is well known, biomass-based processes are often carbon neutral, i.e., do not add additional carbon dioxide to the atmosphere, or have a very low carbon footprint. For these reasons, biomass is the largest and most widespread carbon source for producing renewable energy and is relatively free of fluctuation problems inherent to the wind and solar energy. A comprehensive inventory of biomass resources in the United States potentially available for energy production is available as so-called "billion-ton study" by the U.S. Department of Energy [16,17].

The oldest energy conversion process used by humans is biomass combustion in open air to produce heat. Biomass burning is still a dominant process in many parts of the world and thermochemical conversion of biomass to energy has a long scientific history. Since then, various thermochemical processes for biomass conversion have been developed to overcome the primary limitation of combustion; it only produces thermal energy along with the flue gases. Thermochemical biomass conversion to gaseous and liquid fuels has been studied and practiced for centuries. Production of a number of chemical compounds from biomass is also important application of the thermochemical process. The first such example is charcoal production from wood around 4000 B.C. [16]. The gasification of biomass produces synthetic gas containing CH_4, CO_2, CO and H_2 with impurities depending on the source can be converted to a mixture of CH_4, and H_2 known as synthetic

natural gas or renewable natural gas. A biomass conversion process to renewable natural gas process is shown in Figure 1-4.

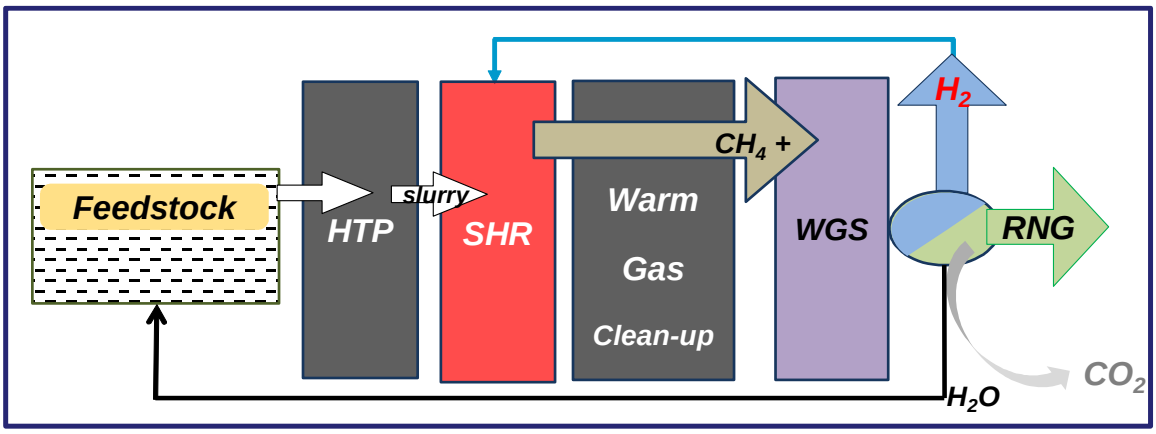

Figure 1-4: Biomass conversion to natural gas via steam hydrogasification [16].

1.2 Biogas

The carbonaceous renewable feedstock's in gaseous form always comes with high CO_2 concentration which is not easy to remove to increase the calorific value of the fuel. Biogas is a carbonaceous feedstock containing CH_4 and CO_2 produced when animal waste, or manure, decomposes via a natural process called anaerobic digestion [18]. Anaerobic digestion reduces odors, pathogens, and waste in an enclosed system by bacteria without the presence of oxygen. Figure 1-5 shows a sample biogas production facility from organic materials in a digester tank. Biogas is a GHG (CH_4 and CO_2) and impacts the air with their GHG activity. Methane is estimated to have global warming potential (GWP) of 28-36 over 100 years [19]. Therefore, in a small scale biogas facility, the biogas is usually flared so that the methane is not released in the atmosphere. CO_2 separation from Renewable

Natural Gas (RNG) sources and storage is useful in this prospect that sometime separated carbon can be used as fuel or raw materials for valuable chemical synthesis although it is capital intensive [20,21]. Even if cost-effective CO_2 separation methods are available, it is highly unlikely that renewable sources will be competitive with fossil CNG or petroleum-based fuels in the open marketplace for transportation fuels. Moreover, commercially available CO_2 separation methods are primarily suited for large-scale industrial process and not for distributed renewable resources. Therefore, renewable fuel production processes to be commercially competitive in the marketplace, it is critical that the carbon lost as CO_2 is converted into a co-product with commercial value.

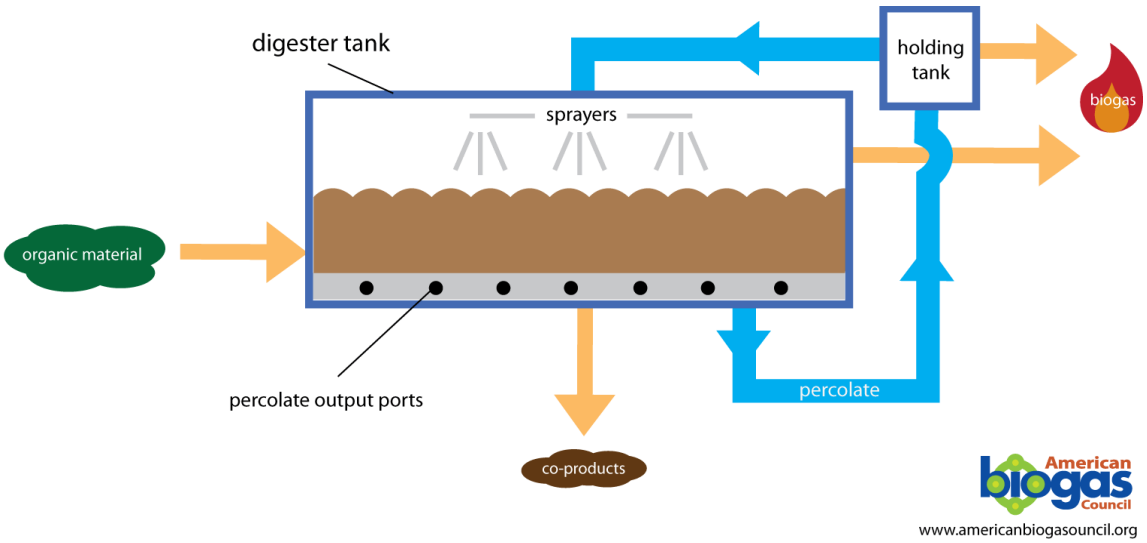

Figure 1-5: The biogas production system from organic materials [22].

Biogas produced from digester tank is cleaned or upgraded increasing the biogas energy content and remove impurities before used in appliances. Large farms usually use biogas to heat and power the facility, flare or supply to an off-farm buyer. Biogas is potentially

used in boilers, internal combustion engine, gas turbine, hot water system, process heaters, space or air heaters, gas fired chillers, combined heat and power, absorption chillers, fuel cells [23]. In places where biogas is not available in large quantities, biogas is released to the atmosphere and/or flared. In a large scale, biogas is used for heat and steam generation which is further utilized for electricity generation. The following statement is taken from California Energy Commission website describes how the landfill gas (LFG) or biogas is used for electricity generation:

"At Royal Farms No. 1 in Tulare, California, hog manure is slurried and sent to a Hypalon-covered lagoon for biogas generation. The collected biogas fuels a 70 kilowatt (kW) engine-generator and a 100 kW engine-generator. The electricity generated on the farm is able to meet monthly electric and heat energy demand. Given the success of this project, three other swine farms (Sharp Ranch, Fresno, and Prison Farm) have also installed floating covers on lagoons. The Knudsen and Sons project in Chico, California, treated wastewater which contained organic matter from fruit crushing and wash down in a covered and lined lagoon. The biogas produce is burned in a boiler. And at Langerwerf Dairy in Durham, California, cow manure is scraped and fed into a plug flow digester. The biogas produced is used to fire an 85 kW gas engine. The engine operates at 35 kW capacity level and drives a generator to produce electricity. Electricity and heat generated is able to offset all dairy energy demand. The system has been in operation since 1982." [24].

The methane potential in form of biogas in the United States is estimated to be 7.9 million tonnes per year, equivalent to 420 billion cubic feet or 431 trillion British thermal units [25]. The methane generation potential is expected to be much higher if lignocellulosic

biomass resources are used. In the future, the estimated amount of methane from renewable resources could reach 4.2 trillion cubic feet per year, equivalent to 4,318 trillion British thermal units [26]. This 4.2 trillion cubic feet per year renewable methane generation could replace about 46% of current natural gas uses in the electricity generation and transportation sector [27]. The amount of energy contained in this 4.2 trillion cubic feet renewable methane per year is equivalent to 35 billion gasoline gallon equivalent is about three times more than current gasoline consumption [28]. This huge amount of gas can reduce the GHG emission in two ways: reducing the use of fossil natural gas and biogas utilization instead of releasing to the atmosphere (as methane has 28-36 GWP compared to CO_2). The biogas utilization as a fuel for electricity generation in a large-scale facility is cost-effective and no attempts have been taken for the small-scale process. Therefore, more applications of biogas are desirable that will enable small-scale biogas utilization strategy. One attractive approach to avoid CO_2 separation from biogas is to convert CO_2 along with CH_4 directly to transportation fuel production or electricity generation. The conversion of CO_2 in presence of CH_4 only is called dry reforming (DR). Catalytic thermochemical DR is prone to coke formation and coke formation usually leads to catalyst deactivation [29]. Coke formation can be alleviated by adding steam and/or increasing the steam/methane (*S*/*C*) ratio of reactant mixture, i.e., by adding steam to biogas feed [30–33]. The product of thermochemical conversion is syngas which consists primarily of hydrogen and carbon monoxide. The syngas produced by dry reforming of a model biogas (60% CH_4, 40% CO_2) to syngas using a Ni/γ-Al_2O_3 produced syngas with an H_2/CO ratio of 1 at 800 °C [34]. Steam addition is required for lowering the coke formation and increasing the H_2/CO ratio

in the syngas. The reforming of biogas in presence of steam enables methane to react with and/or CO_2 referred to as bi-reforming in this study. The bi-reforming reactions take place catalytically temperatures as high as 1073 K for satisfactory methane conversion [35,36]. Synthesis gas is a versatile raw material for chemical and fuel synthesis and hydrogen is commonly used for ammonia production and refineries for hydrotreating and hydrocracking. Syngas is also used for Fischer-Tropsch diesel [37], methanol [38], gasoline [39], or natural gas [40] production.

1.3 Reforming of methane and biogas

Industrially, steam reforming of hydrocarbons, especially natural gas followed by water gas shift is the primary way syngas production [38]. The major component of natural gas is methane and the steam methane reforming is defined by the following reaction:

$$CH_4 + H_2O \leftrightarrow 3H_2 + CO \qquad \Delta H^{\ominus} = 206.1 \text{ kJ/mol} \qquad \text{eq 1-1}$$

In the next stage, CO and steam known as water gas react for more hydrogen production. This reaction is known as water gas shift (WGS) reaction.

$$CO + H_2O \leftrightarrow H_2 + CO_2 \qquad \Delta H^{\ominus} = 41.2 \text{ kJ/mol} \qquad \text{eq 1-2}$$

Hydrogen production via steam methane reforming (SMR) is a multistage reaction that includes impurities removal, reforming reaction in a reformer, WGS, and H_2 separation. A schematic diagram of the production process is shown in Figure 1-6. SMR is performed

catalytically and the catalyst is primarily deactivated due to carbon deposition onto the surface, which is the major obstacle to catalyst stability. Catalyst also encounters the sintering of active phase, the formation of inactive metal oxide or unfavorable interaction with oxide support, which affects catalyst performance adversely [41]. In this context, certain intensification or improvement of support material may help to resolve this problem.

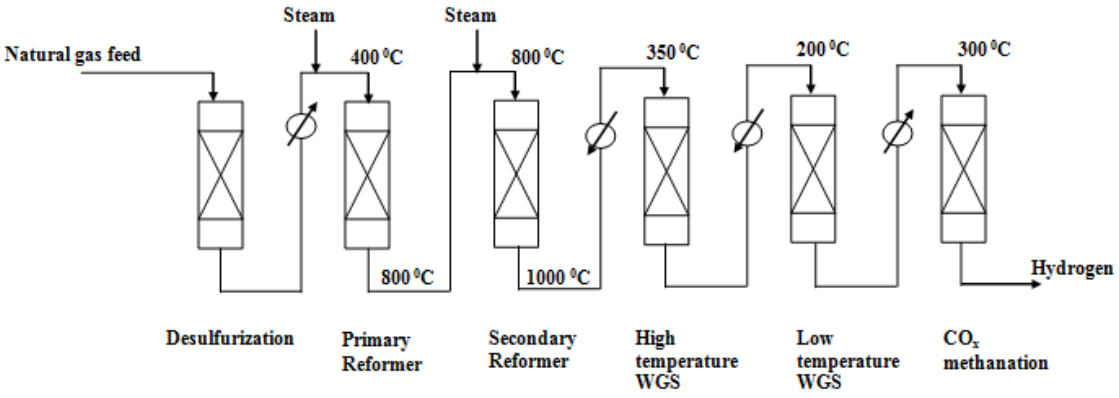

Figure 1-6: Schematic diagram of H_2 production process from steam reforming of natural gas [42].

The dry reforming reaction consumes CO_2 to produce syngas but requires a higher energy input compared to conventional steam reforming.

$$CH_4 + CO_2 \leftrightarrow 2H_2 + 2CO \qquad \Delta H^{\Theta} = 247.3 \text{ kJ/mol} \qquad \text{eq 1-3}$$

The catalyst selection for the reforming process is important since the catalyst plays a key role in feed conversion, product selectivity as well as suppress coke formation. Ni supported over Al_2O_3 is the most widely used catalyst for SMR [35,36]. Rh is known as

the most active element for activation of CH_4 by reforming reaction, and addition of a second metal to modify the structure of catalytic ingredient(s) is necessary for enhancement of syngas selectivity, suppression of coke buildup, and prevention of active metal oxidation [43–47]. Bimetallic combinations are known to perform better than monometallic catalysts, and their selection has shifted from Pt–Rh to Pd–Rh, due to cost impact of precious metals, activity and product selectivity, as well as thermal stability [48]. Rh mixed with Pd enables better metal dispersion owing to surface migration of Pd particles, providing preferential enrichment of the active metals on the surface [49,50]. Alumina support also plays an important role in catalytic reforming of methane because of its surface area, thermal stability, and capacity of maintaining metal dispersion during the reaction. Al_2O_3 supported catalysts activity is remarkably influenced by addition of reducible CeO_2 together with irreducible-but-stabilizing ZrO_2 [51–55]. CeO_2 sinters by itself at high temperature, however, its stability tends to improve with addition of ZrO_2. $CeZrO_2$-modification of Al_2O_3 can not only enhance catalyst activity, thermal stability and metal dispersion, but also reduce coke formation resulting from methane reforming [56–59]. So far, most studies have focused on the effect of $CeZrO_2$-modification of Al_2O_3 for syngas production, via partial oxidation of CH_4 [60,61].

Most commonly used DR catalysts are Ni-based. The problem is, these Ni-based catalysts undergo severe deactivation due to carbon deposition over catalyst surface during DR reactions. Noble metal catalysts are not economically attractive although they are found to be much more resistant to coke deposition than Ni catalysts [62].

The most widely used catalysts for bi-reforming are Ni-based [63]. Although cobalt-based catalysts have been reported to deactivate rapidly by coke formation and oxidation of the active sites by CO_2, promotion by noble metal has been found to be effective. Catalysts based on noble metals are generally more active and less sensitive to coke formation, but their high cost restricts their use for scale-up of the process. Pt-promoted cobalt catalysts [64] have shown high activity for bi-reforming. The role of Pt is proposed to stabilize the highly dispersed and reduced bimetallic nanoparticles.

The promotion of Ni-based catalysts by lanthanide group metals (La, Ce) has also been investigated. CeO_2 has been found to gasify the deposited coke on the catalyst surface by storing and delivering active oxygen [62,65,66].

In one of the few studies of bi-reforming, Olah et al. [67] used NiO deposited on MgO under 7 atm and 830 °C and the catalyst was found to be active and stable. They used a molar ratio 3/2.4/1.2 for $CH_4/H_2O/CO_2$ and observed stable activity for 320 h with an H_2/CO product ratio of 2/1. The selectivity for CO and H_2 were 100% and 98% respectively and conversions of both CH_4 and CO_2 were in the range of 70-75%. The undesired formation of carbon was prevented by the presence of steam. As an endothermic reaction, the positive effect of increasing temperature from 830 to 910 °C was that the conversion increased 15%, although the H_2/CO ratio changed little (1.99 to 1.97). An increase in pressure from 7 atm to 28 atm reduced the conversion from 71% to 52%, consistent with thermodynamics, while the H_2/CO ratio increases slightly from 1.99 to 2.02. Moreover, doubling the steam and CO_2 amount at 7 atm enhanced the CH_4 conversion from 71% to 85%.

One of the industrially significant results by Olah et al. [67] was that they were able to adjust the H_2/CO ratio in the product gases by changing the CO_2/H_2O ratio in the feed gas stream. Similar results have been reported by Choudhary's group [68–71], where they studied the effect of reactant composition on the H_2/CO ratio for the oxy-CO_2 methane reforming process. For bi-reforming reactions carried out by the same group [72,73], the product H_2/CO ratio was varied from 1.5 to 2.5 by manipulating the relative concentrations of stream and CO_2 in the feed. The catalyst for SMR and DR is commercially available in the market whereas catalyst for bi-reforming is still under development. To overcome these issues, one may be motivated to design a catalyst favorable for the bi-reforming reactions in terms of activity, stability, and resistance to coke formation.

Next, the type of reactor used for SMR reaction has an influence on the process efficiency. Most of the available study on dry reforming and bi-reforming are either done in a tubular reactor or with process simulator which is not suited, and heat transfer is a critical issue for the reforming reactions. In case SMR reaction is used for fuel processing in a solid oxide fuel cell (SOFC), the milli-structured micro-reactor or micro-channel reactor can reduce fuel reformer size more than the tubular reactor [74,75]. Reactor selection is dependent on mass and heat transfers, pressure drop and spatial limitation, and the use of integrated heat exchanger type reactor like a concentric tubular reactor, catalytic wall reactor, and micro-channel reactor has shown the process efficiency can be improved by reducing the energy supply from electric furnace [75–79]. Hwang et al.'s micro-channel reactor with a porous Ni plate catalyst performed satisfactorily as an energy-intensive device for hydrogen production [75].

1.4 CO_2 conversion utilization and Life Cycle Assessment

CO_2 produced via fossil fuel use in industry contribute towards GWP requires the individual plants to include implementing combined heat and power systems (that is, recovering waste heat produced during combustion), adding carbon capture and storage (CCS) [80]. The separation of this CO_2 from the industrial effluent and renewable carbonaceous feedstock is cost intensive and venting the CO_2 after separation leads to loss of major portion of carbon. In addition, converting CO_2 into commercially valuable products will also improve the economic viability of renewable and non-renewable carbon-based energy production by creating additional revenue streams, significantly decreasing net GHG emissions. Several technology options to convert CO_2 into higher value fuels and chemicals are currently available, including well-known pathways for methanol and dimethyl ether (DME) production [81–83]. Among CO_2 hydrogenation products, methanol is attractive, for it is a hydrogen carrier medium and can be directly used as transportation fuel. However, these pathways are commercially feasible under very few circumstances and search for improved technology is ongoing [84–86].

Methanol is an industrial chemical that is primarily synthesized from natural gas. The most widely used conversion pathway is steam reforming of natural gas followed by the conversion of the resulting syngas into methanol. A simplified flow diagram of methanol synthesis is given in Figure 1-7 (Process Analytics in Methanol Plants, Siemens AG 2007) [87]. The description of the methanol synthesis process below is adapted from the document ‘Process Analytics in Methanol Plants’ published by Siemens AG (2007), and other references [87,88].

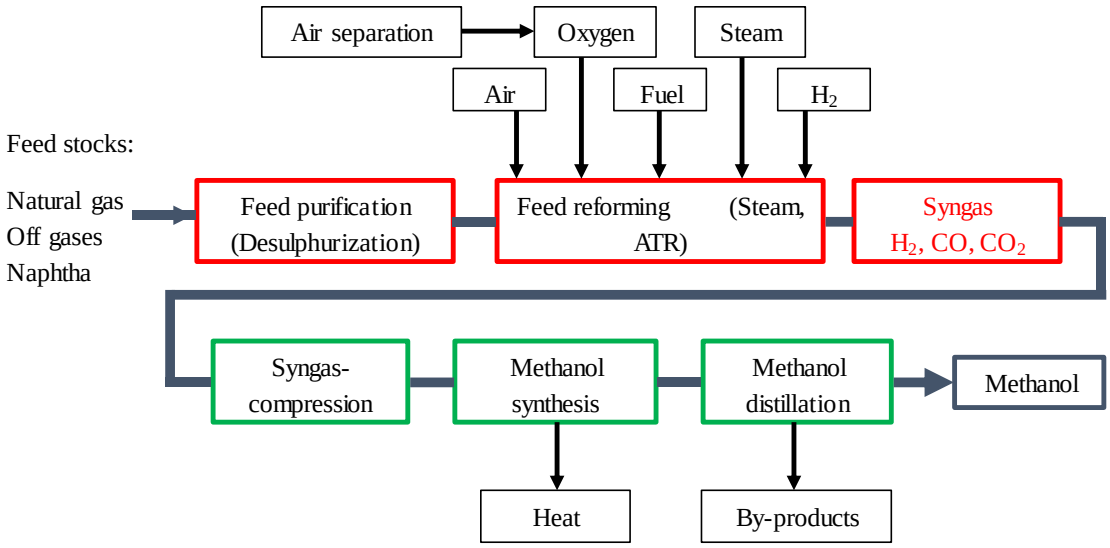

Figure 1-7: Generic flow diagram of the methanol synthesis process [87].

Feed purification: During this step, the natural gas feed is compressed, and sulfur is removed from the gas stream by hydro-desulfurization. The desulfurized gas is cooled and flows to the saturator where it encounters hot water over a bed of packing. The saturated gas contains most of the steam required for later reforming. Additional steam, generated in the boiler, is made up to the gas stream to achieve the required 'steam to carbon ratio' for the reforming.

Feed reforming (Syngas generation): Syngas is composed of H_2, CO and CO_2, whereas the ratio of H_2/CO is important in view of the process efficiency using a certain catalyst material. Syngas is produced mainly from natural gas (NG) through a reforming process. A number of reforming technologies are available, with or without using air or oxygen SMR, Partial Oxidation (POX), Autothermal Reforming (ATR). After cooling, syngas is

compressed to synthesis pressure, which ranges from 40 to 110 bar. A brief description of the reforming technology options is given below [87].

Methanol Synthesis: The synthesis gas is fed to the methanol synthesis reactor at about 130-250 °C. The compressed gas is preheated to reaction temperatures inside the tubes as it flows through the hot catalyst bed. The hot reacted gas leaves the converter and provides heat to the saturator water circuit and the loop interchanger before finally being cooled. Crude methanol is separated from the uncondensed gases and the gases are recirculated back to the converter via the circulator.

Methanol Distillation: The crude methanol passes to a methanol distillation section, where it is stabilized and reduced to an economic water content for transport. Purge gas from the methanol synthesis cascade is treated to recover hydrogen for recycling.

Table 1-1: Global Warming Potentials of the key GHGs [89].

GHG Name	100 Year GWP
Carbon dioxide (CO_2)	1
Methane (CH_4)	25
Nitrous Oxide (N_2O)	298
Chlorofluorocarbons(CFC-12)	10,900
Hydrofluorocarbons (HFC-134a)	1,430

The new technologies must demonstrate a life cycle approach environmental superiority over alternative pathways towards the product before entering the market. GHG emission,

as well as criteria pollutant emission, are considered as the crucial component for environmental superiority. The key GHGs considered by the Life cycle assessment (LCA) and their GWP compared to CO_2 is given in Table 1-1. The GWPs are the 100 years warming potential values published by the Intergovernmental Panel on Climate Change (IPCC) in 2007 and are often referred to as the IPCC 2007 GWPs [89].

LCA models iteratively calculate the energy use and emissions associated with specific pathways using large databases consisting of information on various stages of the pathways and some user-specified input values. Figure 1-8 shows the processes typically included in an LCA and the system boundaries [90].

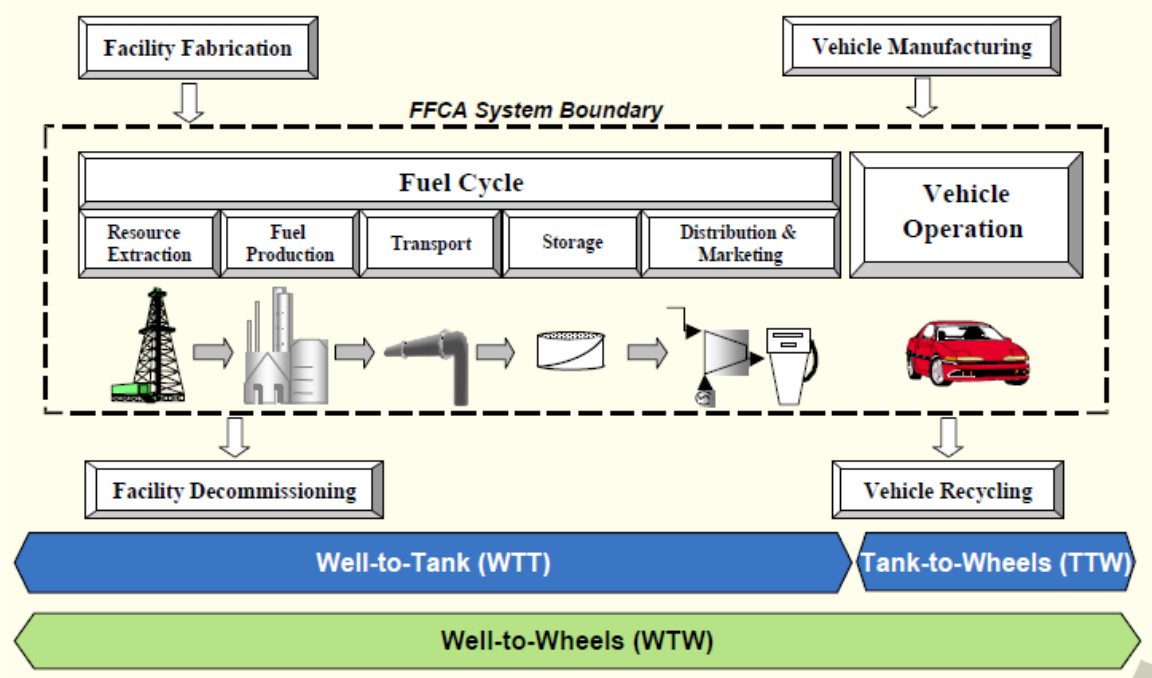

Figure 1-8: Typical processes and system boundaries included in an LCA study [90].

The Greenhouse Gases, Regulated Emissions, and Energy Use in Transportation (GREET) model, an LCA tool developed by Argonne National Laboratory (ANL), widely used in emission study of fuel production pathways, especially in the United States [91]. GHGenius is an LCA tool developed for Natural Resources Canada over the past decade. The model can evaluate a number of conventional and alternative fuels and production pathways. While GHGenius and GREET are similar, Excel-based life cycle models, there are significant detailed differences in terms of the system boundaries, the fuel pathways modeled, and the default data stored in the models. GREET uses US data only. The GHGenius data used in the calculations for pathways based in Canada are from reports published by Statistics Canada, Natural Resources Canada, Environment Canada and the National Energy Board [92].

The energy uses of a fuel production pathway are calculated by the LCA model in the below listed category:

Total and fossil energy used per unit of energy produced for each stage of the fuel production steps

Total energy used per kilometer driven for the fuel used in vehicles

Fossil energy used per kilometer driven for the fuel used in vehicles

The proportions of types of energy used for each stage of the fuel production cycle

1.5 Biogas in transportation

About one fifth of the world's primary energy requirements is met by natural gas widely used by the domestic, commercial and industrial users [93]. Pretreated natural gas is a

mixture of hydrocarbons with minor impurities containing N_2, O_2 and CO_2. Methane is the largest hydrocarbon component in the natural gas, and composition of methane usually varies from 85 to 98% also contains ethane (C_2H_6), propane (C_3H_8), butane (C_4H_{10}), inert nitrogen (N_2) and carbon dioxide (CO_2) [94,95]. Methane composition in biogas also varies over a wide range of 35-60%. The CO_2 content in upgraded biogas varies in a wide range depending on the source and/or production method. The Variable Natural Gas Vehicle (VNGV) is a Natural Gas Vehicle (NGV) that can operate on any arbitrary mixture of CH_4 and CO_2, thus allowing the use of RNG including biogas for transportation without comprehensive gas cleanup/upgrading.

NGV can be attractive for their low fuel prices on an energy-equivalent basis relative to gasoline [96]. A significant increase in the number of NGVs running on RNG is needed to make an impact on net GHG and criteria pollutant emissions reduction. Comprehensive gas cleanup/upgrading of RNG resources to meet current NGV fuel specifications is often not economically feasible. On the contrary, the presence of inert gas (like CO_2) in the RNG could provide the benefit of reducing NO_x emission, since it plays as the Exhaust Gas Recirculation (EGR) control of the engine. NGV typically operate with stoichiometric air-to-fuel ratio control with a three-way catalyst (TWC) to control the emissions of NOx. One method for reducing NOx emissions further is with EGR. EGR is the process of recirculating some of the exhaust with fresh air and fuel to minimize the Nitrogen forming species. RNG has high levels of CO_2 which could provide the same NO_x emissions reduction benefit of EGR but without the EGR technology. A schematic diagram of the idea is shown in Figure 1-9. This has two benefits, 1) the EGR system is not needed thus

reducing engine costs and 2) the separation process is not needed thus reducing the RNG costs.

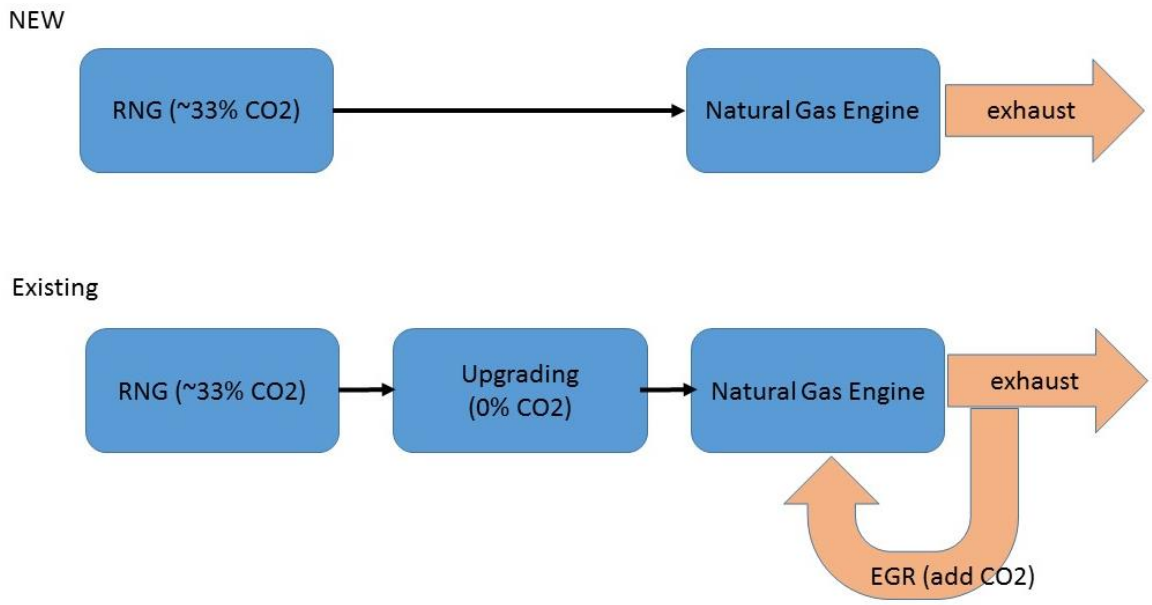

Figure 1-9: The concept of biogas utilization in a VNGV over the EGR technology.

The two key enabling technologies needed by a VNGV are (1) on-board, real-time detection of key fuel properties (such as Wobbe Index, Methane Index, and Inert gas composition) and (2) adaptive combustion control in the engine for a wide range of fuel variations. On-board detection of fuel properties is an essential part of adaptive engine control determining the engine combustion mode and combustion control, and integration of emission control systems. Among the fuel properties, Wobbe Index (WI), the ratio of a calorific value of a fuel to the square root of its specific gravity, is a well-known, critical factor for fuel interchangeability. WI is not only related to VNGV but is also used in a wide variety of equipment and processes that involve natural gas combustion. The major natural

gas users sometimes require a process that must fulfill certain characterizing natural gas qualities such as Methane Number (MN), Wobbe Index to make sure that natural gas vehicles, devices, or appliances operate safely and efficiently. The composition of the combustion gas affects the thermodynamic properties especially thermal conductivity and sound velocity in the gas medium. The change in these properties can be accounted for the change in methane MN or WI [97].

WI, the ratio of a calorific value of a fuel to the square root of its specific gravity, is a well-known, critical factor for fuel interchangeability. WI is not only related to VNGV but is also used in a wide variety of equipment and processes that involve natural gas combustion. WI for natural gas is approximate twice the WI of biogas [97]. Gas appliances are designed to produce a certain thermal input, WI provides a sufficient measure for this application [98]. The calorific values of gaseous fuels containing alkane hydrocarbons are not measured frequently and an average number is assumed as the value. Therefore, the price of the gaseous fuel is usually based on a nominal average value or a value obtained by the periodic checking [99].

The NM is a natural gas property similar to the octane number of gasoline in which it describes the ability of natural gas to withstand compression before ignition. Fuels with higher methane numbers are more capable of resisting combustion knocking, while fuels with lower methane numbers may pose performance problems for NGV engines due to their higher amounts of ethane, propane, and heavier hydrocarbons that can cause combustion knocking. Pure methane has an MN of 100 and pure hydrogen has an MN of 0 (zero) [100]. The MN of a gas mixture is a function of hydrocarbon composition in the

natural gas. Industrially MN higher than 70/80 is preferable depending on the type of operation. MN drops significantly with the increase in hydrogen composition in the gas mixture and hydrogen composition can be more than 20% in the future [101]. Engines can run with the gas of different MN by proper tuning for the operational condition.

In an environment where the gas composition varies frequently, an accurate estimation or prediction of WI and MN is critical since their variation significantly impacts the combustion/operation efficiency and CO_2 emission [102] as well as cogeneration engines knocking [103]. There are several methods to characterize the quality of combustion gas. Most of these methods rely on the measurement of hydrogen to carbon ratio in the fuel, which can be obtained through a comprehensive component analysis [103,104]. These complex, expensive, and bulky size of existing quality measurement systems can be used by NG suppliers alone, thereby prevent its use for the consumer or small/medium scale natural gas industry. There is a need exists for equipment and methods to ease the transition from conventional fossil-based fuels to the widespread adoption of RNG fuels while reducing or eliminating the need for EGR technology.

The overall objective of this dissertation is to develop pathways that can lead to cost-effective and efficient technologies for renewable energy generation, with an emphasis on CO_2 utilization.

1.6 Organization of this thesis

The study is designed to enhance the utilization of biogas and the overall study direction is presented in Figure 1-10.

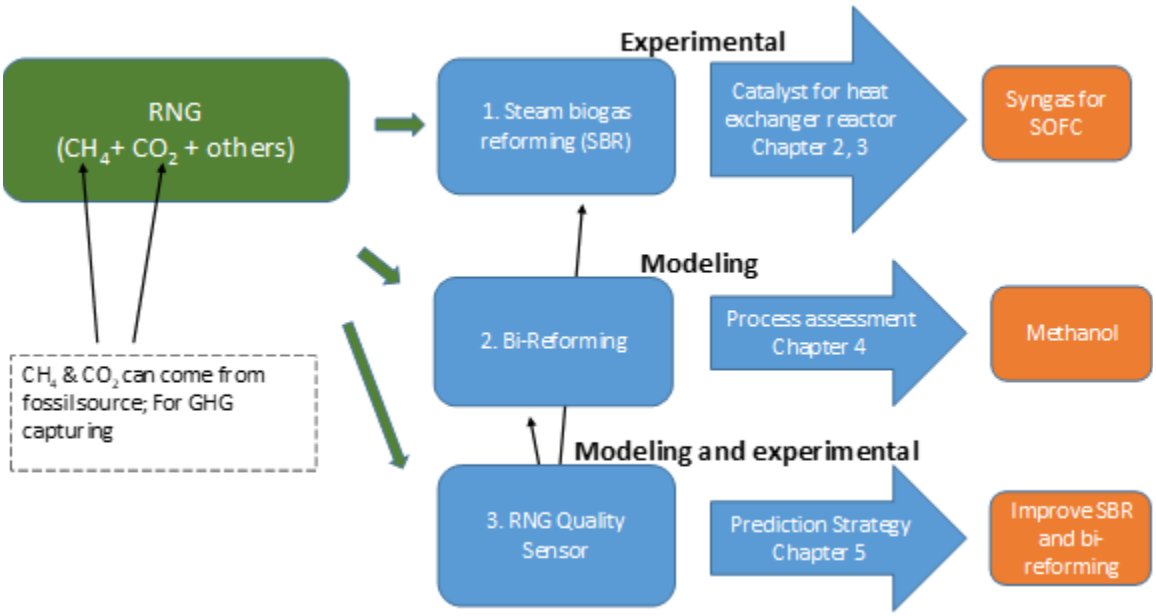

Figure 1-10: Development of technologies to enable increased RNG use

A list of the thesis chapters is provided below.

Introduction: A brief overview of renewable energy utilization technologies are provided.

CO2 conversion to syngas through the steam-biogas reforming process: A brief description steam biogas reforming catalysts are provided. The experimental results are compared to the simulation results.

Effects of CeZrO2-Al2O3 support composition of metal-foam-coated Pd-Rh catalysts for the steam-biogas reforming reaction: Experimental data of the steam biogas reforming over

a metal-foam-coated catalyst is used to find a suitable catalyst support material composition.

Techno-economic and Life Cycle Analysis of CO2 Conversion to Methanol through Bi-reforming: A life cycle analysis has been performed for methanol production using syngas produced via steam and CO_2 reforming of methane.

Predicting Wobbe Index and Methane Number of a Renewable Natural Gas by the Measurement of Simple Physical Properties: A model is developed for estimating Wobbe Index, Methane Number and gas composition of a biogas, anaerobic digester gas and natural gas mixture. The model uses the temperature, pressure, thermal conductivity of the gas mixture and sound in the mixed gas medium.

Conclusions and recommendations: A summary of the experimental and simulation results are presented for this work.

1.7 References

[1] E. McFarland, Unconventional chemistry for unconventional natural gas, Science 338 (2012): 340-342.

[2] United Nations Framework Convention on Climate Change (UNFCC), Report of the Conference of the Parties on its Fifteenth Session, Copenhagen, December 2009.

[3] Intergovernmental Panel on Climate Change. Climate change 2014: Mitigation of climate change, Cambridge University Press (Vol. 3) (2015) 511-597.

[4] M. Meinshausen, N. Meinshausen, W. Hare, S.C.B. Raper, K. Frieler, R. Knutti, D.J. Frame, M.R. Allen, Greenhouse-gas emission targets for limiting global warming to 2 °C, Nature 458 (2009) 1158–62.

[5] C. McGlade, P. Ekins, The geographical distribution of fossil fuels unused when limiting global warming to 2 °C, Nature 517 (2015) 187-190.

[6] G. Marland, A.F. Turhollow, CO2 emissions from the production and combustion of fuel ethanol from corn, Energy 16 (1991) 1307-1316.

[7] E.E. Powell, G.A. Hill, Carbon dioxide neutral, integrated biofuel facility, Energy 35 (2010) 4582-4586.

[8] W.P. Nel, C.J. Cooper, Implications of fossil fuel constraints on economic growth and global warming, Energy Policy 37 (2009) 166-180.

[9] M. Jakob, J. Hilaire, Climate science: Unburnable fossil-fuel reserves, Nature 517 (2015) 150-152.

[10] International Energy Agency. Electricity generation by fuel,

https://www.iea.org/statistics/?country=WORLD&year=2016&category=Electricity&indicator=ElecGenByFuel&mode=chart&categoryBrowse=false&dataTable=ELECTRICITYANDHEAT&showDataTable=false [accessed 5 October 2018].

[11] California Public Utilities Comission. California Renewables Portfolio Standard (RPS), http://www.cpuc.ca.gov/renewables/ [accessed 19 October 2018].

[12] United States Environmental Protection Agency. State Renewable Energy Resources, https://www.epa.gov/statelocalenergy/state-renewable-energy-resources [accessed 19 October 2018].

[13] California Air Resources Board. California's 2030 Climate Commitment: Renewable resources for the half of the state's electricity by 2030, https://www.arb.ca.gov/html/fact_sheets/2030_renewables.pdf [accessed 15 October 2018].

[14] California Energy Cmission. Landfill Gas Power Plants, http://www.energy.ca.gov/biomass/landfill_gas.html [accessed 19 October 2018].

[15] United States Environmental Protection Agency. Landfill Methane Outreach Program: Landfill Gas Energy Project Data, https://www.epa.gov/lmop/landfill-gas-energy-project-data#project [accessed 19 October 2018].

[16] C.S. Park, P.S. Roy, S.H. Kim. Current Developments in Thermochemical Conversion of Biomass to Fuels and Chemicals, in: Y. Yun (Eds.), Gasification for Low-grade Feedstock, InTechOpen, 2018, pp. 19-41.

[17] M.H. Langholtz, et al., 2016 Billion-ton report: Advancing domestic resources for a thriving bioeconomy, volume 1: Economic availability of feedstocks, No.

ORNL/TM-2016/160. Oak Ridge National Lab.(ORNL), Oak Ridge, TN (United States), 2016.

[18] United States Environmental Protection Agency. Learn About Biogas Recovery, https://www.epa.gov/agstar/learn-about-biogas-recovery [accessed 19 October 2018].

[19] United States Environmental Protection Agency. Greenhouse Gas Emissions: Understanding Global Warming Potentials, https://www.epa.gov/ghgemissions/understanding-global-warming-potentials [accessed 19 October 2018].

[20] E.G. Lindfeldt, O.W. Mats, System study of carbon dioxide (CO2) capture in bio-based motor fuel production, Energy 33 (2008) 352-361.

[21] H.S. Kheshgi, C.P. Roger, Sequestration of fermentation CO2 from ethanol production, Energy 30 (2005) 1865-1871.

[22] American Biogas Council. BiogasSystems: Dry System, http://americanbiogascouncil.org/images/dryBiogasSystems_large.gif [accessed 15 October 2018].

[23] Biogas Utilization and Cleanup, https://articles.extension.org/pages/30312/biogas-utilization-and-cleanup [accessed 15 October 2018].

[24] California Energy Cmission. Anaerobic Digestion, https://www.energy.ca.gov/biomass/anaerobic.html [accessed 15 October 2018].

[25] National Renewable Energy Laboratory. Energy Analysis: Biogas Potential in the United States, , https://www.nrel.gov/docs/fy14osti/60178.pdf [accessed 15 October 2018].

[26] The National Petroleum Council (NPC). Renewable Natural Gas for Transportation: An Overview of the Feedstock Capacity, Economics, and GHG Emission Reduction Benefits of RNG as a Low-Carbon Fuel, www.npc.org/FTF_Top, 2013 [ccessed 2013': n.d.

[27] Monthly Energy Review: Energy Consumption by Sector. (2013a). U.S. Energy Information Administration (EIA). [accessed 2013].

[28] United States Energy Information Administration. Refiner Motor Gasoline Sales Volumes, EIA.

www.eia.gov/dnav/pet/pet_cons_refmg_d_nus_VTR_mgalpd_a.htm, 2013 [accessed 2013]

[29] S. Damyanova, B. Pawelec, K. Arishtirova, J.L.G. Fierro, Biogas reforming over bimetallic PdNi catalysts supported on phosphorus-modified alumina, Int. J. Hydrogen Energy 36 (2011) 10635-10647.

[30] V. Chiodo, A. Galvagno, A. Lanzini, D. Papurello, F. Urbani, M. Santarelli, S. Freni, Biogas reforming process investigation for SOFC application, Energy Convers. Manag. 98 (2015) 252-258.

[31] P. Kolbitsch, C. Pfeifer, H. Hofbauer, Catalytic steam reforming of model biogas, Fuel 87 (2008) 701-706.

[32] P. Gangadharan, C.K. Krishna, H.L. Helen, Evaluation of the economic and environmental impact of combining dry reforming with steam reforming of methane, Chem. Eng. Res. Des. 90 (2012) 1956-1968.

[33] A. Galvagno, V. Chiodo, F. Urbani, S. Freni, Biogas as hydrogen source for fuel cell applications. Int. J. Hydrogen Energy 38 (2013) 3913-3920.

[34] V. Rathod, P.V. Bhale, Experimental Investigation on Biogas Reforming for Syngas Production over an Alumina based Nickel Catalyst, Energy Procedia 54 (2014) 236-245.

[35] D. Li, Y. Nakagawa, K. Tomishige, Methane reforming to synthesis gas over Ni catalysts modified with noble metals, Appl. Catal. A Gen. 408 (2011) 1-24.

[36] J. Xu, F.F. Gilbert, Methane steam reforming, methanation and water-gas shift: I. Intrinsic kinetics. AIChE J. 35 (1989) 88-96.

[37] M.E. Dry, The Fischer-Tropsch process: 1950-2000. Catal. Today 71 (2002) 227-241.

[38] J.G. Jakobsen, J. Sehested, I. Chorkendorff, Noble metal catalysts for methane steam reforming, Technical University of Denmark (2010).

[39] J. Topp-Jørgensen, Topsøe Integrated Gasoline Synthesis - The Tigas Process, Stud. Surf. Sci. Catal. 36(1988) 293-305.

[40] J.R. Rostrup-Nielsen, K. Pedersen, J. Sehested, High temperature methanation: Sintering and structure sensitivity, Appl. Catal. A Gen. 330 (2007) 134-138.

[41] V. Dal Santo, A. Gallo, A. Naldoni, M. Guidotti, R. Psaro, Bimetallic heterogeneous catalysts for hydrogen production, Catal. Today 197 (2012) 190-205.

[42] NPETL. Primary steam reforming, https://nptel.ac.in/courses/103103026/module2/lec26/2.html [accessed 16 October 2018].

[43] D. Pakhare, J. Spivey, A review of dry (CO2) reforming of methane over noble metal catalysts, Chem. Soc. Rev. 43 (2014) 7813-7837.

[44] M.H. Halabi, M.H.J.M. De Croon, J. Van der Schaaf, P.D. Cobden, J.C. Schouten, Low temperature catalytic methane steam reforming over ceria–zirconia supported rhodium. Appl. Catal. A Gen. 389 (2010) 68-79.

[45] J. Wei, E. Iglesia. Structural requirements and reaction pathways in methane activation and chemical conversion catalyzed by rhodium, J. Catal. 225 (2004) 116-127.

[46] V. Dal Santo, A. Gallo, A. Naldoni, M. Guidotti, R. Psaro, Bimetallic heterogeneous catalysts for hydrogen production, Catal. Today 197 (2012) 190-205.

[47] X. Wang, R.J. Gorte, A study of steam reforming of hydrocarbon fuels on Pd/ceria, Appl. Catal. A Gen. 224 (2002) 209-218.

[48] S.B. Kang, S.J. Han, I.S. Nam, B.K. Cho, C.H. Kim, S.H. Oh, Detailed reaction kinetics for double-layered Pd/Rh bimetallic TWC monolith catalyst, Chem. Eng. J. 241 (2014) 273-287.

[49] F. Tao, et al., Reaction-driven restructuring of Rh-Pd and Pt-Pd core-shell nanoparticles, Science 322 (2008) 932-934.

[50] B.T. Sneed, et al., Nanoscale-phase-separated Pd–Rh boxes synthesized via metal migration: An archetype for studying lattice strain and composition effects in electrocatalysis, J. Am. Chem. Soc. 135 (2013) 14691-14700.

[51] C. Berger-Karin, S. Wohlrab, U. Rodemerck, E.V. Kondratenko, The tremendous effect of trace amounts of Rh on redox and catalytic properties of CeO2-TiO2 and Al2O3 in CH4 partial oxidation, Catal. Commun. 18 (2012) 121-125.

[52] P. Fornasiero, R. Dimonte, G.R. Rao, J. Kaspar, S. Meriani, A.0. Trovarelli, M. Graziani, Rh-loaded CeO2-ZrO2 solid-solutions as highly efficient oxygen exchangers: dependence of the reduction behavior and the oxygen storage capacity on the structural-properties, J. Catal.151 (1995) 168-177.

[53] C. Bozo, F. Gaillard, N. Guilhaume, Characterisation of ceria–zirconia solid solutions after hydrothermal ageing, Appl. Catal. A Gen. 220 (2001) 69-77.

[54] C.E. Hori, H. Permana, K.S. Ng, A. Brenner, K. More, K.M. Rahmoeller, D. Belton, Thermal stability of oxygen storage properties in a mixed CeO2-ZrO2 system, Appl. Catal. B Environ. 16 (1998): 105-117.

[55] M.M.V.M. Souza, M. Schmal, Methane conversion to synthesis gas by partial oxidation and CO2 reforming over supported platinum catalysts, Catal. Lett. 91 (2003) 11-17.

[56] H.-S. Roh,, H.S. Potdar, K.-W. Jun, Carbon dioxide reforming of methane over co-precipitated Ni-CeO2, Ni-ZrO2 and Ni-Ce-ZrO2 catalysts, Catal. Today 93 (2004) 39-44.

[57] S. Kurungot, T. Yamaguchi, Stability improvement of Rh/γ-Al2O3 catalyst layer by ceria doping for steam reforming in an integrated catalytic membrane reactor system, Catal. Lett. 92 (2004) 181-187.

[58] M.P. Yeste, J.C. Hernández, S. Bernal, G. Blanco, J.J. Calvino, J.A. Pérez-Omil, J.M. Pintado, Redox behavior of thermally aged ceria-zirconia mixed oxides. Role of their surface and bulk structural properties, Chem. Mater. 18 (2006) 2750-2757.

[59] K. Kusakabe, K.I. Sotowa, T. Eda, Y. Iwamoto, Methane steam reforming over Ce-ZrO2-supported noble metal catalysts at low temperature. Fuel Process. Technol. 86 (2004) 319-326.

[60] G. Nahar, V. Dupont Hydrogen production from simple alkanes and oxygenated hydrocarbons over ceria–zirconia supported catalysts: Review, Renew. Sust. Energy Rev. 32 (2014) 777-796.

[61] L.V. Mattos, E. Rodino, D.E. Resasco, F.B. Passos, F.B. Noronha, Partial oxidation and CO2 reforming of methane on Pt/Al2O3, Pt/ZrO2, and Pt/Ce–ZrO2 catalysts, Fuel Process. Technol. 83 (2003), 147-161.

[62] K.Y. Koo, S.H. Lee, U.H. Jung, H.S. Roh, W.L. Yoon, Syngas production via combined steam and carbon dioxide reforming of methane over Ni–Ce/MgAl2O4 catalysts with enhanced coke resistance, Fuel Process. Technol. 119 (2014) 151-157.

[63] M.M. Danilova, Z.A. Fedorova, V.A. Kuzmin, V.I. Zaikovskii, A.V. Porsin, T.A. Krieger, Combined steam and carbon dioxide reforming of methane over porous nickel based catalysts, Catal. Sci. Technol. 5 (2015) 2761-2768.

[64] S.S. Itkulova, G.D. Zakumbaeva, Y.Y. Nurmakanov, A.A. Mukazhanova, A.K. Yermaganbetova, Syngas production by bireforming of methane over Co-based alumina-supported catalysts, Catal. Today 228 (2014) 194-198.

[65] K.Y. Koo, H.S. Roh, U.H. Jung, W.L. Yoon, Combined H2O and CO2 reforming of CH4 over Ce-promoted Ni/Al2O3 catalyst for gas to liquid (GTL) process: Enhancement of Ni-CeO2 interaction, Catal. Today 185 (2012) 126-130.

[66] H.S. Roh, K.Y. Koo, U.H. Joshi, W.L. Yoon, Combined H2O and CO2 Reforming of Methane Over Ni-Ce-ZrO2 Catalysts for Gas to Liquids (GTL), Catal. Lett. 125 (2008) 283-288.

[67] G.A. Olah, A. Goeppert, M. Czaun, G.S. Prakash, Bi-reforming of Methane from Any Source with Steam and Carbon Dioxide Exclusively to Metgas (CO–2H2) for Methanol and Hydrocarbon Synthesis, J. Am. Chem. Soc. 135 (2012) 648-650.

[68] V.R. Choudhary, K.C. Mondal, T.V. Choudhary, Oxy-CO2 reforming of methane to syngas over CoOx/CeO2/SA-5205 catalyst, Energy Fuels, 20 (2006) 1753-1756.

[69] V.R. Choudhary, K.C. Mondal, T.V. Choudhary, Oxy-CO2 reforming of methane to syngas over CoOx/MgO/SA-5205 catalyst, Fuel 85 (2006) 2484-2488.

[70] V.R. Choudhary, K.C. Mondal, CO2 reforming of methane combined with steam reforming or partial oxidation of methane to syngas over NdCoO3 perovskite-type mixed metal-oxide catalyst, Appl. Energy 83 (2006) 1024-1032.

[71] V.R. Choudhary, B.S. Uphade, A.S. Mamman, Simultaneous steam and CO2 reforming of methane to syngas over NiO/MgO/SA-5205 in presence and absence of oxygen, Appl. Catal. A Gen. 168 (1998) 33-46.

[72] V.R. Choudhary, A.M. Rajput, Simultaneous Carbon Dioxide and Steam Reforming of Methane to Syngas over NiO−CaO Catalyst, Ind. Eng. Chem. Res. 35 (1996) 3934-3939.

[73] T.V. Choudhary, V.R. Choudhary, Energy-efficient syngas production through catalytic oxy-methane reforming reactions, Angew. Chem., Int. Ed. 47 (2008) 1828-1847.

[74] M. Mbodji M, J.M. Commenge, L. Falk, D. Di Marco, F. Rossignol, L. Prost, S. Valentin, R. Joly, P. Del-Gallo, Steam methane reforming reaction process intensification by using a millistructured reactor: Experimental setup and model validation for global kinetic reaction rate estimation, Chem. Eng. J. 207 (2012) 871-884.

[75] K.-R. Hwang, C.-B. Lee, S.-W. Lee, S.-K. Ryi, J.-S. Park, Novel micro-channel methane reformer assisted combustion reaction for hydrogen production, Int. J. Hydrogen Energy 36 (2011) 473-481.

[76] G. Kolios, J. Frauhammer, G. Eigenberger, Efficient reactor concepts for coupling of endothermic and exothermic reactions, Chem. Eng. Sci. 57 (2002) 1505-1510.

[77] T.G. Ghang, S.M. Lee, K.Y. Ahn, Y. Kim, An experimental study on the reaction characteristics of a coupled reactor with a catalytic combustor and a steam reformer for SOFC systems, Int. J. Hydrogen Energy 37 (2012) 3234-3241.

[78] K. Venkataraman, E.C. Wanat, L.D. Schmidt, Steam reforming of methane and water-gas shift in catalytic wall reactors, AIChE J. 49 (2003) 1277-1284.

[79] G.D. Stefanidis, D.G. Vlachos, N.S. Kaisare, M. Maestri, Methane steam reforming at microscales: Operation strategies for variable power output at millisecond contact times, AIChE J. 55 (2009) 180-191.

[80] Union of Concerned Scientists. Tapping Renewables and Efficiency to Meet Carbon Standards for Power Plants Reducing Carbon Emissions from Power Plants, https://www.ucsusa.org/sites/default/files/legacy/assets/documents/clean_energy/Tapping-Renewables-and-Efficiency-to-Meet-Carbon-Standards-for-Power-Plants.pdf [accessed 19 October 2018].

[81] West Virginia Coal Association. Japan Helps Iceland Convert CO2 into Liquid Hydrocarbon Fuels, https://www.wvcoal.com/research-development/japan-helps-iceland-convert-co2-into-liquid-hydrocarbon-fuels [accessed 19 October 2018].

[82] Carbon Recycling International. Carbon Recycling International implements power-to-fuel technology in Germany, http://carbonrecycling.is/news/2016/2/18/carbon-recycling-international-implements-power-to-fuel-technology-in-germany [accessed 19 October 2018].

[83] West Virginia Coal Association. Germany to Convert Coal Power Plant CO2 into Methanol, https://www.wvcoal.com/research-development/germany-to-convert-coal-power-plant-co2-into-methanol [accessed 19 October 2018].

[84] W.M. Budzianowski, Negative carbon intensity of renewable energy technologies involving biomass or carbon dioxide as inputs, Renew. Sust. Energy Rev. 16 (2012) 6507-6521.

[85] G.A. Olah, Towards oil independence through renewable methanol chemistry, Angew. Chem., Int. Ed. 52 (2013) 104-107.

[86] Unites States Energy Information Administration. Annual Energy Outlook 2013: with Projections to 2040, http://www.eia.gov/forecasts/aeo/pdf/0383(2013).pdf [accessed 19 October 2018].

[87] Siemens. Process Analytics in Methanol Plants,

https://www.industry.usa.siemens.com/automation/us/en/process-instrumentation-and-analytics/process-analytics/pa-case-studies/Documents/PIACS-00014-1015-Methanol.pdf [accessed 19 October 2018].

[88] S. Lögdberg, H.A. Jakobsen, Natural Gas Conversion: The Reforming and Fischer-Tropsch Processes, TKP 4145 Reactor technology (2010).

[89] Intergovernmental Panel on Climate Change. IPCC fourth assessment report: climate change 2007, Cambridge, 104p (2007).

[90] California Energy Commission. Full Fuel Cycle Assessment Well To Tank Energy Inputs, Emissions, And Water Impacts, (2007).

[91] Argonne National Laboratory. Energy Systems: GREET Model,

https://greet.es.anl.gov/ [accessed 19 October 2018].

[92] GHGenius. Frequently Asked Questions,

http://www.ghgenius.ca/index.php/modelling-resources/frequently-asked-questions [accessed 19 October 2018].

[93] T. Briggs, The combustion and interchangeability of natural gas on domestic burners, Combustions 4 (2014) 67-87.

[94] M. Schoell, The hydrogen and carbon isotopic composition of methane from natural gases of various origins, Geochim. Cosmochim. Acta. 44 (1980) 649-661.

[95] A.-H. Kakaee, A. Paykani, M. Ghajar, The influence of fuel composition on the combustion and emission characteristics of natural gas fueled engines, Renew. Sustain. Energy Rev. 38 (2014) 64-78.

[96] A. Wiley, T. Hunt, Pipeline & Gas Journal. CNG As Vehicle Fuel Looming Larger, https://pgjonline.com/magazine/2011/november-2011-vol-238-no-11/features/cng-as-vehicle-fuel-looming-larger [accessed 18 July 2018].

[97] P.S. Roy, C. Ryu, C.S. Park, Predicting Wobbe Index and methane number of a

renewable natural gas by the measurement of simple physical properties, Fuel 224 (2018) 121-127.

[98] D. Ferguson, Fuel interchangeability considerations for gas turbine combustion, No. DOE/NETL-IR-2008-014; NETL-TPR-1913. National Energy Technology Laboratory (NETL), Pittsburgh, PA(United States), Morgantown, WV(United States), Albany, OR(United States), 2007.

[99] W.B. Kude, A.N.J. Pearman, Method and apparatus for determining the Wobbe index of gaseous fuels, U.S. Patent 4,359,284 (1982).

[100] G. Diderich, P. Scherm, Requirements on the quality of natural gas, The European Association of Internal Combustion Engine Manufacturers, https://www.euromot.eu/wp-content/uploads/2018/02/EUROMOT-Position-Gas-Quality-2017-11-09-.pdf, 2017 [accessed 19 October 2018].

[101] Müller W, Caterpillar JR. Variation of Natural Gas Composition Challenges for Power Generation One powerful future, CIMAC International Council on Combustion Engines,

https://www.cimac.com/cms/upload/events/circles/circle_2014_PowerGen/2_Mueller_CAT_Variation_of_Natural_Gas_Composition_Challenges_V2_final.pdf [accessed 19 October 2018].

[102] U. Kramer, M. Ferrera, H. Künne, D.C. Moreira, I. Magnusson, Natural Gas/Methane Fuels: European Automotive Fuel Quality and Standardization Requirements, http://www.gason.eu/documents/get_doc/90 [accessed 19 October 2018].

[103] D. Puente, F.J. Gracia, I. Ayerdi, Thermal conductivity microsensor for determining the Methane Number of natural gas, Sensors Actuators B Chem. 110 (2005) 181-189.

[104] T.A. Grimley, An overview of the AGA gas quality management, https://asgmt.com/wp-content/uploads/pdf-docs/2012/1/019.pdf [accessed 19 October 2018].

CHAPTER 2 CO_2 CONVERSION TO SYNGAS THROUGH THE STEAM-BIOGAS REFORMING PROCESS

2.1 Abstract

The steam-biogas reforming (SBR) process to convert biogas to a high hydrogen syngas was studied experimentally and using Aspen Plus simulations. An integrated renewable power generation system where the SBR process was coupled with a Solid Oxide Fuel Cell (SOFC) was studied using the Aspen Plus model. The experimental work was conducted over a metal-foam-coated [Pd(7)-Rh(1)]/[$CeZrO_2$(25)-Al_2O_3(75)] catalyst in a Heat Exchanger Platform (HEP) reactor. SBR simulations were conducted for biogas feeds with CH_4/CO_2 ratios of 40/60, 50/50 and 60/40 at S/C ratios of 1.00 to 2.00 over a temperature range of 873 to 1123 K. The experimental data show that positive CO_2 conversion was attainable only at temperatures higher than 1073 K, although the equilibrium based simulation predicts positive CO_2 conversion through most of the operating temperature range. Energy efficiency of the overall system was approximately 40% at temperatures of 948 K and above. Coke formation over the Pd-Rh catalyst was estimated to be 1.05~2.88% of the carbon input to the system. Fresh and used catalysts were characterized by BET adsorption, porosimetry, CO chemisorption and Scanning Electron Microscopy. The results show that the proposed system can provide a viable approach to utilizing distributed renewable methane resources for localized power generation.

2.2 Introduction

The distributed nature of renewable energy sources, particularly carbon based resources, is a major barrier to achieving economically viable utilization. Landfill gas (LFG) and biogas are the primary sources of renewable methane around the world. However, LFG sources are often not developed or are flared due to economic constraints. Of the facilities under operation, most achieve low thermal efficiencies, typically in the range of 20 to 40% with 25% being the most common value [1]. New technology options with improved efficiency but reduced costs are necessary to enable increased utilization.

LFG normally contains 40-60% CO_2 along with moisture and other contaminants. Although gas compositions from different sources vary widely, there are several contaminants and compounds that are commonly found in most LFG streams: sulfur compounds, halogenated compounds, ammonia, silicon compounds and siloxanes, and particulate matter [2]. The contaminants must be removed from the raw LFG during the upgrading process. Technologies for LFG cleanup includes water scrubbing, cryogenic separation, physical absorption, chemical absorption, pressure swing adsorption, membrane separation, in-situ upgrading and biological upgrading methods [2]. Depending on the source of LFG, the energy consumption of the cleanup process is about 0.05~0.15 MJ/MJ LFG [2] which has a significant impact on the net process efficiency.

Converting the CO_2 in the LFG along with CH_4 into syngas (H_2+CO), instead of separating and venting it, can offer multiple benefits that are discussed elsewhere [3]. The research team has experimentally evaluated the combined steam and CO_2 reforming of methane, referred to as ‘bi-reforming’ or Steam Biogas Reforming [3–6]. The chemical reactions

associated with methane reforming are listed below. Since both CH_4 and CO_2 are present in LFG, combined reforming with steam and CO_2 is particularly attractive. The product syngas can be converted into electricity in conventional systems or in a Solid Oxide Fuel Cell (SOFC), as proposed in this study.

SMR: $CH_4 + H_2O \rightarrow 3H_2 + CO$	$\Delta H^\theta = 206.1$ kJ/mol	eq 2-1
WGS: $CO + H_2O \rightarrow H_2 + CO_2$	$\Delta H^\theta = -41.2$ kJ/mol	eq 2-2
DR: $CH_4 + CO_2 \rightarrow 2H_2 + 2CO$	$\Delta H^\theta = 247.3$ kJ/mol	eq 2-3
CH_4 Dehydrogenation: $CH_4 \rightarrow 2H_2 + C$	$\Delta H^\theta = 74.82$ kJ/mol	eq 2-4
SBR reaction: $2CH_4 + H_2O + CO_2 \rightarrow 5H_2 + 3CO$	$\Delta H^\theta = 453.4$ kJ/mol	eq 2-5

The dry reforming (DR) reaction is more energy intensive compared to the well-known steam reforming reaction (SMR) and is prone to coke formation through the CH_4 dehydrogenation reaction. Carbon deposition over the catalyst surface is rapid and inhibits catalyst activity. Steam addition to the dry reforming reaction leads to significant mitigation of coke deposition.

Once the CH_4 is converted to H_2, fuel cells offer an important technology option for power generation in small to medium scale localized projects that do not require expansive infrastructure. Fuel cells are commercially used in a wide range of applications, including but not limited to: medium to large power stations, distributed generation in buildings, small/portable power supply equipment, and auxiliary power units in vehicles [7]. The

degree of hydrogen purity required by fuel cells is dependent on the type of fuel cell and the desired application. Systems with high hydrogen purity requirement are generally not suited for renewable energy projects due to the costs associated with high grade purification. Fuel cells that can tolerate other gas species, especially carbon monoxide, are highly desirable since natural gas reforming produces syngas (H_2+CO) that must be upgraded to pure hydrogen. From this perspective, suitable candidates for such applications include Molten Carbonate Fuel Cells (MCFC) and Solid Oxide Fuel Cells (SOFC). These fuel cells can use H_2 streams with higher CO concentrations and therefore offer the possibility of coupled reforming and fuel cell systems [8]. SOFCs are among the most studied fuel cell options due to their high conversion efficiencies and the potential ability to handle other fuels in addition to H_2 [7,9,10]. Here, we study the conversion of CH_4, CO_2, and steam into a high hydrogen syngas using the 'bi-reforming' reaction in a heat exchanger platform (HEP) reactor. This syngas is then used as the fuel in an SOFC. The energy required for the bi-reforming reaction is supplied by combustion of the SOFC flue gas in alternating compartments of the same HEP reactor.

Steam biogas reforming has been studied using a number of different systems. Galvagno et al., have reported syngas composition from biogas-steam reforming over a wide range of temperatures and pressures using Aspen Plus simulations and over a commercial Ni/Al_2O_3 catalyst [11]. The study also reported that the process thermal efficiency for syngas production through the steam biogas reforming process is between 85 and 95% (efficiency is defined as the ratio of energy out from the reformer to energy in to the reformer) which decreases with increasing temperature. The integration of reforming

systems with fuel cells has also been reported in the literature before [11–14]. Chiodo et al., studied the integration of a reforming reaction process with a fuel cell system and found the fuel utilization rate (rate of conversion of fuel input to the fuel cell into electricity) to be approximately 60 to 85% for SOFCs [12]. They also show that for SOFC fuel utilization rates of 55% or less, the integrated reforming process can be sustained through the heat generated by the SOFC and flue gas combustion. Miyake et al., showed that the syngas produced from biogas reforming over $Ni/LaAl_2O_3$ catalyst is an effective feedstock for the SOFC process [15]. Biogas reforming processes coupled with fuel cell systems studied by Farhad et al., [16] and Trendewicz et al., [17] achieved 42.4% and 51.6% electricity generation efficiency, respectively. Van herle et al., showed that the integrated biogas to electricity process efficiency (for plants under operation in Switzerland) can be in the range of 18-36% with the electrical efficiency of the stack at 42% [18].

Angeli et al., used Ni(10)CeZrLa and Rh(1)CeZrLa steam biogas reforming catalysts to achieve 50% methane conversion at 823 K with a steam to methane ratio of 3.0 [19]. The study reports drop in catalyst performance with high deactivation rates when in use for longer time periods (5% after 55 h). The catalysts performance was poor compared to equilibrium predictions. Process parameters (steam to methane ratio, optimum operating condition) also play an important role in improving efficiency and optimization efforts in lab scale studies are reported in the literature [20-23].

Previously reported experimental data using Pd and Rh based catalysts show that bimetallic combination of catalysts perform better than monometallic catalysts by enhancing syngas selectivity, suppressing coke buildup, and mitigating active metal oxidation [6,24–26].

Also, $CeZrO_2$-modification of Al_2O_3 as catalytic support material leads to improved catalyst activity, thermal stability and metal dispersion, and reduces coke formation resulting from methane reforming [6,27–29].

The Pd, Pt, Rh are among the most activity metals for CH_4 reforming by CO_2 or steam [30]. The rate of reaction for steam methane reforming on Pd, Pt, Rh catalysts are essentially the same [31]. The study also reports the identical rates for the water gas shift reaction. Promoting Ni with Rh, Pt, Pd or Ru, increases to the catalyst activity and lessen the carbon formation than monometallic Ni catalysts [32-35]. Pd is among the rare earth metals that shows highest CO selectivity during the reforming process and resist to hot spot formation inside the reactor [36]. The CO selectivity improves 5 times or more with a small addition of Pd with Ni catalysts [37]. Pd addition prevents the oxidation of the bi-metallic catalysts is essential for steam biogas-reforming reaction [35]. Bradford & Vannice claimed that Pd catalyst do not participate in CH_4 decomposition or oxidation of coke to form CO [38, 39].

Rh is the most active catalyst for methane activation. Fischer and Tropsch [40] reported that the group VIII metals (Ni, Ru, Rh, Pt, Pd, Ir) catalyze the conversion of CH_4 to syngas, and Rh is considered as the most stable group VIII metals for the CH_4 conversion [41]. The bond-order bond-energy conservation analysis suggests that the CH_4 and CO_2 dissociation are much better over Rh [42]. SMR and DR on Rh by thermodynamically consistent microkinetic model claims that CH_4 consumed by pyrolysis and carbon oxidation by OH* ($CH_4 \rightarrow C^* \rightarrow CO^*$) independent of the co-reactant. The co-reactant, either CO_2 or H_2O, supply the oxidizer, OH^* which is enhanced by Rh activity [43, 44].

Rh, the most active component for CH_4, CO_2 activation and Pd is equally active for CH_4 reforming by CO_2 or steam. Rh provides the added benefit of coke removal whereas Pd is better for CO selectivity makes the combination best for dry reforming with high CO selectivity and low syngas ratio.

The effect of Pd-Rh ratio was selected at 7:1 in one of my earlier studies [45]. The Pd/Rh catalyst was tested with Pd, Pd(7)-Rh(1), and Pd(3)-Rh(1) loading. The catalysts were supported on unmodified alumina. [Pd(7)–Rh(1)] catalyst performed better with respect to CH_4 conversion as well as H_2 and CO yields as shown in Figure 2-1 even though Rh loading is higher in [Pd(3)-Rh(1)] catalyst.

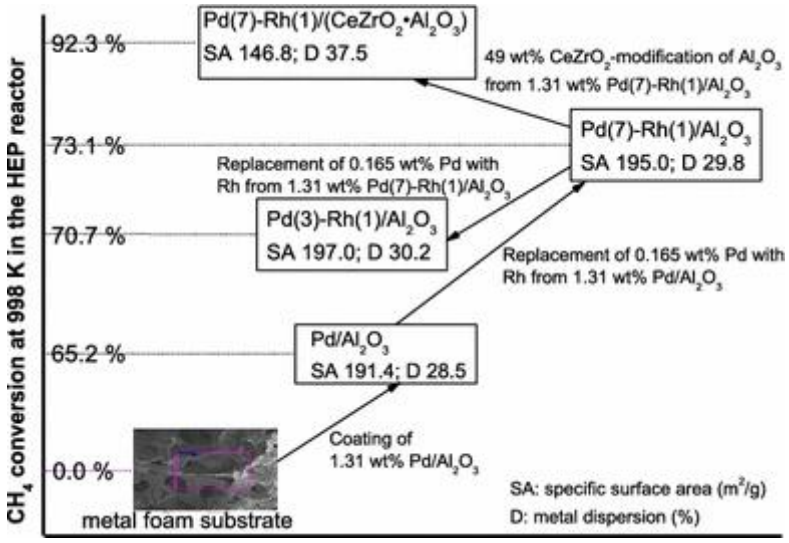

Figure 2-1: The effect of Pd-Rh ratio in steam biogas reforming process [45].

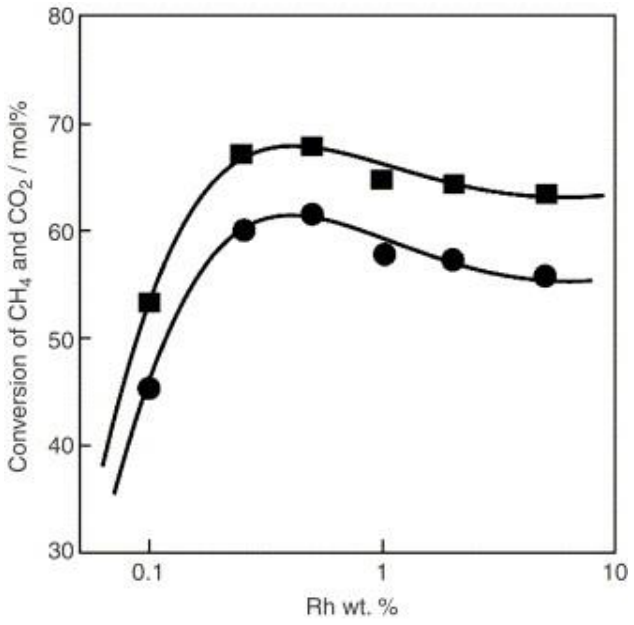

Figure 2-2: Dry reforming feed conversion activity of different loading amounts of Rh [46].

The Rd catalyst loading can lead either increased or decreased feed conversion beyond the optimum loading. The study performed by Hou et. al. reports that there is an optimum Rh loading as shown in Figure 2-2 [46]. The suppression of coke formation compared for Pd, Pd(7)-Rh(1), and Pd(3)-Rh(1) loading in catalyst as shown in Figure 2-3. Therefore, the additional Rh loading from the optimum condition leads to improved coke formation resistance and reduced feed conversion.

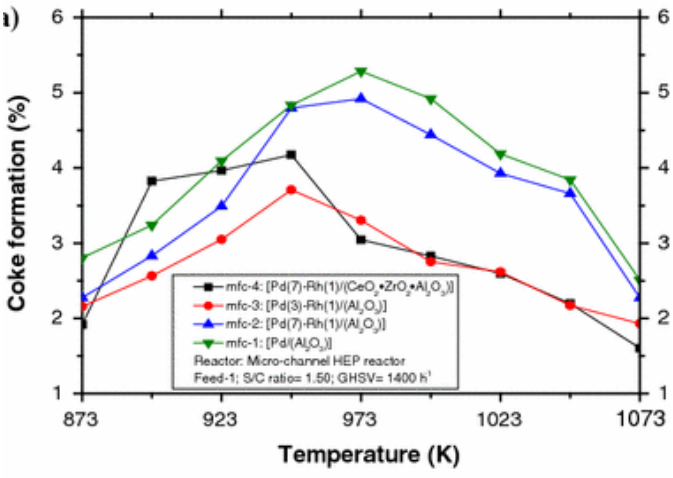

Figure 2-3: Coke formation from the SRB reaction over catalysts with variable Pd-Rh loading ratio [45].

The catalytic support material for reforming reactions study includes SiO_2, La_2O_3, ZrO_2, TiO_2, CeO_2, Al_2O_3, and MgO to minimize the coke formation [39]. The study by Nagaoka and Aika report that the Pd loaded catalyst is very active and selective, but carbon formation results the catalyst deactivation for the dry reforming reaction [47]. The study demonstrated that the addition of Ce or La suppress the coke formation. A small amount of CeO_2 addition with the Pd/Al_2O_3 catalyst reduce the activation energy of steam reforming of CH_4, and improved reaction rates and the oxygen storage capacity significantly participate in coke formation reduction [48]. Pd or Pt dispersion decreases with increasing CeO_2 loading. In a ceria supported catalyst, CH_4 over ceria produce syngas and reduced ceria CeO_{2-n} which react with CO_2 and/or steam to produce CO and H_2 [49]. The study by Dong et. al., over $Ni/Ce_{0.15}Zr_{0.85}O_2$ catalyst reported that the catalyst have two active site in a steam methane reforming: active metal for methane activation, and

active metal and $Ce_xZr_{1-x}O_2$-support for steam [50]. Steam biogas reforming mechanism is bi-functional: CH_4 is activated on the active metal and steam/CO_2 activation on the active metal & catalytic support components. Ozkara-Aydinoglu et al. reported the effect of promoter Ce on Pt/ZrO_2 catalyst [51]. They suggested from spectroscopy (XPS) study that the co-impregnation of Ce adds to the cationic character of active metal which increases the oxygen transfer properties of the catalytic support. The oxygen transfer property makes it more resistant to coke deposition.

The role of ceria-containing CeO_2-Al_2O_3, $Ce_xZr_{1-x}O_2$, and $CeZrO_x$-Al_2O_3 supports are attractive. The ability to store, release, and transfer oxygen species is acquired due to CeO_2 addition, enhance the ability to prevent carbon formation [52]. Pt/$Ce_{0.2}Zr_{0.8}O_2$ attributed to the greater density of oxygen vacancies compared to Pt/ZrO_2 favors coke removal from the surface and provides better stability [53]. Based on the study, CH_4 and CO_2 conversion decreased by steam addition over Pt/ZrO_2 due to significant amount of coke deposition whereas Pt/$Ce_xZr_{1-x}O_2$ is fairly steady even with the steam. Therefore, Ce addition to the catalyst support was performed with the hope that the catalytic support material modification will have significant improvement on CO_2 and steam activation, and coke formation reduction.

Ni-Fe-Cr-Al foams have a high strength and oxidation resistance over the life time High temperature operation [54]. Ni-Fe-Cr-Al metal foam enhance the radial heat transfer by 30% compared to conventional ceramic pellets and reduce the tube wall temperature. The metal foams enhance the reaction rate and decrease the pressure drop and energy cost of the operation [55].

Performance analysis of the integrated reforming and end-use systems is a crucial step in selecting viable approaches and optimizing specific combinations. The steam biogas reforming process combined with a SOFC system represents a potentially viable approach and experimental work has been performed on the catalyst. However, the process has not been studied in detail as an integrated system. There are no reports available in the literature that compare experimental data and simulation results for the proposed system over a range of conditions to identify the preferred operating parameters. This study investigates the performance of the steam-biogas reforming process coupled with SOFC system using a custom built Aspen Plus process model. The simulation results are presented and where relevant, are compared with experimental data obtained over a metal-foam-coated Pd-Rh based catalyst in a compact HEP reactor.

2.3 Simulation and Experimental

2.3.1 Simulation model

Aspen Plus is a well-known simulation tool that has the ability to model complex chemical processes using built-in process units and physical/chemical property databases. An Aspen Plus model of the integrated system consisting of the fuel reformer, combustor and SOFC simulator process blocks was created for this study. The combustor burns the SOFC stack flue gas and provides heat to fuel reformer located in alternating compartments of the heat exchanger platform (HEP) reactor. Stoichiometric reactor blocks are used to simulate the individual components (SOFC, combustor and reformer). Figure 2-4 depicts the process

block diagram of the integrated system. Initially, CH_4, CO_2 and water are mixed and heated up before entering the fuel reformer.

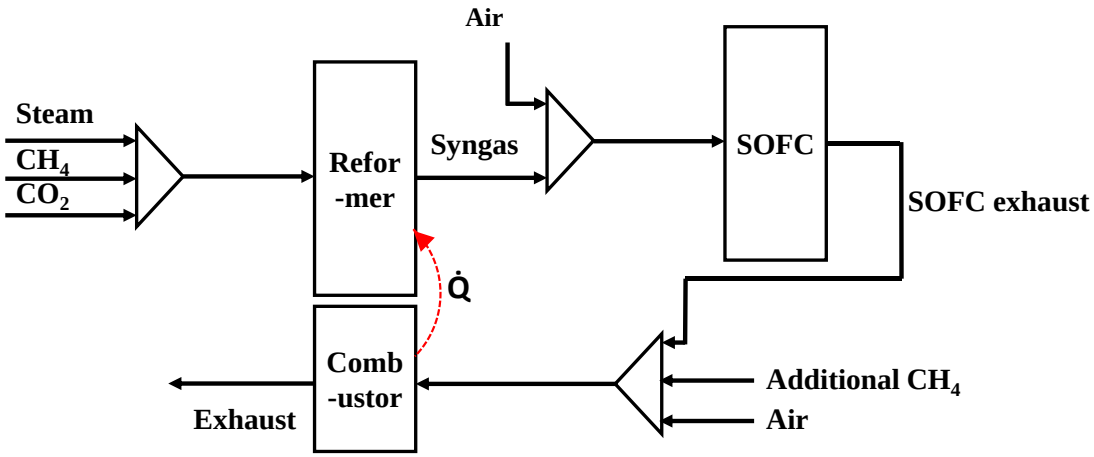

Figure 2-4: Process block diagram for the SOFC-integrated steam-biogas reforming process.

The feed stream is converted to reformate consisting of mostly syngas, which is directed to the fuel cell along with the air needed for the oxidation of H_2 and CO in the SOFC anode. Flue gas from the fuel cell stack is then fed to the combustor coupled with the fuel reformer. The reformer is modeled using a built in equilibrium reactor that uses the Peng-Robinson equation of state. The combustor coupled with the reformer is a stoichiometric reactor that completely burns the combustible components of the SOFC stack flue gas. The simulation model is used to determine all the material and energy stream rates and the compositions. Equilibrium reactant conversion and product distribution for the SBR process were evaluated for biogas feeds having CH_4/CO_2 ratios of 40/60, 50/50 and 60/40. The process was evaluated at steam/CH_4 (S/C) ratios (mole/mole ratio) of 1.00 to 2.00 with 0.25

increments over a temperature range of 873 K to 1123 K. The major assumptions used in the model are:

- Equilibrium is determined through Gibbs free energy minimization.
- Elemental carbon formation is not considered.
- The SOFC converts 70% of H_2 and CO in the reformate gas into electricity.
- SOFC stack flue gas combustion in the HEP reactor uses 40% excess air.
- Additional fuel (CH_4) is supplied to the combustor if needed.

2.3.2 Experimental

2.3.2.1 Catalyst

A supported Pd-Rh catalyst was prepared by coating the metal-oxide composites onto metal foam strips made of Ni-Cr-Al alloy. The catalytic composites were made by loading 1.31 wt% Pd(7)-Rh(1) clusters on $CeZrO_2$-modified Al_2O_3 powder having $CeZrO_2/Al_2O_3$ wt. ratio of 25/75. Catalyst preparation procedure is described in detail elsewhere [5]. The Pd-Rh catalyst was characterized by nitrogen adsorption and porosimetry (Micromeritics, ASAP 2010), CO pulse chemisorption (BEL, BelCat Analyzer) and Scanning Electron Microscope (JEOL, JSM-5610). Physical properties and chemical composition of the Pd-Rh catalyst free of the metal foam substrate are respectively listed in

Table 2-1 and Table 2-2.

Table 2-1: Physical properties of the metal-foam-coated Pd-Rh/($CeZrO_2$-Al_2O_3) catalyst.

BET surface area (m^2/g)	Pore volume (cm^3/g)	Pore size (nm)	Metal dispersion (%)
125.4	0.519	15.0	43.9

Table 2-2: Chemical composition of the catalytic Pd-Rh/($CeZrO_2$-$Al2O_3$) composite wash-coat.

Catalyst	Active metal (wt%)	Oxide (wt%)
Pd-Rh/($CeZrO_2$-Al_2O_3)	Pd-1.15, Rh-0.16	Al_2O_3 74.0, $CeZrO_2$ 24.7

Surface and cross-section SEM images of the metal-foam-coated Pd-Rh catalyst are presented in Figure 2-5. The EDX data for fresh and used catalysts obtained by using a transmission electron spectroscopy (TEM, Hitachi Ltd., H-7600) is taken as an evidence for any coke deposition. Average metal particle size of the catalyst was less than 2.5 nm as calculated from metal dispersion data.

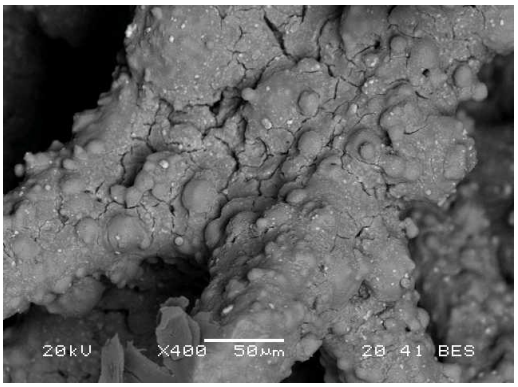

SEM image: catalyst surface

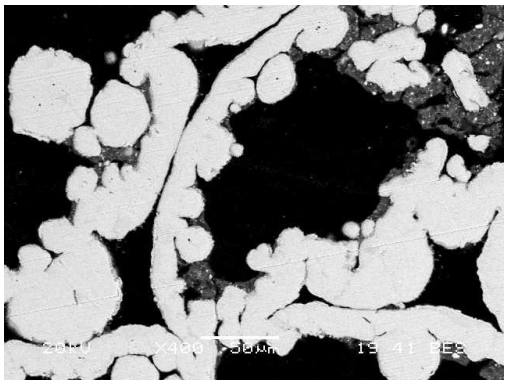

SEM image: catalyst cross-section

Figure 2-5: SEM images of the metal-foam-coated Pd-Rh/($CeZrO_2$-Al_2O_3) catalyst.

2.3.2.2 SBR reaction experiments

Reaction runs were conducted in the multichannel HEP reactor (Catacel/Johnson-Matthey), described in previous articles [5]. Metal-foam-coated Pd-Rh catalyst strips were inserted into the reforming side of the reactor through which the reformer feed stream was passed under atmospheric pressure at GHSV (Gas Hourly Space Velocity) of 1,400 h^{-1}. Several K-type thermocouples installed at different axial positions in the reactor were used to measure the catalyst bed temperature. Combustion side of the HEP reactor was packed with metal-foam-coated catalyst strips prepared by loading Pd-Pt clusters on $CeZrO_2$-modified Al_2O_3 powder. Thermocouples were also installed on the combustion side of the reactor in the same manner as described above. The HEP reactor was enclosed inside a temperature-programmed furnace interfaced with a personal computer. The biogas feeds used in the experimental work consisted of 60% CH_4 and 40% CO_2. Product gas composition from the SBR reaction was analyzed on a dry basis by using a residual gas

analyzer (Cirrus, MKS Technologies). Reaction runs were performed at S/C ratio of 1.50 in the range of 873 K to 1123 K. SBR performances were evaluated using the following equations:

CH_4 conversion = $\left(\frac{(CH_4)_{in}-(CH_4)_{out}}{(CH_4)_{in}}\right)_{reformer}$

CO_2 conversion = $\left(\frac{(CO_2)_{in}-(CO_2)_{out}}{(CO_2)_{in}}\right)_{reformer}$

H_2/CO ratio of the product gas = $\left(\frac{(H_2)_{out}}{(CO)_{out}}\right)_{reformer}$

Overall system efficiency = $\frac{\text{MW of SOFC}}{\text{MJ/s of } CH_{4_{in}} + \text{MJ/s of additional fuel}_{in}}$

Coke formation (%) =

$$\left(\frac{\text{moles of carbon in the feed} - \text{moles of gaseous carbon in the product gas}}{\text{moles of carbon in the reforming feed}}\right)_{reformer}$$

2.4 Results and discussion

2.4.1 Simulation

The SBR process evaluated over a wide range of S/C ratios, temperatures and CH_4/CO_2 ratios using the Aspen Plus simulation model is shown in Figure 2-4. The impact of temperature and S/C ratio on the feed conversion and other performance metrics was studied. Higher CH_4 conversion is expected for the SBR process compared to dry reforming of CH_4 alone. Equilibrium CH_4 conversion obtained were higher than 50% at

873 K for all the S/C ratio used in the study as shown in Figure 2-6. CH_4 conversion increased by 15% when S/C ratio increased from 1.00 to 2.00, and the difference in CH_4 conversion due to S/C ratio attenuated with increase in temperature. For all the S/C ratios studied, CH_4 conversion reached a maximum of 95% at a temperature of 1023 K and was steady above this temperature.

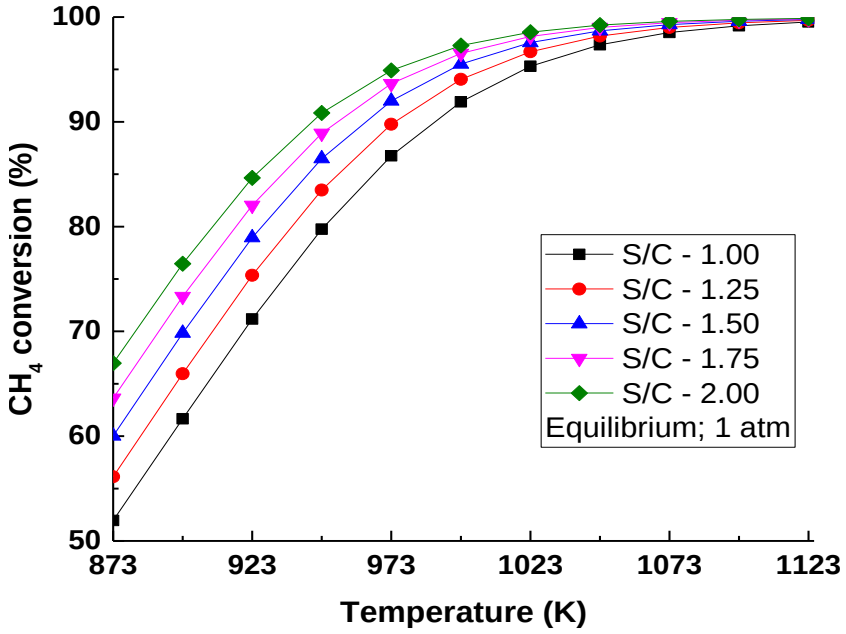

Figure 2-6: SBR CH_4 conversion at equilibrium via simulation (CH_4/CO_2 ratio of 60/40).

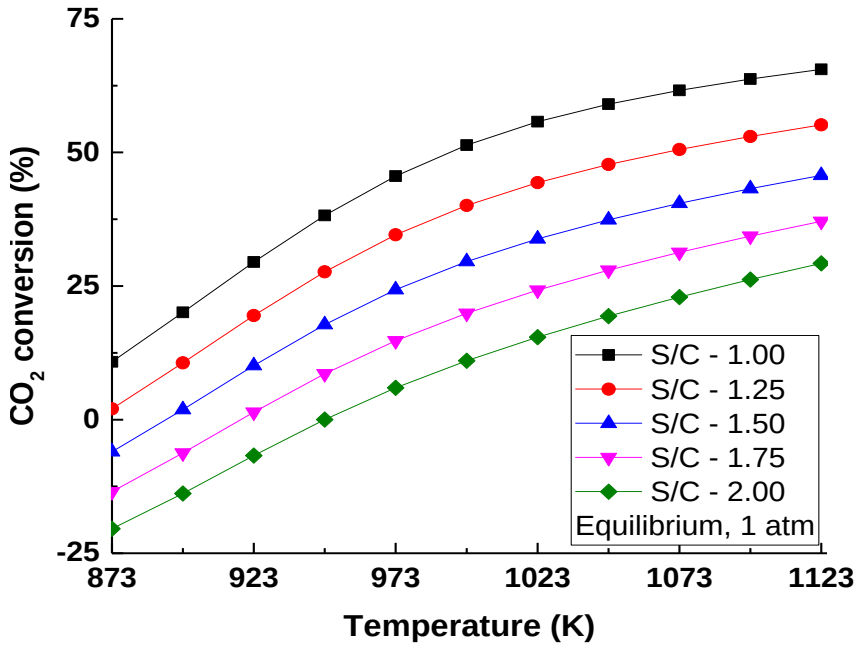

Figure 2-7: SBR CO_2 conversion at equilibrium via simulation (CH_4/CO_2 ratio of 60/40).

Equilibrium CO_2 conversion is negative at some temperatures as shown in Figure 2-7. Negative CO_2 conversion indicates net CO_2 generation by the reforming process which decreases with increasing temperature and decreasing S/C ratio. At 950 K and above, CO_2 conversion becomes positive which implies net CO_2 consumption by the process. Reformer temperatures 1023 K or above represent attractive operating conditions with higher than 90% CH_4 conversion and 25% CO_2 conversion for S/C ratios of 1.50 or less.

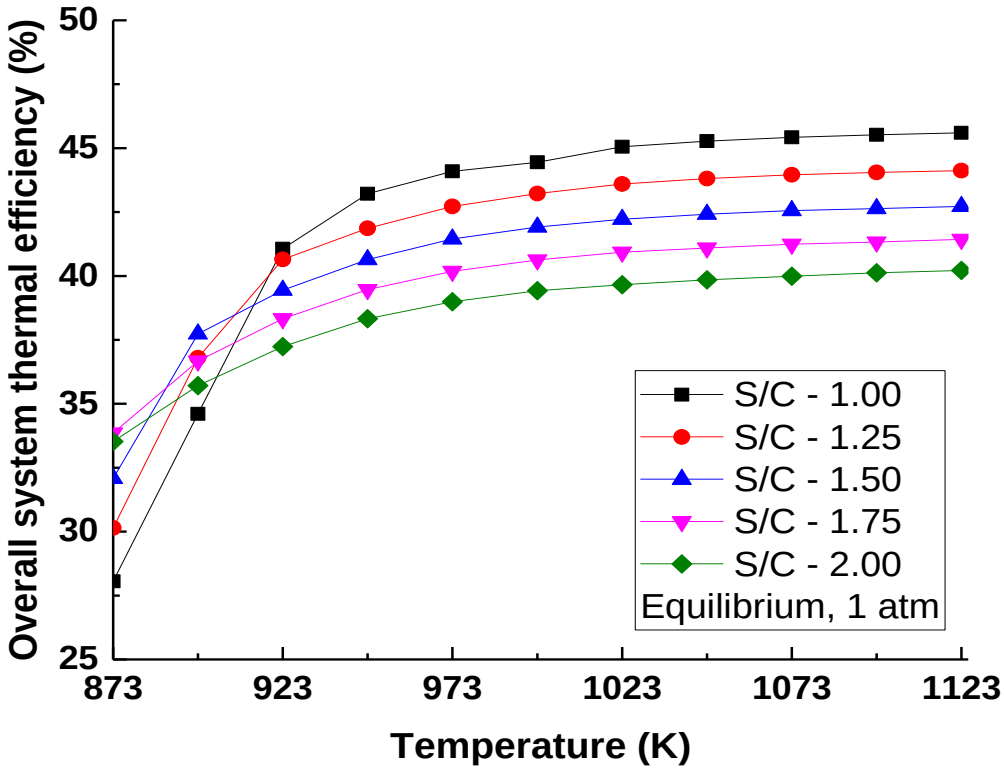

Figure 2-8: Overall system efficiency (%) for the SBR equilibrium process integrated with SOFC for the biogas feed with CH_4/CO_2 ratio of 60/40.

The SBR reaction occurs inside the HEP reactor with CH_4 being the only energy containing species in the reformer feed. H_2 and CO from the reformer are sent to the SOFC whereas the unreacted CH_4 is supplied back to the combustor located inside the HEP reactor. Heat supply is necessary for the SBR reactions, steam generation and feed pretreatment. All the heat required for the reformer is supplied by the combustion of the unreacted CH_4 from the reformer, H_2 and CO unused by the SOFC and additional fuel in form of CH_4 if needed. Figure 2-8 shows the overall system efficiency for different S/C ratios as a function of temperature. The efficiency initially increases with temperature and stabilizes at

approximately 1023 K. At lower temperatures, higher S/C ratio leads to higher CH_4 conversions as well as increased syngas production and SOFC output.

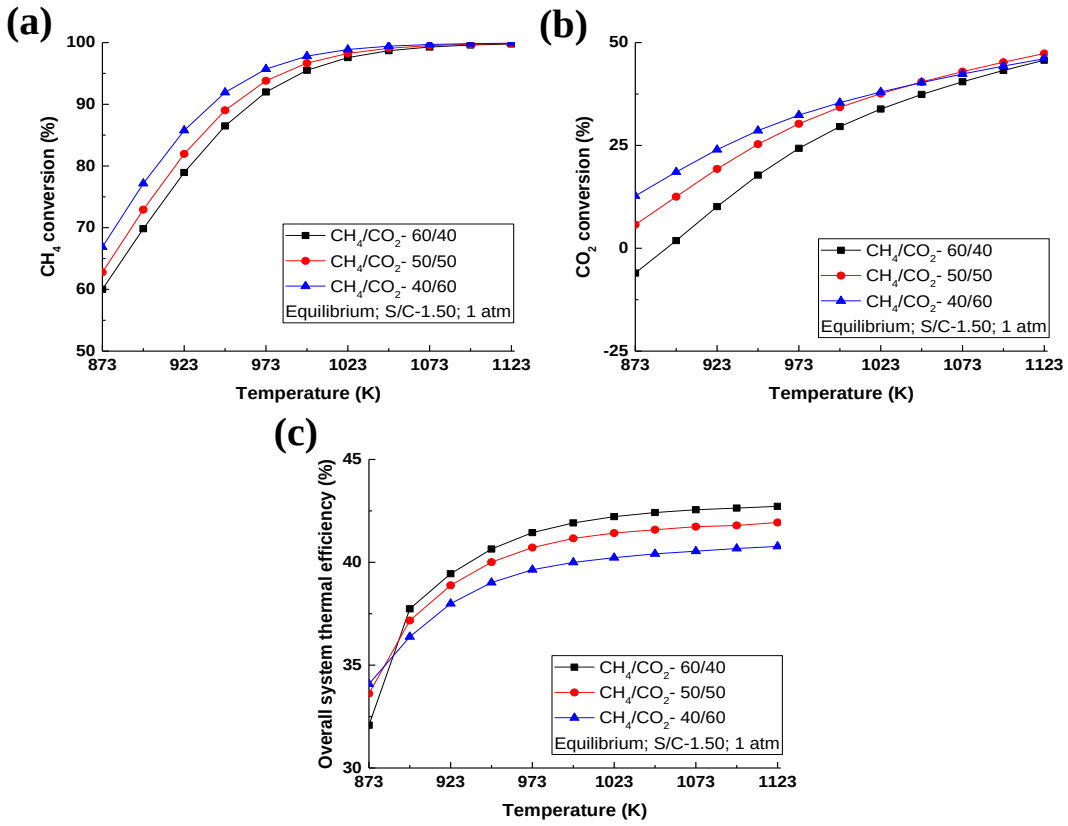

Figure 2-9: SBR equilibrium performance for biogas feed with different CH_4/CO_2 ratios: (a) CH_4 conversion; (b) CO_2 conversion; (c) overall system efficiency.

CH_4/CO_2 ratio is often dependent on the biogas source and is also varied to check the process performance. S/C is maintained at 1.50 at atmospheric pressure while checking the

effect of CH_4/CO_2 ratio on process performance. CH_4 conversion increases with decreasing CH_4 concentration in the feed, and at temperatures above 1073 K CH_4 conversion is mostly independent of the feed composition as shown in Figure 2-9 (a). A similar trend can be observed for CO_2 conversion, as shown in Figure 2-9 (b). Overall system efficiency increases with increasing CH_4/CO_2 ratio as shown in Figure 2-9 (c).

2.4.2 Catalytic SBR comparison with simulation results

The metal foam supported catalysts, Pd-Rh/Al_2O_3 modified with $CeZrO_2$, demonstrated better performance for steam biogas reforming process during earlier studies [6]. Based on the previously reported experimental results, [Pd(7)-Rh(1)/$CeZrO_2$(25)-Al_2O_3(75)] was selected as the reforming catalyst for this study. The equilibrium data obtained by Aspen Plus process simulation is compared with the experimental data.

Experimental CH_4 conversion is lower than the equilibrium value over the entire temperature range studied as shown in Figure 2-10. A similar trend for CH_4 conversion has been reported in the literature [56, 57]. Above 1000 K, the conversion is independent of temperature and the gap between experimental and equilibrium data is also attenuated. The experimental CO_2 conversion data show significant deviation from the equilibrium values. CO_2 conversion also increases with temperature and the trend has been observed previously [57].

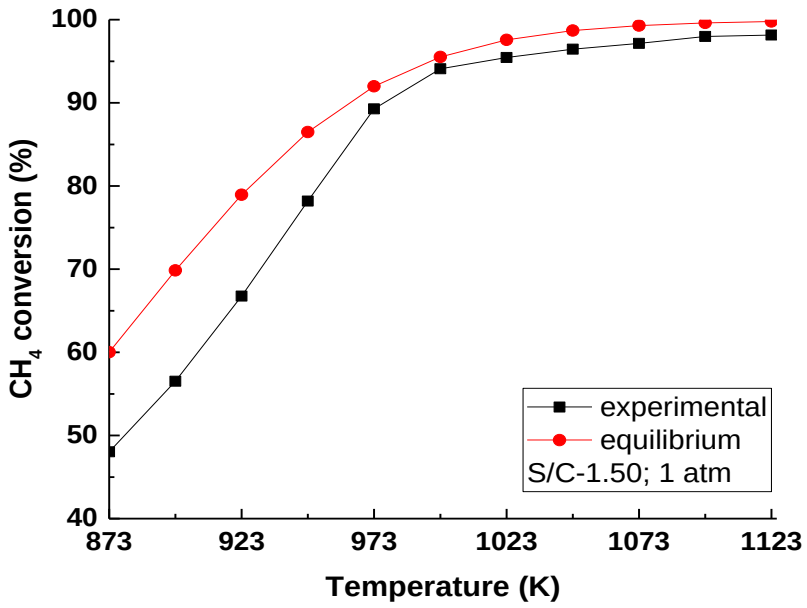

Figure 2-10: CH_4 conversion (%) compared between SBR equilibrium simulation and experimental results for the biogas feed with CH_4/CO_2 ratio of 60/40.

The CO_2 is produced by WGS reaction and consumed by both DR and Reverse WGS (RWGS). The WGS reaction thermodynamics is favored at relatively low temperatures whereas RWGS is favored over a higher temperature range [58]. Moreover, CO_2 conversion by dry reforming also increases with an increase in temperature. In this experimental study, at temperatures below 1073 K, net CO_2 consumption is not attained due to the WGS reaction dominating; this changes at temperatures of 1073 K and above.

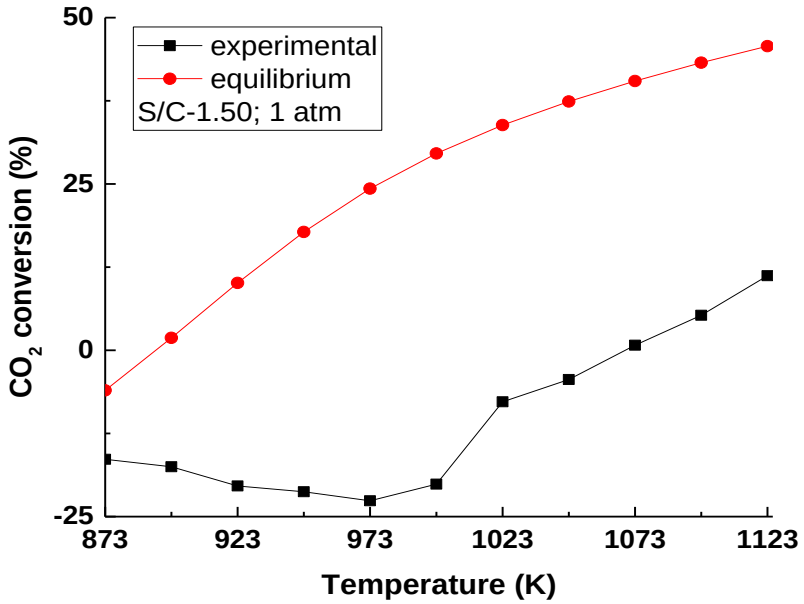

Figure 2-11: CO_2 conversion (%) compared between SBR equilibrium simulation and experimental results for the biogas feed with CH_4/CO_2 ratio of 60/40.

The difference between equilibrium and experimental data for CO_2 consumption is shown in Figure 2-11 and a similar trend was observed by Ashrafi et. al., [56]. They reported that the equilibrium CO_2 conversion decreases with S/C ratio at S/C ratios of 2.00 or higher. Their reported equilibrium CO_2 conversion data at S/C ratio of 2.71 ranged from -37% to 5% in the temperature range of 873 K to 1123 K whereas experimental CO_2 conversion ranged from about -27% to 10% in the same temperature zone which is comparable with this study.

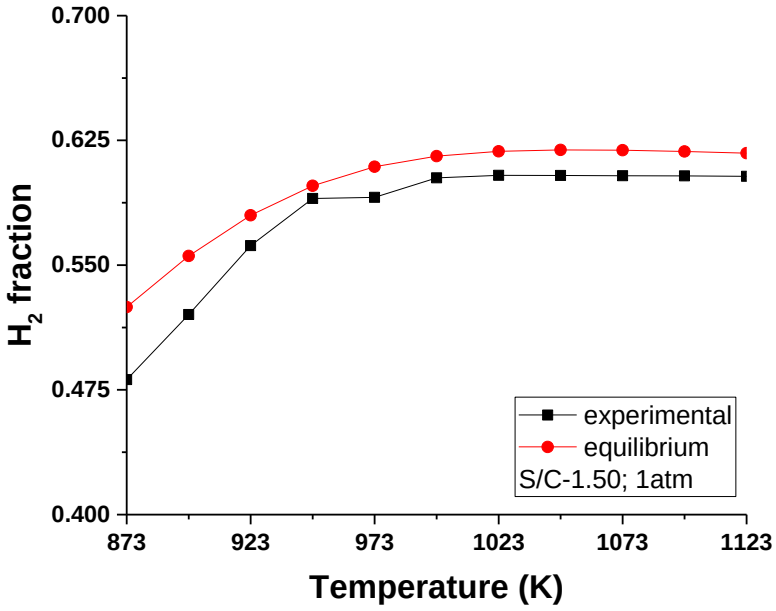

Figure 2-12: H_2 fraction of product syngas compared between SBR equilibrium simulation and experimental results for the biogas feed with CH_4/CO_2 ratio of 60/40.

Figure 2-12 compares the variation of experimental and equilibrium H_2 fractions in syngas (excluding steam in calculation) with temperature. The experimental values align well with the equilibrium predicted product gas hydrogen fraction. The experimental H_2/CO ratios, however, are noticeably higher than the equilibrium predicted values (Figure 2-13). Experimental CH_4 conversions and H_2 fractions are close to the equilibrium values whereas CO_2 conversions are significantly lower than the equilibrium values. This indicates that the steam reforming reaction dominates the dry reforming reaction in the experiments and suggests water gas shift activity. The trend and the H_2/CO ratio values obtained are similar to the values reported in earlier studies [56]. High H_2/CO ratio (H_2 rich syngas) is preferred for the SOFC as H_2 is the major feedstock for electrochemical processes.

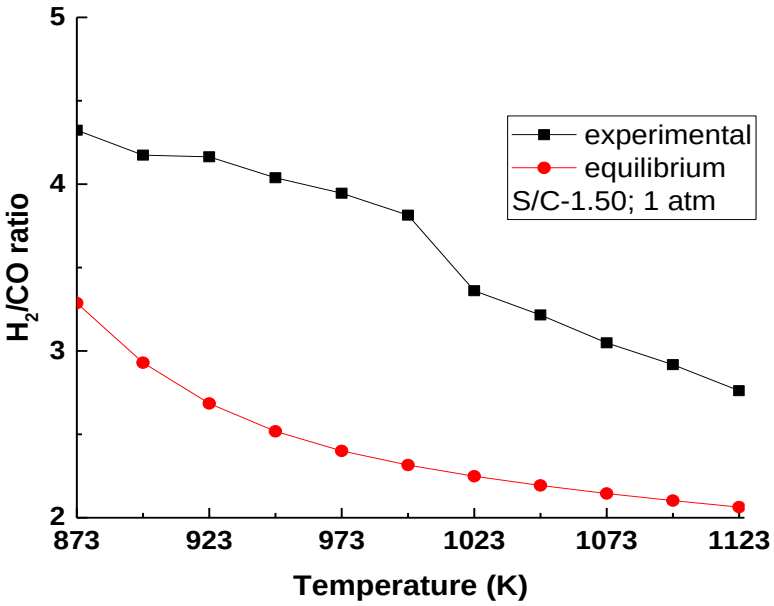

Figure 2-13: H_2/CO ratio of product syngas compared between SBR equilibrium simulation and experimental results for the biogas feed with CH_4/CO_2 ratio of 60/40.

Details of the HEP reactor system coupled with the SOFC as well as the overall system efficiency calculations are shown in Figure 2-14. The sample calculation is based on SBR experimental results over the metal foam coated catalyst at 1023 K and 1 atm. with an S/C ratio of 1.50.

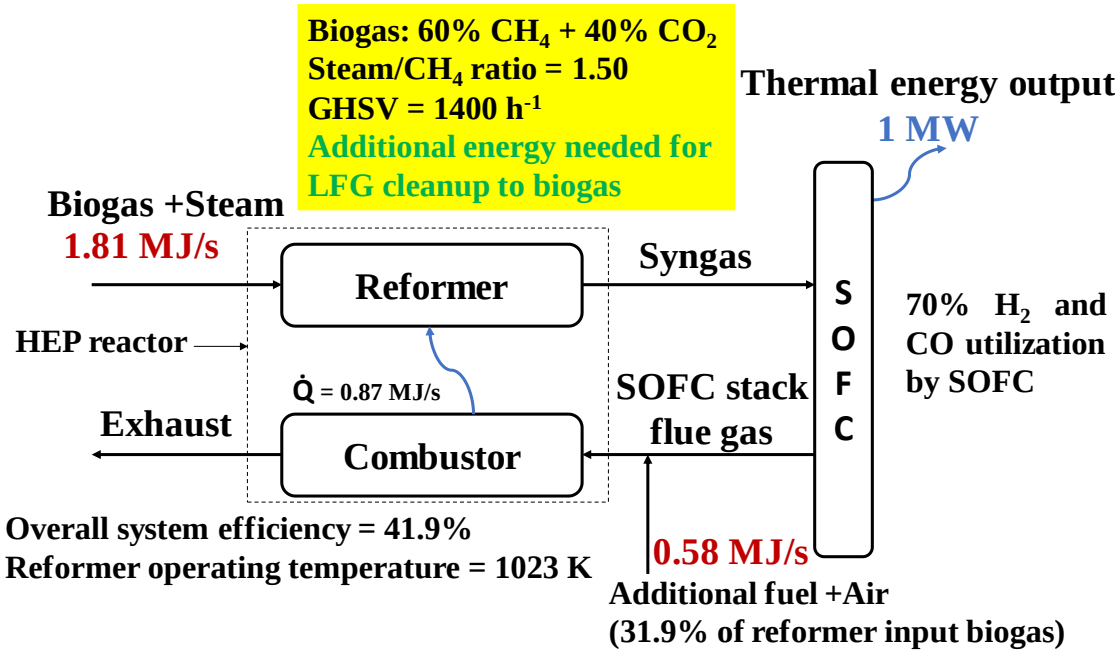

Figure 2-14: A schematic process flow diagram for calculating the overall efficiency of the integrated SBR and SOFC system.

The higher the CH_4 conversion the lower the CH_4 concentration in the SOFC exhaust and thus necessitates additional fuel supply to the combustor. Higher operating temperatures lead to higher CH_4 conversion and improved overall system efficiency as shown in Figure 2-15. Once the overall system efficiency is above 40%, it does not increase significantly with increasing temperature. At temperatures above 973 K there are no significant differences between the equilibrium and experimentally predicted system efficiencies, making this the minimum preferable operating temperature.

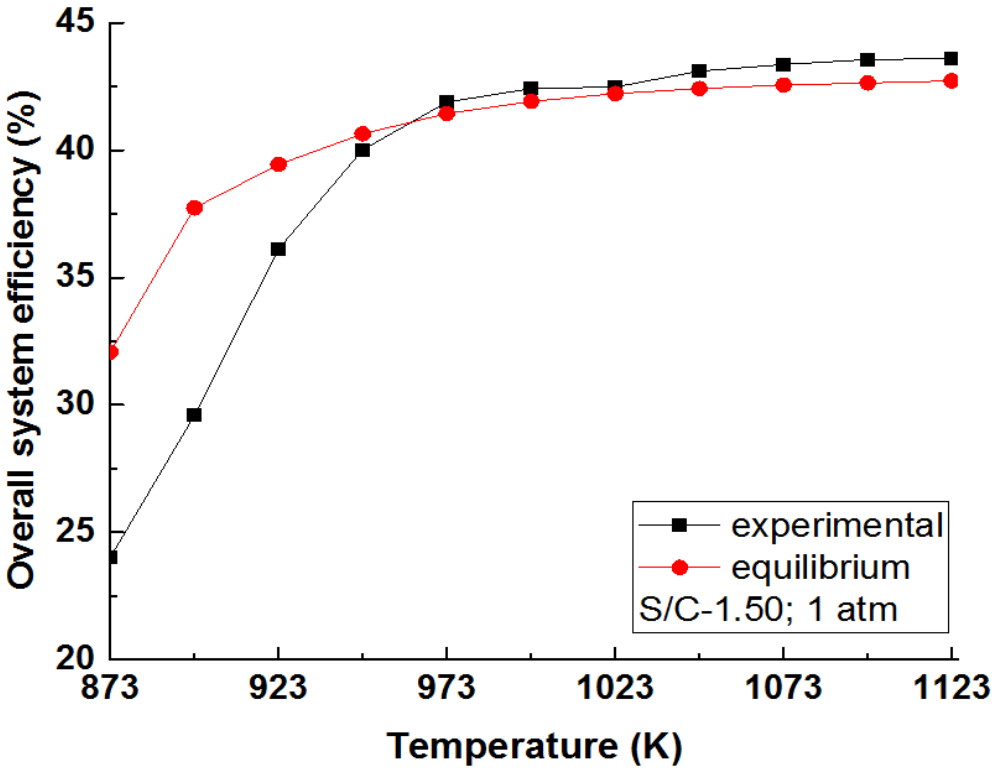

Figure 2-15: Overall system efficiency (%) compared between SBR equilibrium simulation and experimental results for the biogas feed with CH_4/CO_2 ratio of 60/40.

Table 2-3: Coke formation (%) from the SBR reaction over the Pd-Rh catalyst. (Coke formation percentage was evaluated based on carbon balance by subtracting the carbon in the product gases from the carbon in biogas feed.)

Temperature (K)	923	948	973	998	1023	1048	1073	1098	1123
Coke formation (%)	1.05	1.24	1.63	1.98	2.16	2.44	2.88	2.31	2.20

Data shown in Table 2-3 presents the coke formation from steam-biogas reforming process. There are no comparable studies reported in the literature on coke formation during the SBR process. The observed coke deposition is significantly lower than during the dry

reforming process, which is expected. Coke accumulation in this study increases with temperature until 1073 K and decreases at higher temperatures and comparable with our previous study [3]. The catalyst was checked with Energy-dispersive X-ray spectroscopy (EDX) data for coke formation evidence and the results are shown in Figure 2-16.

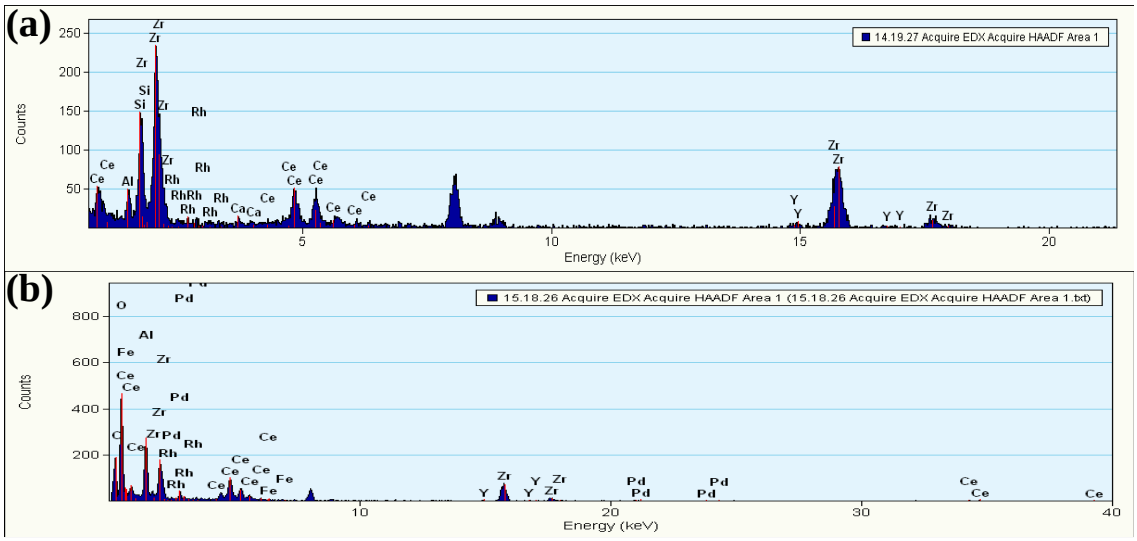

Figure 2-16: EDX data for the fresh (a) and used (b) catalyst as an evidence for coke formation.

The EDX data shows no coke existence in the fresh catalyst and evidence of coke deposition in the used catalyst. The significantly reduced coke deposition compared to literature data can be attributed to $CeZrO_2$ modification of the catalyst by the following mechanism [59].

$CH_4 \rightarrow C + 2H_2$; $C + CeZrO_2 \rightarrow CO + CeZrO_{(2-x)}$; $CO_2/H_2O + CeZrO_{(2-x)} \rightarrow CO/H_2 + CeZrO_2$

2.5 Conclusions

A renewable energy system to produce electricity from biogas feed by integrating the SBR process with an SOFC was evaluated through experimental and modeling study. The system performance was evaluated using the Aspen Plus process simulation tool and through SBR experiments over a metal-foam-coated 1.31 wt% [Pd(7)-Rh(1)]/[$CeZrO_2$(25)-Al_2O_3(75)] catalyst. The results of this study are summarized below:

1. For biogas feeds with CH_4/CO_2 ratios of 40/60, 50/50 and 60/40, and S/C ratio of 1.00 to 2.00, higher than 90% CH_4 conversion and net positive CO_2 conversion were attainable at temperatures of 1073 K and above under atmospheric pressure. The overall system efficiency increased with decreasing S/C ratios at temperatures of 923 K and above.

2. For S/C ratio of 1.50, the overall system efficiency increased with increasing CH_4 concentration in biogas feed whereas CH_4 and CO_2 conversions increased with decreasing CH_4 concentration in biogas feed.

3. For the biogas feed with CH_4/CO_2 ratio of 60/40 and at S/C ratio of 1.50, experimental CH_4 conversion was comparable with the equilibrium value at 973 K and above whereas experimental CO_2 conversion was much less than the equilibrium value throughout the temperature range tested: net positive CO_2 conversion was achieved only at 1073 K and above.

4. For the biogas feed composition and S/C ratio described above, experimental H_2/CO ratio of product syngas was greater than the equilibrium value throughout the temperature

range tested due to WGS reaction effect. The integrated system can achieve energy efficiency values of 40% or higher at reformer temperatures of 948 K and above.

5. Coke formation (%) from the SBR process in this work is estimated to be 1.05~2.88% of the carbon input to the system and is comparable with our previous study.

Acknowledgements

This work was supported by the California Energy Commission through Energy Innovation Small Grant No. 57825A/13-08G. Kiseok Kim is grateful to Yeungnam University for the 2015 Research Abroad Grant. Authors acknowledge contributions by Kyle Hunter, Vincent Van, Annie Chang and Sean Franco.

2.6 References

[1] US EPA, Landfill Gas Energy Project Data and Landfill Technical Data. https://www.epa.gov/lmop/landfill-Gas-Energy-Project-Data-and-Landfill-Technical-Data#states, 2016 [accessed December 7, 2016].

[2] Q. Sun, H. Li, J. Yan, L. Liu, Z. Yu, X. Yu, Selection of appropriate biogas upgrading technology-a review of biogas cleaning, upgrading and utilisation, Renew. Sust. Energy Rev. 51 (2015) 521-532.

[3] P.S. Roy, C.S. Park, A.S.K. Raju, K. Kim, Steam-biogas reforming over a metal-foam-coated (Pd-Rh)/($CeZrO_2$-Al_2O_3) catalyst compared with pellet type alumina-supported Ru and Ni catalysts, J. CO2 Util. 12 (2015) 12-20.

[4] P.S. Roy, A.S.K. Raju, K. Kim, Influence of S/C ratio and temperature on steam reforming of model biogas over a metal-foam-coated Pd-Rh/($CeZrO_2$-Al_2O_3) catalyst, Fuel 139 (2015) 314-320.

[5] P.S. Roy, N.-K. Park, K. Kim, Metal foam-supported Pd-Rh catalyst for steam methane reforming and its application to SOFC fuel processing, Int. J. Hydrogen Energy 39 (2014) 4299-4310.

[6] P.S. Roy, M.S. Kang, K. Kim, Effects of Pd-Rh Composition and $CeZrO_2$-Modification of Al_2O_3 on Performance of Metal-Foam-Coated Pd-Rh/Al_2O_3 Catalyst for Steam Reforming of Model Biogas, Catal. Letters. 144 (2014) 2021-2032.

[7] H.J. Alves, C. Bley Junior, R.R. Niklevicz, E.P. Frigo, M.S. Frigo, C.H. Coimbra-Araújo, Overview of hydrogen production technologies from biogas and the applications in fuel cells, Int. J. Hydrogen Energy 38 (2013) 5215-5225.

[8] D. Hotza, J.C. Diniz da Costa, Fuel cells development and hydrogen production from renewable resources in Brazil, Int. J. Hydrogen Energy 33 (2008) 4915-4935.

[9] J. Xuan, M.K.H. Leung, D.Y.C. Leung, M. Ni, A review of biomass-derived fuel processors for fuel cell systems, Renew. Sustain. Energy Rev. 13 (2009) 1301-1313.

[10] A. Naidja, C.R. Krishna, T. Butcher, D. Mahajan, Cool flame partial oxidation and its role in combustion and reforming of fuels for fuel cell systems, Prog. Energy Combust. Sci. 29 (2003) 155-191.

[11] A. Galvagno, V. Chiodo, F. Urbani, F. Freni, Biogas as hydrogen source for fuel cell applications, Int. J. Hydrogen Energy 38 (2013) 3913-3920.

[12] V. Chiodo, A. Galvagno, A. Lanzini, D. Papurello, F. Urbani, M. Santarelli, S. Freni, Biogas reforming process investigation for SOFC application, Energy Convers. Manag. 98 (2015) 252-258.

[13] J. Staniforth, K. Kendall, Biogas powering a small tubular solid oxide fuel cell, J. Power Sources. 71 (1998) 275-277.

[14] Y. Takahashi, Y. Shiratori, S. Furuta, K. Sasaki, Thermo-mechanical reliability and catalytic activity of Ni-Zirconia anode supports in internal reforming SOFC running on biogas, Solid State Ionics. 225 (2012) 113-117.

[15] M. Miyake, M. Iwami, K. Goto, K. Iwamoto, K. Morimoto, M. Shiraishi, K. Takatori, M. Takeuchi, S. Nishimoto, Y. Kameshima, Intermediate-temperature solid oxide fuel cell employing reformed effective biogas: Power generation and inhibition of carbon deposition, J. Power Sources 340 (2017) 319-324.

[16] S. Farhad, F. Hamdullahpur, Y. Yoo, Performance evaluation of different configurations of biogas-fuelled SOFC micro-CHP systems for residential applications, Int. J. Hydrogen Energy 35 (2010) 3758-3768.

[17] A.A. Trendewicz, R.J. Braun, Techno-economic analysis of solid oxide fuel cell-

based combined heat and power systems for biogas utilization at wastewater treatment facilities, J. Power Sources 233 (2013) 380-393.

[18] J. Van herle, Y. Membrez, O. Bucheli, Biogas as a fuel source for SOFC co-generators, J. Power Sources 127 (2004) 300-312.

[19] S.D. Angeli, L. Turchetti, G. Monteleone, A.A. Lemonidou, Catalyst development for steam reforming of methane and model biogas at low temperature, Appl. Catal. B Environ. 181 (2016) 34-46.

[20] J.D. Silva, C.A.M. de Abreu, Modelling and simulation in conventional fixed-bed and fixed-bed membrane reactors for the steam reforming of methane, Int. J. Hydrogen Energy 41(2016) 11660-11674.

[21] X. Chen, J. Jiang, K. Li, S. Tian, F. Yan, Energy-efficient biogas reforming process to produce syngas: The enhanced methane conversion by O2, Appl. Energy 185 (2017) 687-697.

[22] C.E. Tuna, J.L. Silveira, M.E. da Silva, R.M. Boloy, L.B. Braga, N.P. Pérez, Biogas steam reformer for hydrogen production: Evaluation of the reformer prototype and catalysts, Int. J. Hydrogen Energy 43 (2017) 2108-2120.

[23] G. Nahar, D. Mote, V. Dupont, Hydrogen production from reforming of biogas: Review of technological advances and an Indian perspective, Renew. Sustain. Energy Rev. 76 (2017) 1032-1052.

[24] D. Pakhare, J. Spivey, A review of dry (CO 2) reforming of methane over noble metal catalysts, Chem. Soc. Rev. 43 (2014) 7813-7837.

[25] R.B. Duarte, M. Olea, E. Iro, T. Sasaki, K. Itako, J.A. van Bokhoven, Transient Mechanistic Studies of Methane Steam Reforming over Ceria-Promoted Rh/Al_2O_3 Catalysts, ChemCatChem 6 (2014) 2898-2903.

[26] V. Dal Santo, A. Gallo, A. Naldoni, M. Guidotti, R. Psaro, Bimetallic heterogeneous catalysts for hydrogen production, Catal. Today 197 (2012) 190-205.

[27] C. Berger-Karin, S. Wohlrab, U. Rodemerck, E. V. Kondratenko, The tremendous effect of trace amounts of Rh on redox and catalytic properties of CeO_2-TiO_2 and Al_2O_3 in CH_4 partial oxidation, Catal. Commun. 18 (2012) 121-125.

[28] C. Bozo, F. Gaillard, N. Guilhaume, Characterisation of ceria–zirconia solid solutions after hydrothermal ageing, Appl. Catal. A Gen. 220 (2001) 69-77.

[29] M.M.V.M. Souza, M. Schmal, Methane Conversion to Synthesis Gas by Partial Oxidation and CO_2 Reforming over Supported Platinum Catalysts, Catal. Letters 91 (2003) 11-17.

[30] M. Masai, H. Kado, A. Miyake, S. Nishiyama, S. Tsuruya, Methane reforming by carbon dioxide and steam over supported Pd, Pt, and Rh catalysts, In Studies in Surface Science and Catalysis 36 (1988) 67-71. Elsevier.

[31] R. Craciun, B. Shereck, R.J. Gorte, Kinetic studies of methane steam reforming on ceria-supported Pd, Catal. Letters 51 (1988) 149-153.

[32] Z. Hou, T. Yashima, Small amounts of Rh-promoted Ni catalysts for methane reforming with CO2, Catal. Letters 89 (2003), 193-197.

[33] M. García-Diéguez, I.S. Pieta, M.C. Herrera, M.A. Larrubia, L.J. Alemany, RhNi nanocatalysts for the CO2 and CO2+ H2O reforming of methane. Catal. Today 172 (2011) 136-142.

[34] B. Pawelec, S. Damyanova, K. Arishtirova, J.L.G. Fierro, L. Petrov, Structural and surface features of PtNi catalysts for reforming of methane with CO2, Appl. Catal. A Gen. 323 (2007) 188-201.

[35] B. Steinhauer, M.R. Kasireddy, J. Radnik, A. Martin, Development of Ni-Pd bimetallic catalysts for the utilization of carbon dioxide and methane by dry reforming, Appl. Catal. A Gen. 366 (2009) 333-341.

[36] Y. Mukainakano, B. Li, S. Kado, T. Miyazawa, K. Okumura, T Miyao, K. Tomishige, Surface modification of Ni catalysts with trace Pd and Rh for oxidative steam reforming of methane, Appl. Catal. A Gen. 318 (2007) 252-264.

[37] M. Nurunnabi, Y. Mukainakano, S. Kado, T. Miyazawa, K. Okumura, T Miyao, K. Tomishige, Oxidative steam reforming of methane under atmospheric and pressurized conditions over Pd/NiO–MgO solid solution catalysts. Appl. Catal. A Gen. 308 (2006) 1-12.

[38] M.C. Bradford, M.A. Vannice, The role of metal-support interactions in CO2 reforming of CH4, Catal. Today 50 (1999) 87-96.

[39] D. Pakhare, J. Spivey, A review of dry (CO2) reforming of methane over noble metal catalysts, Chem. Soc. Rev. 43 (2014) 7813-7837.

[40] F. Fisher, H. Tropsch, Conversion of methane into hydrogen and carbon monoxide, Brennst.-Chem. (1928) 9.

[41] J. Wei, E. Iglesia, Structural requirements and reaction pathways in methane activation and chemical conversion catalyzed by rhodium, J Catal. 225 (2004) 116-127.

[42] M.J. Hei, H.B. Chen, J. Yi, Y.J. Lin, Y.Z. Lin, G. Wei, D.W. Liao, CO2-reforming of methane on transition metal surfaces, Surf. Sci. 417 (1998) 82-96.

[43] M. Maestri, D.G. Vlachos, A. Beretta, G. Groppi, E. Tronconi, Steam and dry reforming of methane on Rh: Microkinetic analysis and hierarchy of kinetic models, J. Catal. 259 (2008) 211-222.

[44] J.R. Rostrupnielsen, J.B. Hansen, CO2-reforming of methane over transition metals, J. Catal. 144 (1993) 38-49.

[45] P.S. Roy, M.S. Kang, K. Kim, Effects of Pd–Rh Composition and CeZrO2-Modification of Al2O3 on Performance of Metal-Foam-Coated Pd–Rh/Al2O3 Catalyst for Steam Reforming of Model Biogas, Catal. Letters 144 (2014) 2021-2032.

[46] Z. Hou, P. Chen, H. Fang, X. Zheng, T. Yashima, Production of synthesis gas via methane reforming with CO2 on noble metals and small amount of noble-(Rh-) promoted Ni catalysts, Int. J. Hydrogen Energy 31 (2006) 555-561.

[47] K. Nagaoka, K. Aika, Effect of additives on the stability of Pd/Al2O3 for carbon dioxide reforming of methane, Bulletin Chem. Soc. Japan 74 (2001) 1841-1846.

[48] L.S.F. Feio, C.E. Hori, S. Damyanova, F.B. Noronha, W.H. Cassinelli, C.M.P. Marques, J.M.C. Bueno, The effect of ceria content on the properties of Pd/CeO2/Al2O3 catalysts for steam reforming of methane, Appl. Catal. A Gen. 316 (2007) 107-116.

[49] M.H. Halabi, M.H.J.M. De Croon, J. Van der Schaaf, P.D. Cobden, J.C. Schouten, Low temperature catalytic methane steam reforming over ceria–zirconia supported rhodium, Appl. Catal. A Gen. 389 (2010) 68-79.

[50] W.S. Dong, H.S. Roh, K.W. Jun, S.E. Park, Y.S. Oh, Methane reforming over Ni/Ce-ZrO2 catalysts: effect of nickel content, Appl. Catal. A Gen. 226 (2002) 63-72.

[51] M. García-Diéguez, I.S. Pieta, M.C. Herrera, M.A. Larrubia, L.J. Alemany, Improved Pt-Ni nanocatalysts for dry reforming of methane, Appl. Catal. A Gen. 377 (2010) 191-199.

[52] P. Van Beurden, On the catalytic aspects of steam-methane reforming. Energy Research Centre of the Netherlands (ECN), Technical Report I-04-003 (2004).

[53] F.B. Noronha, A. Shamsi, C. Taylor, E.C. Fendley, S. Stagg-Williams, D.E Resasco, Catalytic performance of Pt/ZrO2 and Pt/Ce-ZrO2 catalysts on CO2 reforming of CH4 coupled with steam reforming or under high pressure, Catal. Letters 90 (2003) 13-21.

[54] G. Walther, U. Gaitzsch, T. Büttner, B. Kieback, T. Weißgärber, R. Kolvenbach, M. Lincke, Applications of Metal Foam as Catalyst Carrier.

[55] S.T. Kolaczkowski, S. Awdry, T. Smith, D. Thomas, L. Torkuhl, R. Kolvenbach, Potential for metal foams to act as structured catalyst supports in fixed-bed reactors, Catal. Today 273 (2016) 221-233.

[56] M. Ashrafi, T. Pröll, C. Pfeifer, H. Hofbauer, Experimental Study of Model Biogas Catalytic Steam Reforming: 1. Thermodynamic Optimization, Energy & Fuels 22 (2008) 4182-4189.

[57] D.G. Avraam, T.I. Halkides, D.K. Liguras, O.A. Bereketidou, M.A. Goula, An experimental and theoretical approach for the biogas steam reforming reaction, Int. J. Hydrogen Energy 35 (2010) 9818-9827.

[58] V. Choudhary, B.. Uphade, A. Mamman, Simultaneous steam and CO2 reforming of methane to syngas over NiO/MgO/SA-5205 in presence and absence of oxygen, Appl. Catal. A Gen. 168 (1998) 33-46.

[59] H.-S. Roh, H.S. Potdar, K.-W. Jun, Carbon dioxide reforming of methane over co-precipitated Ni–CeO2, Ni–ZrO2 and Ni–Ce–ZrO2 catalysts, Catal. Today 93 (2004) 39-44.

CHAPTER 3 EFFECTS OF $CEZRO_2$-AL_2O_3 SUPPORT COMPOSITION OF METAL-FOAM-COATED PD-RH CATALYSTS FOR THE STEAM-BIOGAS REFORMING REACTION

3.1 Abstract

Biogas conversion to syngas by steam reforming was studied over metal-foam-coated Pd-Rh catalysts with variable $CeZrO_2$-Al_2O_3 support compositions. Catalysts with a higher $CeZrO_2/Al_2O_3$ ratio exhibited greater CH_4 and CO_2 conversions and higher H_2/CH_4 yields, while displaying lower H_2/CO ratios and reduced coke formation. Catalytic stability tests over 200 hours showed CH_4 and CO_2 conversion rates of 93~97% and 0~5%, respectively. $CeZrO_2$-modification of the catalyst leads to reduction in the BET area and metal dispersion. Sintering was observed in used catalysts; however, there was no clear correlation between the extent of morphological deterioration and the $CeZrO_2/Al_2O_3$ ratio of the catalyst support.

3.2 Introduction

Biogas is an important renewable resource that is often left unused due to its distributed nature and the high cost of development for commercial use. Direct biogas emissions to the atmosphere cause significant harm due to methane's role as a short lived climate pollutant (SLCP). Therefore, biogas development and utilization for energy production can considerably reduce net greenhouse gas (GHG) emissions [1]. Methane in the biogas can either be combusted directly as a fuel or can be converted into syngas through the steam-

biogas reforming (SBR or bi-reforming) process which combines steam-methane reforming with dry (or CO_2) reforming of methane [2]. The benefits of the later approach have been detailed in previous studies by the authors. Syngas consists of H_2 and CO and is a versatile feedstock that can be used for fuels, chemicals and power production [3, 4].

Biogas typically consists of 35~75% CH_4 and 15~50% CO_2 along with moisture. Additional water in the form of steam has to be added to the SBR system since coke formation is a serious problem encountered when CH_4 is reformed with CO_2 without sufficient steam or in the absence of steam. The steam to carbon ratio is also a critical parameter affecting CH_4 and CO_2 conversion during the SBR reaction. Major reactions involved in the SBR process are listed below [5–7]:

SMR: $CH_4 + H_2O \rightarrow 3H_2 + CO$; $\Delta H° = 206.1$ kJ/mol eq 3-1

DRM: $CH_4 + CO_2 \rightarrow 2H_2 + 2CO$; $\Delta H° = 247.3$ kJ/mol eq 3-2

WGS: $CO + H_2O \rightarrow H_2 + CO_2$; $\Delta H° = -41.2$ kJ/mol eq 3-3

DM (Dehydrogenation of Methane): $CH_4 \rightarrow C + 2H_2$; $\Delta H° = 78.4$ kJ/mol eq 3-4

Commercial SMR catalysts for syngas production are mostly nickel-based and are supported on alumina [8]. Dry reforming and bi-reforming are not commercial technologies and the catalysts are still under development for these processes [2, 9–11]. Jakobsen et al. studied SMR and DRM reactions over a Ru/ZrO_2 catalyst in the low

temperature range (700~850 K), reporting CH_4 conversions below 35% [7]. Angeli et al. studied CH_4 bi-reforming over Ni-Rh on La_2O_3–ZrO_2 and La_2O_3–CeO_2–ZrO_2 catalysts at 673–823 K with a feed CH_4/CO_2 ratio of unity and a relatively large steam/CH_4 ratio (S/C = 3), reporting 5~10% less CH_4 conversions than the equilibrium values [12]. The stability tests, conducted for over 50 h, showed a trend of decreasing methane conversions. Other materials that have been evaluated for steam/dry reforming of methane include Ni-La_2O_3 [13], Ni-In/SiO_2 [14], Ni/MgO [15], Ni-MgO-Al_2O_3 [16], Ni/MgO-CeO_2 [17], Fe_2O_3-Al_2O_3-CuO catalyst with Ba, Ca, Mg and Sr [18], Cu-CeO_2-ZrO_2 [19], Co-MgO [20], Co/CeO_2 [21], Fe, Mn, Co and Cu supported on Al_2O_3 [22].

Research has shown that CeO_2-modification of the SBR catalyst support material significantly improves catalytic performance and as an active ingredient, performance of Rh is superior to that of Ni [12]. Compared with nickel, noble metals lead to reduced coke formation in biogas reforming. However, due to the cost factor of noble metals, research has focused on improving catalysts by adding small quantities of noble metal(s) to nickel or by modifying the catalyst support material with promoters such as CeO_2 or $CeZrO_2$ [23, 24].

A number of studies focusing on noble metal catalysts for methane reforming are available in the literature, including evaluation of bimetallic catalysts prepared by adding a small portion of rhodium, the most active ingredient for activating methane, to another noble metal [25-36]. Our previous publications detailed the performance of substrate-coated Pd-Rh catalysts developed for the SBR process [2, 9–11]. We demonstrated that a certain extent of $CeZrO_2$-modification of the Al_2O_3 support altered the physical characteristics and

improved the SBR activity of a 1.31 wt% Pd-Rh catalyst having the optimum bimetallic composition of Pd(7)-Rh(1) by weight [2]. Our present study focuses on how different $CeZrO_2$-Al_2O_3 support compositions affect the surface structure and SBR performance of the Pd(7)-Rh(1) catalyst coated on a metal foam substrate. The results of this study can be used to design a suitable bimetallic noble metal catalyst for the SBR process.

3.3 Experimental

3.3.1 Catalyst preparation and characterization

Each Pd-Rh catalyst was prepared by coating 7.6 grams of catalytic composites, which consist of active metal ingredients and metal oxide(s) support, onto 0.1 liter metal foam substrate (foam density 1g/cm^3, surface area 13.68 m^2/liter, cell diameter 450 microns, porosity 78.5%) made of Al-Ni-Cr alloy. The catalytic composites were made by loading 1.31 wt% Pd(7)-Rh(1) clusters on $CeZrO_2$-modified Al_2O_3 powder having 6 different Al_2O_3/$CeZrO_2$ ratios: 100/0, 85/15, 75/25, 50/50, 25/75, 0/100 by weight. Catalyst preparation procedure has been described in detail in an earlier study [11]. A slurry containing Pd-Rh, alumina, and ceria-zirconia was made by impregnating the mixed powder of alumina and ceria-zirconia with palladium nitrate and rhodium nitrate solutions, then dispersing the impregnated powder in de-ionized water, and then wet-milling the dispersed powder. The volumes of palladium nitrate and rhodium nitrate solutions were calculated so that the impregnated powder had palladium and rhodium contents of 1.15 wt% and 0.16 wt%, respectively. The slurry was coated onto Al-Ni-Cr alloy foam substrate

by the wash-coating method, and excess slurry was blown away from the substrate by an air-knife. The coated substrate was dried at 393 K in an oven for three hours, and then was calcined at 873 K in a muffle furnace for three hours. For each liter volume of the alloy substrate, nominally 76 grams (dry basis) of the impregnated powder was coated. Noble metals loading in the wash-coat composite is 1.31 wt%, and their overall loading value in the metal foam catalyst is reduced to 0.093 wt% when the weight of metal foam is included. The noble metals/metal foam catalysts were used in this study without further pretreatments.

Table 3-1: The catalytic composites of the Pd-Rh catalysts.

Catalytic composites	Catalyst name	Active ingredients* (wt%)	Oxides support (wt%)
[Pd(7)-Rh(1)]/ [Al_2O_3(100)-$CeZrO_2$(0)]	mfc (100/0)	Pd 1.15, Rh 0.16	Al_2O_3 98.7, $CeZrO_2$ 0.0
[Pd(7)-Rh(1)]/ [Al_2O_3(85)-$CeZrO_2$(15)]	mfc (85/15)	Pd 1.15, Rh 0.16	Al_2O_3 83.9, $CeZrO_2$ 14.8
[Pd(7)-Rh(1)]/ [Al_2O_3(75)-$CeZrO_2$(25)]	mfc (75/15)	Pd 1.15, Rh 0.16	Al_2O_3 74.0, $CeZrO_2$ 24.7
[Pd(7)-Rh(1)]/ [Al_2O_3(50)-$CeZrO_2$(50)]	mfc (50/50)	Pd 1.15, Rh 0.16	Al_2O_3 49.3, $CeZrO_2$ 49.3
[Pd(7)-Rh(1)]/ [Al_2O_3(25)-$CeZrO_2$(75)]	mfc (25/75)	Pd 1.15, Rh 0.16	Al_2O_3 24.7, $CeZrO_2$ 74.0
[Pd(7)-Rh(1)]/ [Al_2O_3(0)-$CeZrO_2$(100)]	mfc (0/100)	Pd 1.15, Rh 0.16	Al_2O_3 0.0, $CeZrO_2$ 98.7

*The active metal composition in the composite material is 1.31 wt%. The active metal loading is 0.093 wt% when th weight of the metal foam support is considered.

Chemical compositions of the (Pd-Rh)/($CeZrO_2$-Al_2O_3) catalysts were measured by the ICP (inductively-coupled plasma) (Agilent Technologies, 5100) method, after scraping catalytic composites from the coated alloy substrate. Catalytic composites of the fresh and used catalysts were characterized for BET surface area and pore structure by nitrogen adsorption and porosimetry (Micromeritics, ASAP 2010) and active metal dispersion was

measured by CO chemisorption at 313 K using CO pulse technique (BEL, BelCat Analyzer). Catalyst morphology was examined by scanning electron microscope (JEOL, JSM-5610). Chemical compositions of the catalytic composites are listed in Table 3-1.

3.3.2 SBR reaction experiments

For evaluating the activity and stability of the metal-foam-coated Pd-Rh/($CeZrO_2$-Al_2O_3) catalysts, SBR reaction runs were conducted at atmospheric pressure in a microchannel heat exchanger platform (HEP) reactor (Catacel/Johnson-Matthey), as described previously [11].

Nine pieces of the substrate-coated Pd-Rh catalyst strips (1 cm width x 1 mm thickness) were inserted into the reformer side of the reactor where the reforming feed was passed at GHSV (Gas Hourly Space Velocity) of 1,400 h^{-1}. The reactant (biogas+steam) flow was 380 sccm and the amount of catalyst used is about 17.5 g, which results in a GHSV of 1,400 h^{-1}. Several K-type thermocouples were used to measure the catalyst bed temperature at different axial positions inside the reactor. The alternate chambers of the HEP reactors were used to conduct combustion over a Pd-Pt catalyst to supply the energy necessary for the reforming reaction. Details are reported in our pervious study [11]. Thermocouples were also installed in the combustor side of the reactor, where a mixture of methane and air was passed over a different set of substrate-coated Pd-Pt catalyst strips to enable combustion.

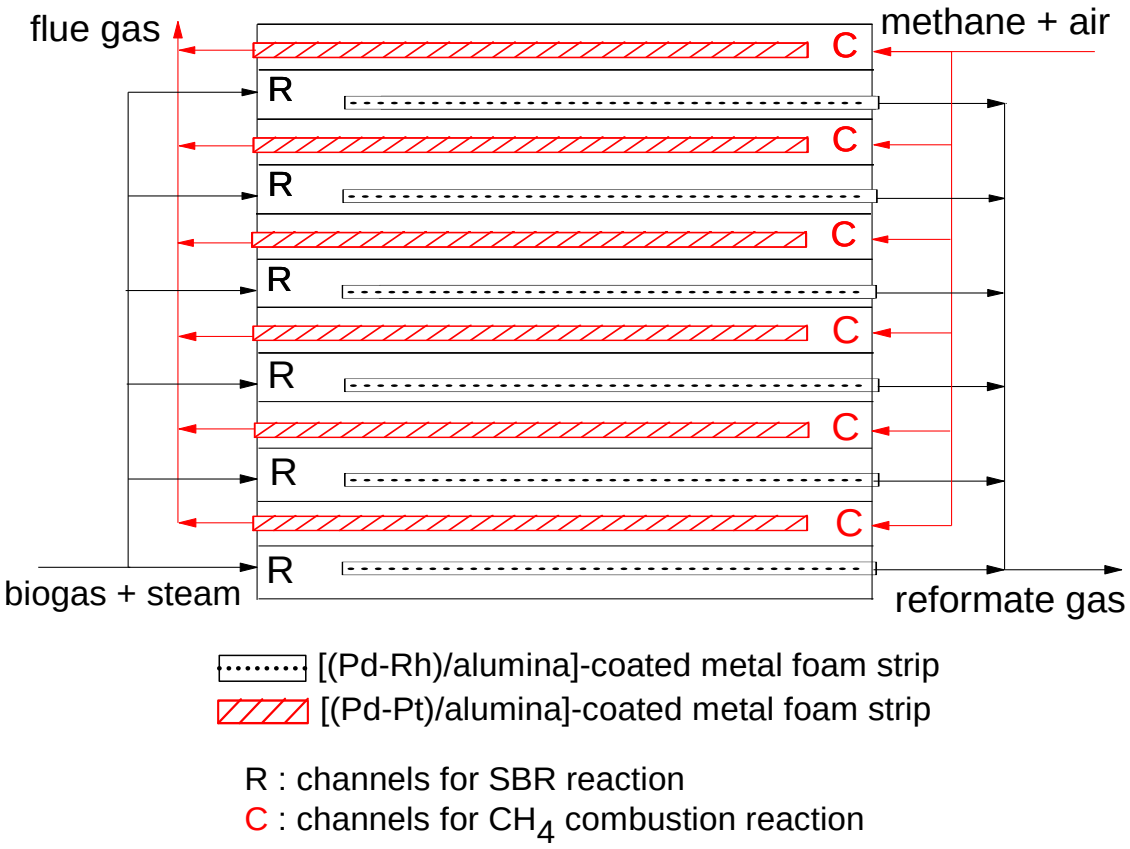

Figure 3-1: Experimental setup of the SBR reaction process inside the HEP reactor [2].

The HEP reactor was enclosed inside a temperature-programmed furnace which was interfaced with a data acquisition system. A schematic diagram of the HEP reactor with the substrate-coated catalysts is shown in Figure 3-1. Catalyst sample placed inside the reactor was heated from room temperature to the reaction temperature at a rate of 5 K/min in reactant gas flow. Gas mixtures were supplied from the manifold consisting of gas cylinders, mixer/vaporizer, and water source. Gas components and water were mixed together and were heated to 433 K in the mixer/vaporizer before entering the reactor. The model biogas feed consisted of 60% CH_4 and 40% CO_2. Product gas composition was

analyzed on a dry basis by using a residual gas analyzer (RGA, Cirrus- MKS Technologies). SBR reaction runs were conducted using a steam/CH_4 (S/C) ratio of 1.50 in the temperature range of 923 to 1123 K. Prior to each reaction run, the catalyst strips were pretreated at 873 K in [10% H_2 + 90% N_2] flow of 200 ml/min for 60 min followed by [40% steam + 60% N_2] flow of 380 ml/min for 30 min in order to remove the deposited coke and oxygen from catalyst surface. Catalytic stability was tested at 1073 K and atmospheric pressure with a S/C ratio of 1.50 for 200 on-stream hours. The reaction temperature was maintained for at least 2.5 h after the target temperature was achieved. Each experiment was repeated at least three times for each catalyst. The standard deviation was measured and was negligible (<2.5%). Catalytic activity was evaluated using the following equations:

CH_4 conversion = $\left(\frac{(CH_4)_{in}-(CH_4)_{out}}{(CH_4)_{in}}\right)_{reformer}$

CO_2 conversion = $\left(\frac{(CO_2)_{in}-(CO_2)_{out}}{(CO_2)_{in}}\right)_{reformer}$

H_2/CO ratio of syngas product = $\left(\frac{(H_2)_{out}}{(CO)_{out}}\right)_{reformer}$

H_2/CH_4 yield = $\left(\frac{(H_2)_{out}}{(CH_4)_{in}}\right)_{reformer}$

3.3.3 Coke formation during the SBR reaction

Coke formation during the SBR reaction is a serious concern since solid carbon (coke) deposition on the catalyst surface leads to deactivation. Two different methods were used

to calculate the extent of coke formation; i.e., the fraction of carbon in the feed that turned into solid carbon:

(1) Coke formation =

$$\left(\frac{\text{moles of gaseous carbon in the feed} - \text{moles of gaseous carbon in the product gas}}{\text{moles of gaseous carbon } (CH_4 \text{ and } CO_2) \text{ in the feed}}\right)_{\text{reformer}}$$

(2) Coke formation =

$$\frac{\text{moles of } CO_2 \text{ in the exhaust during oxidation of used catalyst oxidation over a 10 h period}}{\text{moles of } CH_4 \text{ and } CO_2 \text{ fed to the reformer for 200 h}}$$

The first equation (method 1) has been reported in our previous articles and is straightforward, based on the molar flow rates of CH_4, CO_2 and CO at reformer inlet and outlet [2, 9-11]. Oxidation of the used catalyst sample can also be used to estimate coke formation from the SBR reaction in an alternate manner. The used catalyst was subjected to oxidation in a separate packed bed reactor for 10 h: catalyst samples of approximately 1 gram each were taken from the catalysts used for the 200 h stability test, and then were placed individually in the packed bed reactor for 10 h under an air flow of 200 sccm at 973 K, which is high enough to burn the coke off from the sample. The reactor exhaust was connected to an RGA throughout the course of the oxidation process and the CO_2 concentration in the product gas stream was measured live. The total number of moles of CO_2 produced during the oxidation reaction was used to calculate the total coke deposited on the catalyst using the second equation (method 2). The results from the second method are more reliable than the first method since it is a direct measurement of the deposited carbon and is also not influenced by the accuracy of the RGA.

3.4 Results and discussion

3.4.1 Catalyst activity

Active metals loading of 1.31 wt% Pd-Rh on $CeZrO_2$-Al_2O_3 support is converted to 0.093 wt% Pd-Rh on the metal oxides support plus metal foam substrate, since 7.6 grams of catalytic composites was coated onto 0.1 liter metal foam of 1.0 g/cm^3 density. Despite the small quantity of active metals loading, most of the substrate-coated Pd(7)-Rh(1) catalysts are quite active in view of CH_4 conversion and syngas product yield as observed from the SBR reaction results. The metal-foam-coated (mfc) Pd-Rh catalysts are referred to using the phrase 'mfc (Al_2O_3 weight percentage /$CeZrO_2$ weight percentage)'. Based on this system, the catalyst sample names are: mfc (100/0), mfc (85/15), mfc (75/25), mfc (50/50), mfc (25/75), and mfc (0/100) based on the relative abundance of $CeZrO_2$ in the Al_2O_3 support (Table 3-1).

Catalytic activity of the alloy substrate for the SBR reaction, shown in Figure 3-2, is considered to be minimal. This is due to the substrate being made via heat treatment at 1473 K and its specific surface area being quite small due to the large extent of sintering caused by the heat treatment. At 923 K to 1123 K, the substrate itself, without the catalytic material, exhibited merely 3 to 11% CH_4 conversion from the SBR reaction at the same GHSV that was used for the Pd-Rh catalysts.

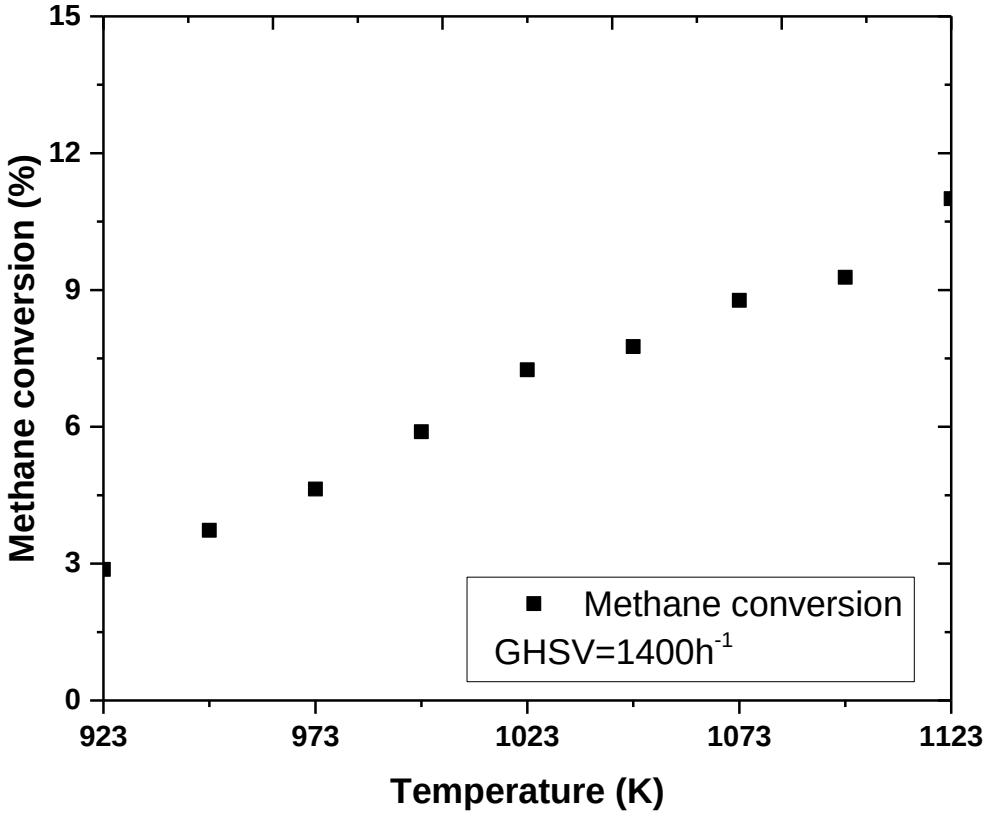

Figure 3-2: CH_4 conversion during the SBR reaction over the blank metal foam support.

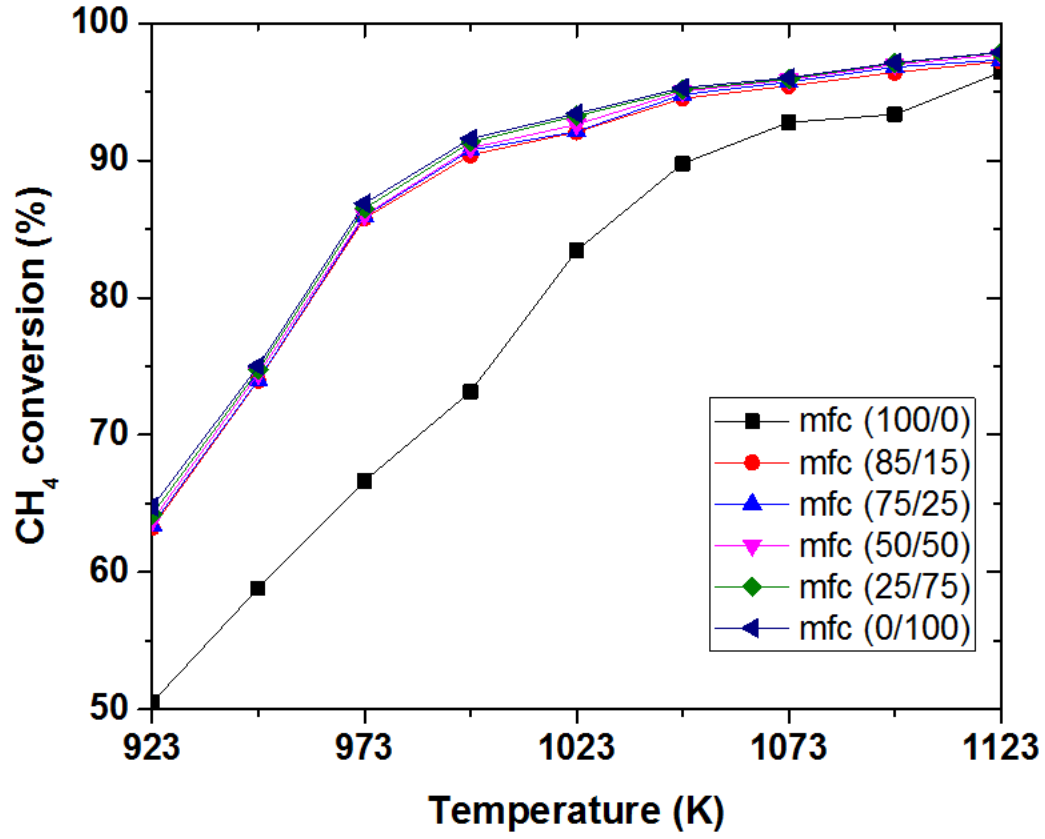

Figure 3-3: CH_4 conversion during the SBR reaction over the Pd-Rh catalysts.

As shown in Figure 3-3, CH_4 conversion from the SBR reaction increased with temperature for all the Pd-Rh catalysts. However, the $CeZrO_2$-modified Pd-Rh catalysts (mfc (85/15), mfc (75/25), mfc (50/50), mfc (25/75), and mfc (0/100)), exhibited higher CH_4 conversion than the unmodified catalyst (the mfc (100/0)) at each reaction temperature, indicating that $CeZrO_2$-modification of the Al_2O_3 support has a positive effect upon CH_4 activation. The CH_4 conversion over the mfc (100/0) catalyst was 5-20% less than the $CeZrO_2$ modified catalysts' values, although the differences were attenuated above 1098 K. At or below 1098 K, CH_4 conversion improvement was most remarkable when $CeZrO_2$ was introduced to the

catalyst support (mfc (85/15)). Further increase in the $CeZrO_2$ percentage maintained CH_4 conversion improvement trend but the improvement margins were significantly smaller. The $CeZrO_2$ modified catalysts exhibited CH_4 conversions greater than 90% at 998 K and above, whereas the mfc (100/0) catalyst did the same only at 1048 K and above. The CH_4 conversion from the SBR reaction over the mfc Pd-Rh/($CeZrO_2$-Al_2O_3) catalyst was in the order of mfc (0/100) > mfc (25/75) > mfc (50/50) > mfc (75/25) > mfc (85/15) > mfc (100/0), consistent with the order of relative $CeZrO_2$ abundance in the Al_2O_3 support. Similar CH_4 conversion improvements during SMR and DRM reactions due to CeO_2- or $CeZrO_2$-modification of supported Ni catalysts have been reported in the literature [37-39].

Figure 3-4 exhibits a complicated pattern of CO_2 conversion versus temperature from the SBR reaction: the CO_2 conversion values decreased with temperature from 923 to 973 K in a negative range, and then reached negative minima at 973 K, above which temperature they turned to increase. This pattern may indicate that from 923 K to 973 K, CO_2 consumption by the DRM and/or RWGS route was far less selective than CO_2 production by the SMR route coupled with WGS route, and then from 973 K and upward, the CO_2 consumption route(s) began to be selective. At temperatures below 1073 K, for all the mfc Pd-Rh catalysts except for the mfc (0/100) catalyst, CO_2 conversion was negative, evidencing that net CO_2 production occurred from the SBR reaction as the result of competition between the DRM and [SMR + WGS] reaction routes [10]. However, at 1073 K and above, all of the mfc Pd-Rh catalysts showed positive CO_2 conversion, e. g., 5.06% at 1073 K and 7.67% at 1123 K for the mfc (0/100) catalyst (supported on $CeZrO_2$) as well as 0.13% at 1073 K and 5.22% at 1123 K for the mfc (100/0) catalyst (supported on Al_2O_3),

demonstrating meaningful achievement of net CO_2 consumption from the SBR reaction. The mfc (0/100) catalyst began to show positive CO_2 conversion (2.10%) at 1048 K, while the rest of the mfc catalysts did the same at 1073 K. The CO_2 conversion trends of the catalysts followed the same trends as CH_4 conversion described above, illustrating the positive effect of $CeZrO_2$-modification upon CO_2 activation. The CO_2 conversion improvement was most pronounced as the catalyst support changed from 75% $CeZrO_2$-25% Al_2O_3 (the mfc (25/75)) to 100% $CeZrO_2$ (the mfc (0/100)) in the range of 998 to 1098 K. The $CeZrO_2$-modification of the catalyst is thought to have a positive effect on CH_4 and CO_2 activation through oxygen storage and oxide reducibility improvement abilities, leading to the improvement of CH_4 and CO_2 conversions [27]. A notable difference in the CH_4 and CO_2 conversion trends is that the effect on CH_4 conversion was most remarkable as the support composition changed from 100% Al_2O_3 (the mfc (100/0)) to 15% $CeZrO_2$-85% Al_2O_3 (the mfc (85/15)) whereas the effect on CO_2 conversion was most remarkable as the support composition changed from 75% $CeZrO_2$-25% Al_2O_3 (the mfc (25/75)) to 100% $CeZrO_2$ (the mfc (0/100)). One possible explanation for this difference is that the threshold of the $CeZrO_2$-modification for CO_2 conversion improvement is higher than that for CH_4 conversion improvement, because CO_2 conversion improvement requires the formation of larger ensembles of active sites on the $CeZrO_2$-Al_2O_3 support.

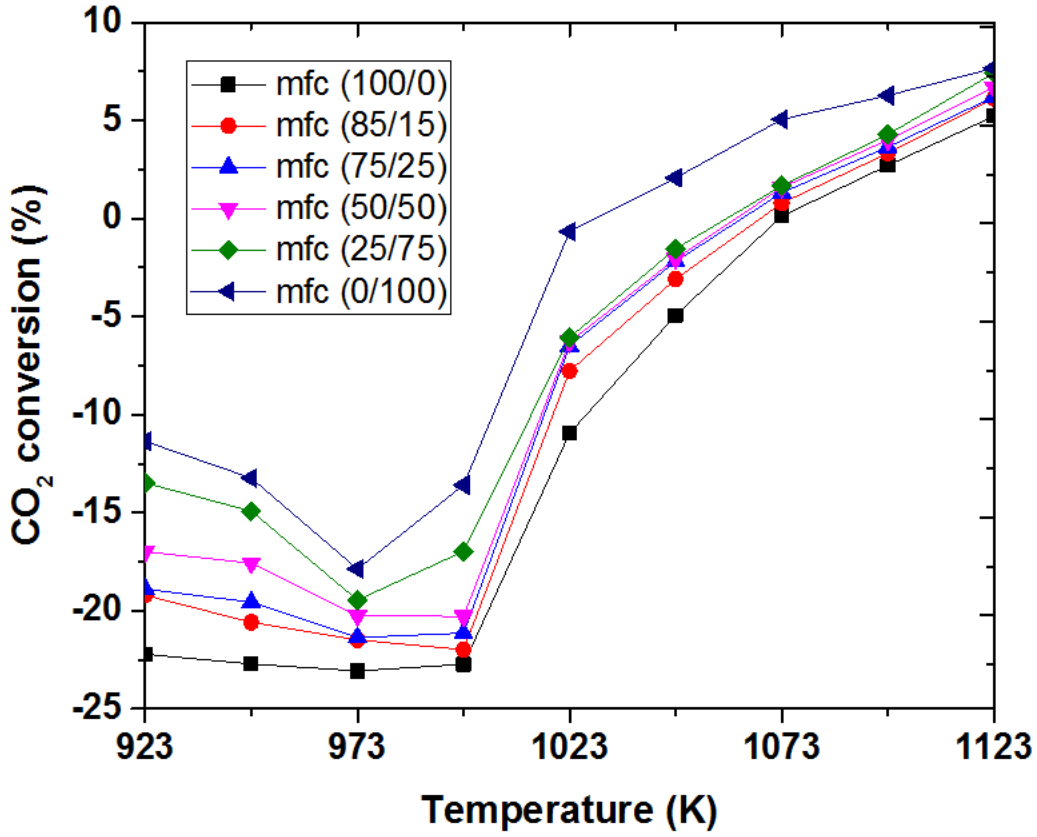

Figure 3-4: CO_2 conversion during the SBR reaction over the Pd-Rh catalysts.

The mfc (0/100) catalyst exhibited lower H_2/CO ratio of the syngas product and higher H_2/CH_4 yield than the other catalysts, as shown in Figure 3-5 and Figure 3-6. This feature is consistent with the significantly higher comparative CO_2 conversion of the mfc (0/100) catalyst than the comparative CH_4 conversion (Figure 3-3 and Figure 3-4), resulting in increased CO production and a lower H_2/CO ratio.

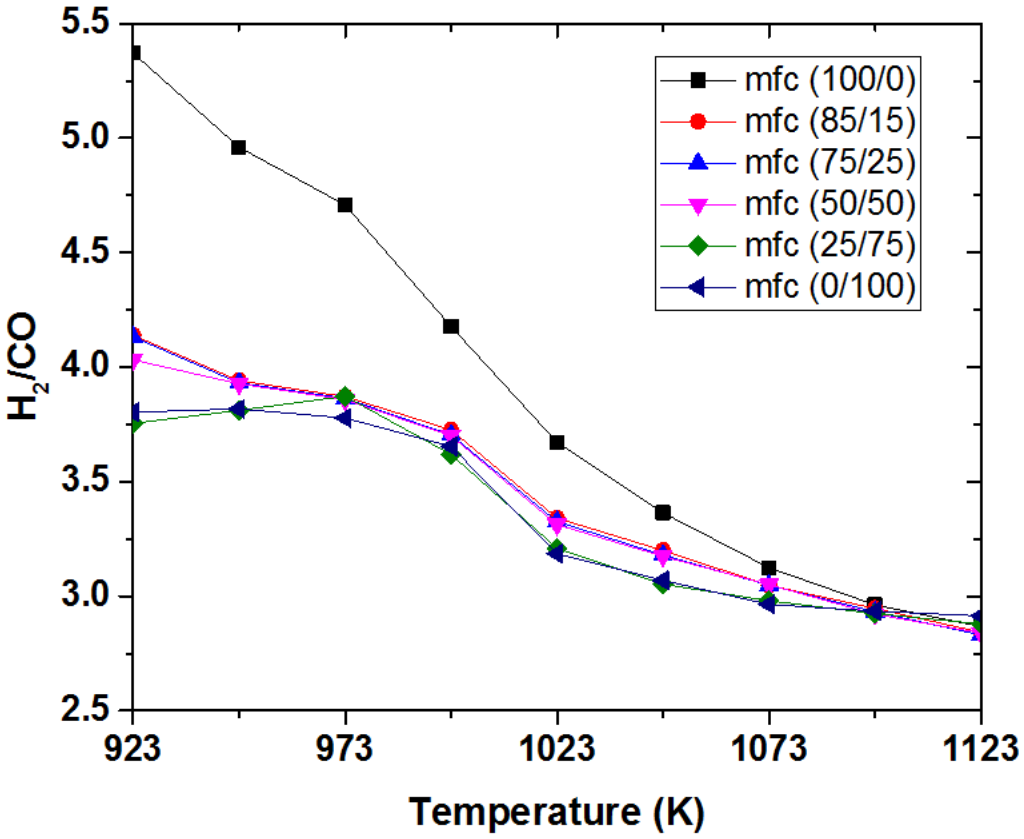

Figure 3-5: H_2/CO ratio of the syngas product from the SBR reaction over the Pd-Rh catalysts.

Over the temperature range of 1023 to 1098 K in which the mfc (0/100) catalyst achieved meaningful conversions of both CH_4 and CO_2, its H_2/CO syngas ratio and H_2/CH_4 yield were 3.19 to 2.93 and 2.91 to 2.94, respectively. Both mfc (0/100) and mfc (75/25) catalysts exhibited nearly identical H_2/CO syngas ratio over this temperature range, whereas the syngas ratio for the other catalysts was higher, with mfc (100/0) exhibiting a significantly higher ratio at lower temperatures.

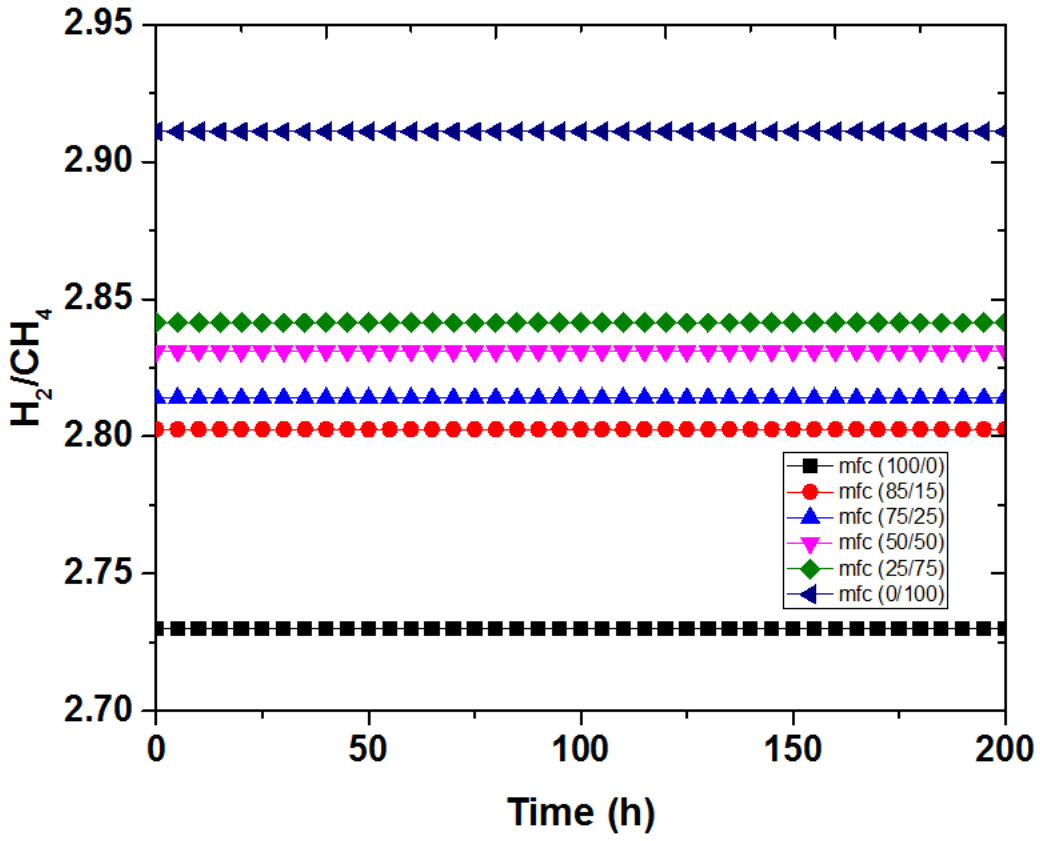

Figure 3-6: H_2/CH_4 yield from the SBR reaction over the Pd-Rh catalysts.

Coke formation values in mol % calculated using method 1 are shown in Table 3-2. For all the catalysts, coke formation increased with temperature until a peak temperature and then decreased. The peak temperature was in the order of mfc (0/100) = mfc (25/75) < mfc (50/50) = mfc (75/25) = mfc (85/15) < mfc (100/0): 948 K for the mfc (0/100) and mfc (25/75) catalysts, 998 K for the mfc (50/50), mfc (75/25) and mfc (85/15) catalysts, and 1023 K for the mfc (100/0) catalyst. Peak value (mol %) of coke formation was in the order of mfc (0/100) (2.79) < mfc (25/75) (3.46) < mfc (50/50) (4.02) < mfc (75/25) (4.23) < mfc (85/15) (4.33) < mfc (100/0) (8.21). The trends show that higher CeZrO2 content in the

Al_2O_3 support resulted in reduced coke formation over the same temperature range. A similar coke formation tendency was observed for CH_4 reforming over Ni/α-Al_2O_3 catalyst with CeO_2- and/or ZrO_2-modification by Pompeo et al. [37]. $CeZrO_2$ in the Al_2O_3 support of the mfc Pd-Rh catalyst is thought to suppress the coke formation during the SBR reaction through the following sequence [2]:

$CH_4 \rightarrow C + 2H_2$; $C + CeZrO_2 \rightarrow CO + CeZrO_{(2-x)}$; $CO_2/H_2O + CeZrO_{(2-x)} \rightarrow CO/H_2 + CeZrO_2$

Table 3-2: Coke formation (mol %) from the SBR reaction over the Pd-Rh catalysts.

T (K)	mfc (100/0)	mfc (85/15)	mfc (75/25)	mfc (50/50)	mfc (25/75)	mfc (0/100)
923	5.82	3.11	3.29	3.51	3.27	2.08
948	6.33	3.84	3.73	3.88	3.46	2.79
973	7.02	3.89	3.77	3.84	3.36	2.57
998	7.40	4.33	4.23	4.02	3.25	1.95
1023	8.21	3.65	3.97	3.78	2.15	1.71
1048	7.76	3.36	3.31	2.97	2.16	1.31
1073	5.45	2.96	2.27	2.12	1.69	1.17
1098	3.26	2.79	2.72	2.11	1.65	1.20
1123	3.01	2.29	2.30	1.86	1.62	1.82

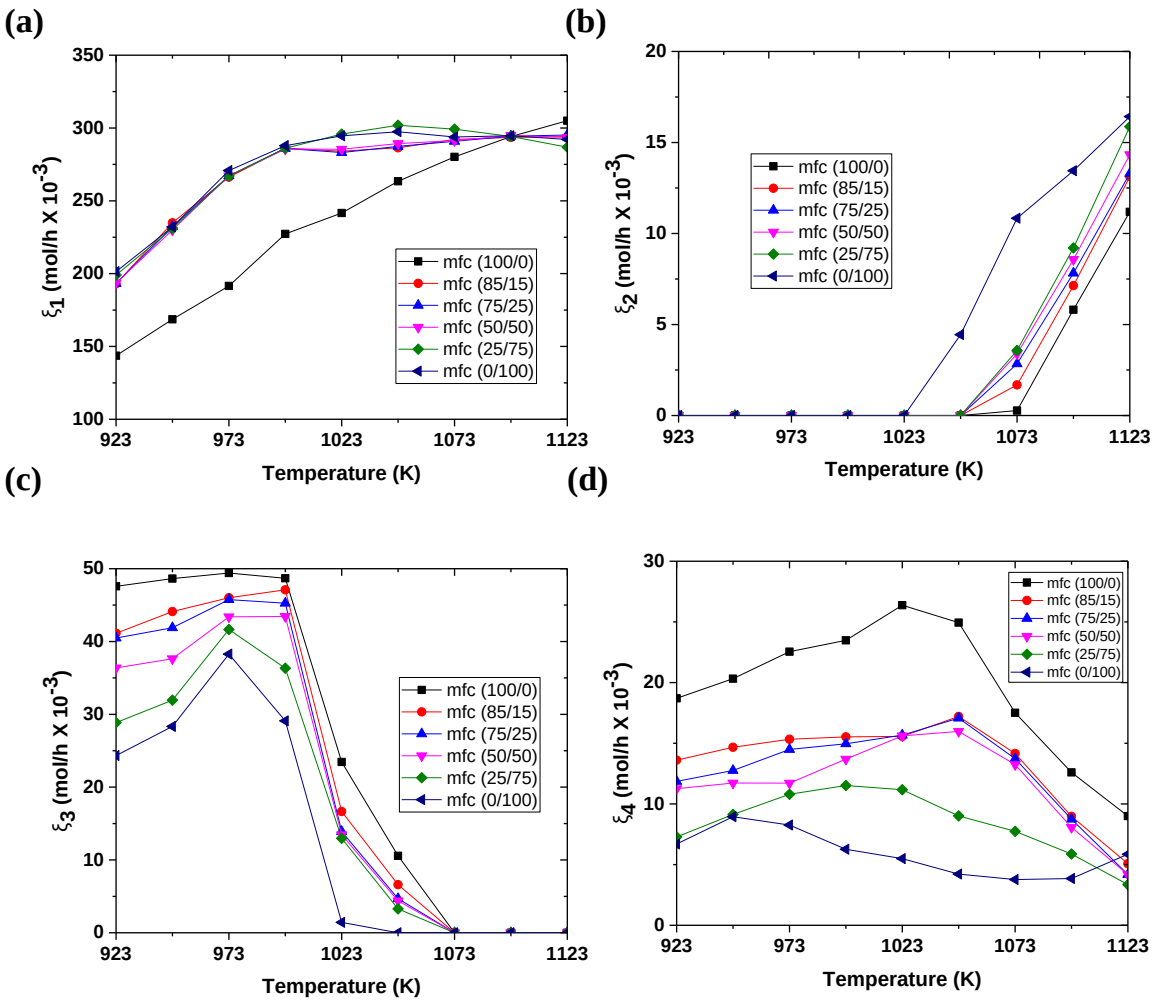

Figure 3-7: Extents of the reaction for the SBR reaction routes (inlet flow rates: CH_4 321.1x10^{-3} mol/h, CO_2 214.2x10^{-3} mol/h; GHSV 1400 h^{-1}; S/C ratio 1.50).

The extent of reaction was calculated for each of the following routes involved in the SBR reaction using the molar balance based on biogas conversion and syngas yield:

route (1): $CH_4 + H_2O \rightarrow 3H_2 + CO$

route (2): $CH_4 + CO_2 \rightarrow 2H_2 + 2CO$

route (3): $CO + H_2O \rightarrow H_2 + CO_2$

route (4): $CH_4 \rightarrow C + 2H_2$

As shown in Figure 3-7, ξ_1, ξ_2, ξ_3 and ξ_4 are the extents of reaction for the reaction routes (1), (2), (3) and (4), respectively, which were evaluated in mol/h for the model biogas and steam fed at GHSV of 1400 h^{-1} and S/C ratio of 1.50. In view of 321.2 x 10^{-3} mol/h CH_4 and 214.2 x 10^{-3} CO_2 in the biogas feed, sum of the extents of reaction for the routes (1), (2) and (4) draws good agreement with CH_4 conversion shown in Figure 3-3, and the difference of those for the routes (2) and (3) reasonably accounts for CO_2 conversion shown in Figure 3-4. Coke removal routes such as $2C + CO_2 \rightarrow 2CO$ and/or $C + H_2O \rightarrow CO + H_2$ were excluded from the molar balance because these routes could not be deconvoluted from the coke formation route (4).

3.4.2 Catalytic stability for 200 on-stream hours

Figure 3-8 shows the SBR performance of each Pd-Rh/($CeZrO_2$-Al_2O_3) catalyst for 200 on-stream hours at 1073 K. The temperature value of 1073 K was selected for the catalytic stability test since the CO_2 conversion became positive at this temperature regardless of the $CeZrO_2/Al_2O_3$ ratio of the catalyst. All the catalysts maintained steady performances with negligible changes during the stability test, indicating that the extent of $CeZrO_2$-modification of the Al_2O_3 support did not affect the resistance to catalyst deactivation for at least 200 on-stream hours. As shown in Figure 3-8 (a), CH_4 conversion was steady in the range of 92.8 to 96.0% respectively for the mfc (100/0), mfc (85/15), mfc (75/25), mfc (50/50), mfc (25/75), and mfc (0/100) catalysts. The CO_2 conversion, shown in Figure 3-8 (b), was also steady from 0.13 to 5.06% for the mfc (100/0), mfc (85/15), mfc (75/25), mfc

(50/50), mfc (25/75), and mfc (0/100) catalysts. As shown in Figure 3-8 (c) and 8(d), H_2/CO ratio of the syngas product was steady at 2.96 to 3.12, while H_2/CH_4 yield was also steady at 2.73 to 2.91, respectively for the mfc (100/0), mfc (85/15), mfc (75/25), mfc (50/50), mfc (25/75), and mfc (0/100) catalysts.

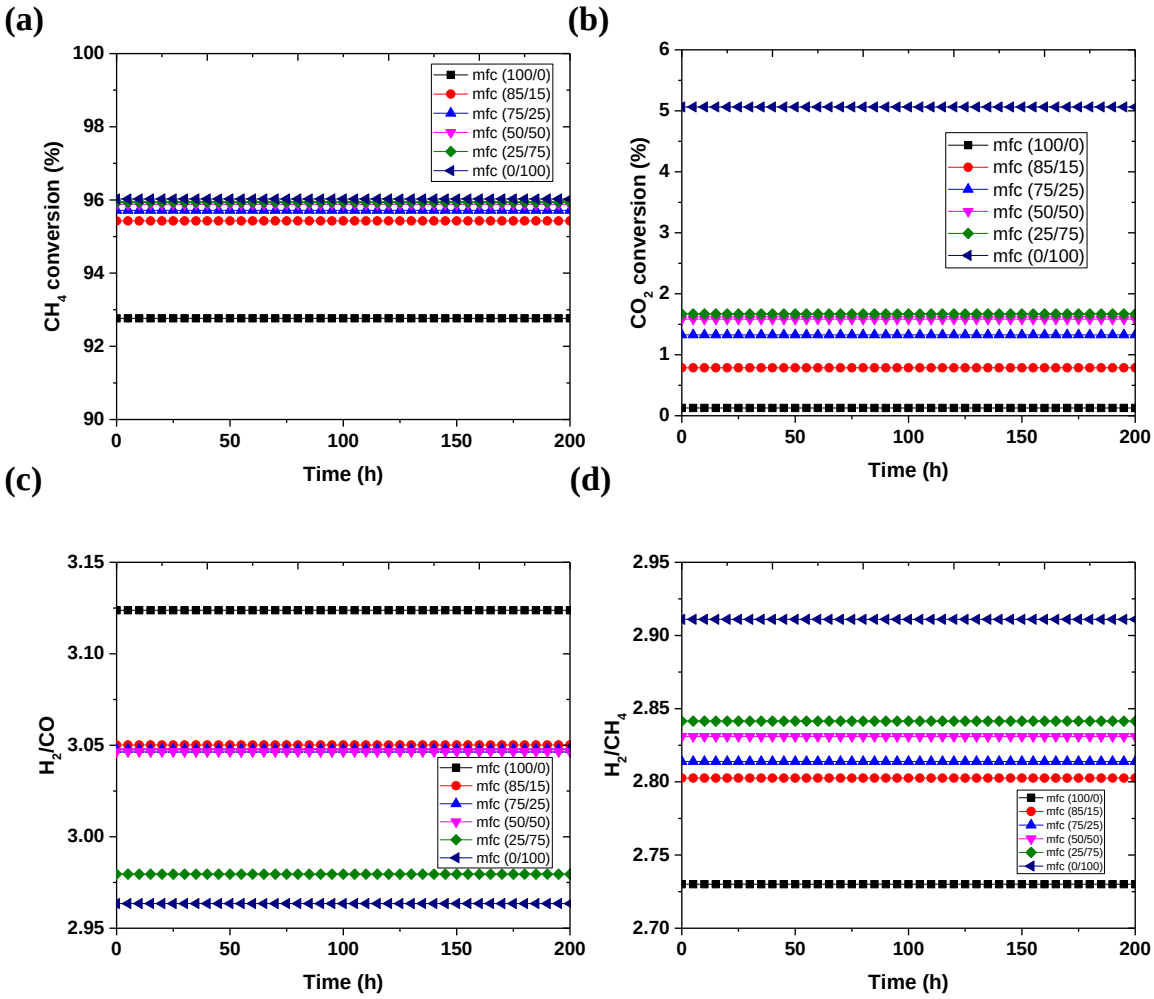

Figure 3-8: Catalytic stability of the Pd-Rh catalysts for the SBR reaction at 1073 K: (a) CH_4 conversion; (b) CO_2 conversion; (c) H_2/CO ratio of syngas product; (d) H_2/CH_4 yield.

Table 3-3: Coke formation (mol %) during the SBR reaction stability test at 1073 K.

Catalyst	Coke formation (mol %)	
	Method 1	Method 2
mfc (100/0)	5.45	2.82
mfc (85/15)	2.96	2.40
mfc (75/15)	2.27	2.40
mfc (50/50)	2.12	2.35
mfc (25/75)	1.69	2.10
mfc (0/100)	1.17	1.97

Each of the Pd-Rh catalysts used for the 200 h stability test was oxidized at 973 K in another packed bed reactor for evaluating coke formation from the SBR reaction by the second method described in section 3.3.3 Coke formation during the SBR reaction. The results for coke formation calculated by method 2 are presented in Table 3-3. The coke formation data from the two methods clearly show that $CeZrO_2$ in the catalyst support played an important role of providing oxygen storage capacity to the Pd-Rh catalyst, and consequently suppressed coke formation from the SBR reaction. The $CeZrO_2$ only supported mfc (0/100) catalyst was least prone to coke deposition whereas the Al_2O_3 supported mfc (100/0) catalyst was most prone to coke deposition.

3.4.3 Catalyst characterization

Although all the Pd-Rh/($CeZrO_2$-Al_2O_3) catalysts maintained steady activity for the SBR reaction for 200 on-stream hours, their thermal stability needed to be examined through catalyst characterization. BET surface area, pore structure and active metal dispersion of the catalytic composites are presented in Table 3-4 for the fresh as well as the used catalysts sampled after 200 h catalytic stability test described above.

Table 3-4: Characterization of the [Pd(7)-Rh(1)]/($CeZrO_2$-Al_2O_3) composites.

Properties / Catalyst	BET surface area (m^2/g)		Pore volume (cm^3/g)		Pore size (nm)		Active metal dispersion (%)	
	fresh	used	fresh	used	fresh	used	fresh	used
mfc (100/0)	126.3	106.3	0.62	0.53	22.1	23.8	52.1	37.3
mfc (85/15)	94.9	81.5	0.46	0.38	18.1	18.9	40.7	30.9
mfc (75/25)	88.3	76.1	0.43	0.36	17.3	17.9	33.1	28.6
mfc (50/50)	84.1	74.3	0.34	0.31	13.5	15.7	30.2	20.4
mfc (25/75)	79.5	72.4	0.36	0.23	9.5	14.4	26.2	18.5
mfc (0/100)	69.8	58.7	0.10	0.12	7.2	13.9	21.0	16.8

$CeZrO_2$-modification of the Al_2O_3 support in the fresh catalysts showed the tendency to decrease BET surface area and active metal dispersion by adversely affecting the catalyst

pore structure. Compared to fresh catalysts, significant reduction of BET surface area was observed in the used catalysts, a tendency also observed by Pompeo et al. in a similar catalyst support modification study [37, 40]. The BET surface area was reduced approximately 9 to 16% in the used catalysts in our study, with no clear correlation between the the extent of reduction and the extent of $CeZrO_2$-modification of the Al_2O_3 support. Pore sizes and pore volumes of the used catalysts increased and decreased in concurrence with the reduction of BET surface area. The exception was the mfc (0/100) catalyst which showed only an increase in the pore size, without pore volume decrease due to its usage by the catalytic stability test. Accompanying these changes, active metal dispersion decreased for the used catalysts by approximately 4 to 15%, again without a clear correlation to the extent of $CeZrO_2$-modification of the Al_2O_3 support.

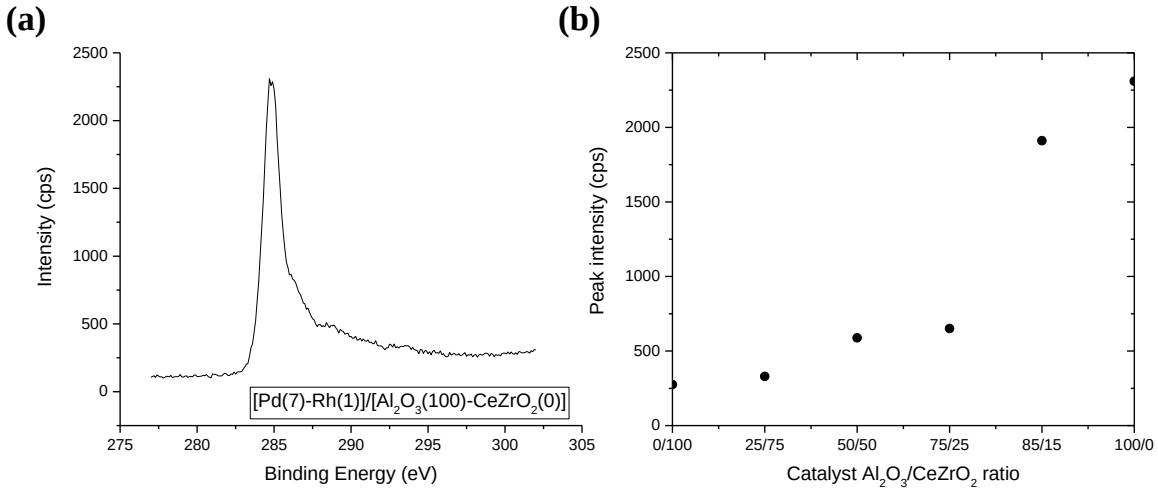

Figure 3-9: XPS data for coke formation: (a) Results of the XPS analysis for used Pd(7)-Rh(1)/[Al_2O_3(100)$CeZrO_2$(0)] catalyst; (b) Peak intensity for carbon from XPS results with varying ratio of Al_2O_3/$CeZrO_2$.

X-ray Photoelectron Spectroscopy (XPS) analysis of the spent catalysts were performed and the results are presented in Figure 3-9. Figure 3-9 (a) shows the XPS analysis of mfc (100/0) for coke deposited over the catalyst. Figure 3-9 (b) shows the change in peak intensity of coke formation over the spent catalysts for the different $Al_2O_3/CeZrO_2$ ratios. The results show the same trend as estimated using the two coke formation calculation methods presented in Table 3-3.

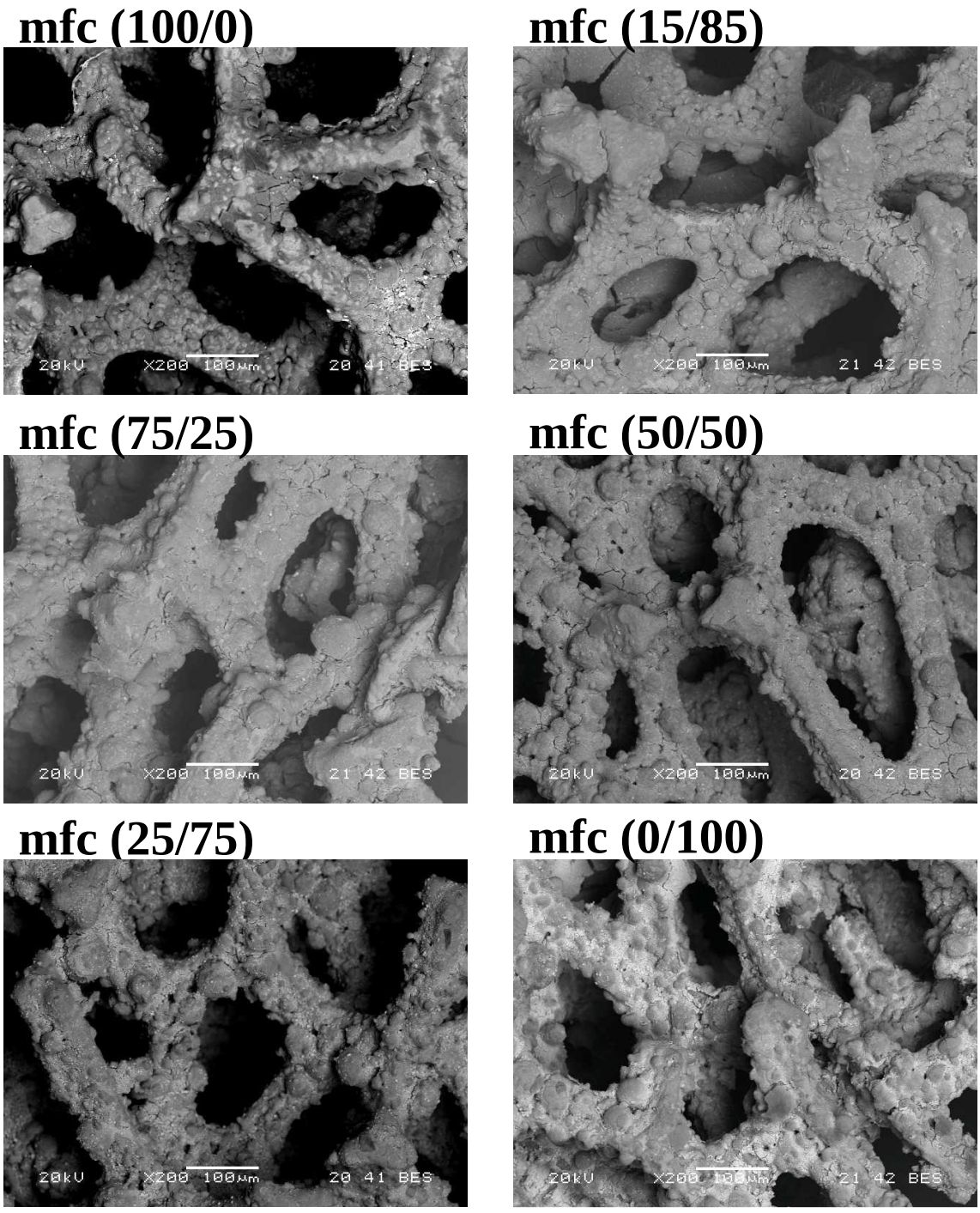

Figure 3-10: SEM images of the fresh Pd-Rh catalysts.

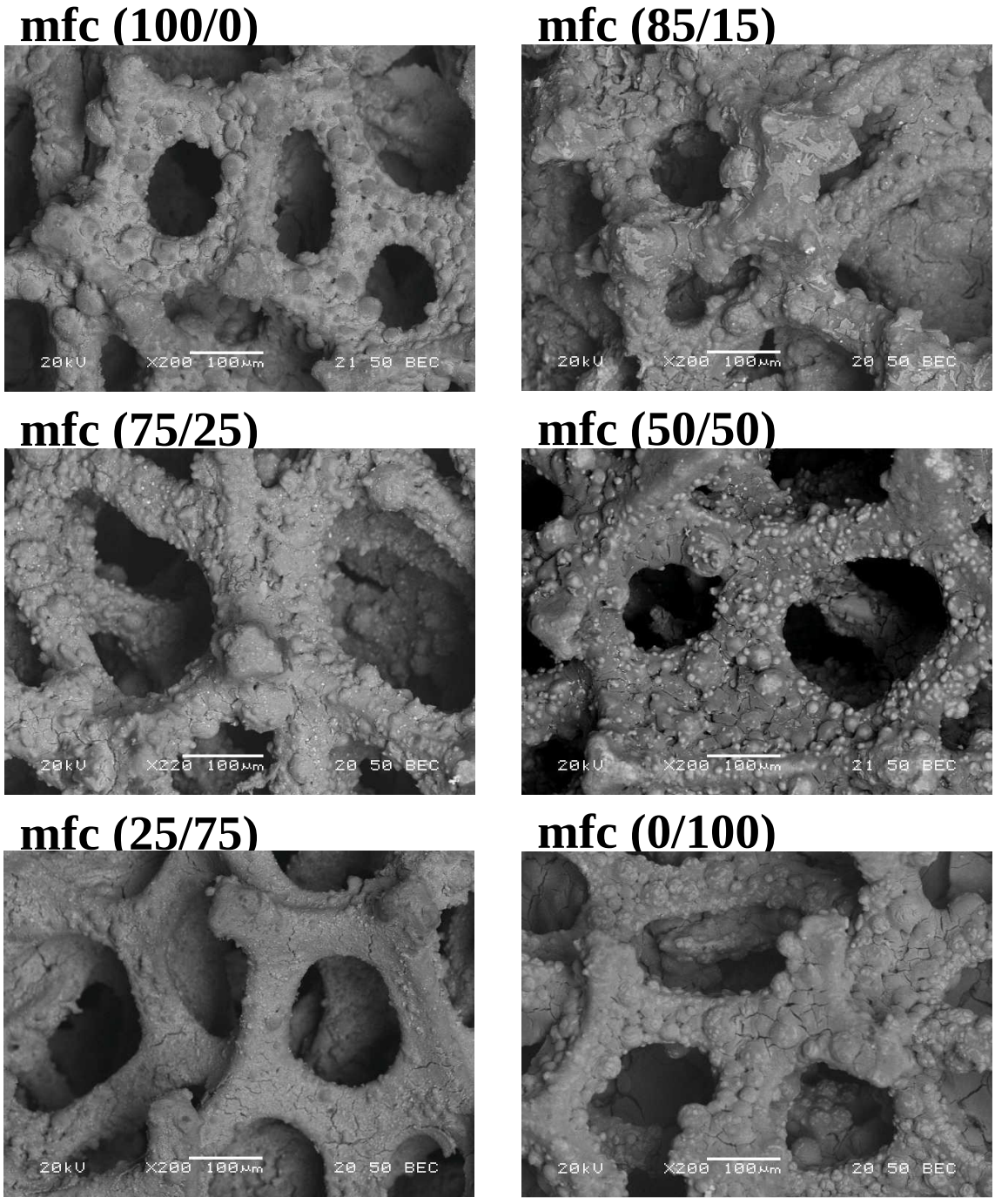

Figure 3-11: SEM images of the Pd-Rh catalysts used in the 200 h catalytic stability test at 1073 K.

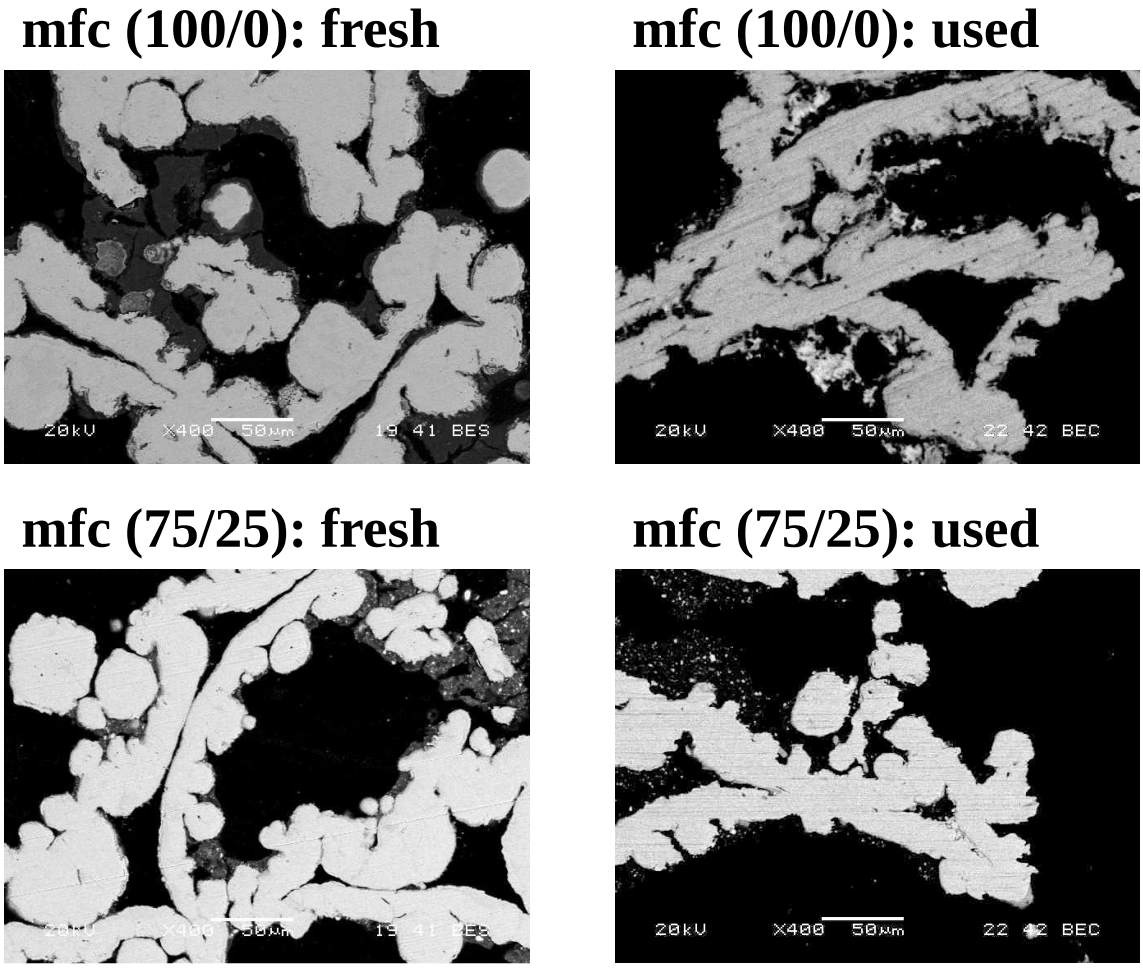

Figure 3-12: Cross-sectional SEM images of the catalysts were taken to further assess the sintering.

Considering that the catalytic activity for the SBR reaction did not degrade during the 200 h catalytic stability test for any of the catalysts, it can be postulated that the catalyst sintering described above is not detrimental enough to negatively affect the catalytic activity. However, it must be acknowledged that the catalytic stability test must be extended to a period much longer than 200 on-stream hours to conclusively understand catalyst sintering and its effect on catalyst activity. Scanning electron microscopic images

of fresh and used Pd-Rh/($CeZrO_2$-Al_2O_3) catalysts are shown in Figure 3-10 and Figure 3-11, respectively. The SEM images show that morphological changes occurred on the catalyst surfaces due to the 200 h catalytic stability test: sintering of the catalyst surface was evidenced by small pebbles which tend to form on the used catalyst surface exposed to high temperature for an extended period. Cross-sectional SEM images of the catalysts were taken to further assess the sintering. The cross-sectional SEM image in Figure 3-12 shows large, smooth pieces on the surface, thus providing evidence to the sintering phenomenon.

3.5 Conclusions

Six metal-foam-coated 1.31 wt% [Pd(7)-Rh(1)]/($CeZrO_2$-Al_2O_3) catalysts were studied to evaluate the effects of the support composition upon their performances for the SBR reaction. The catalytic activity was measured from 923 to 1123 K at atmospheric pressure in a Heat Exchanger Platform reactor operated under an S/C ratio of 1.50 and GHSV of 1400 h^{-1}. The key results are summarized below.

1. Increasing the extent of $CeZrO_2$-modification of the catalyst support resulted in CH_4 and CO_2 conversion improvements for steam reforming of a model biogas consisting of 60% CH_4 and 40% CO_2.

2. The CH_4 and CO_2 conversion improvements were accompanied by a decrease in the H_2/CO ratio of the syngas product and an increase in the H_2/CH_4 yield. This allows the SBR process to be potentially configured to meet the needs of downstream processes.

3. Increased relative abundance of $CeZrO_2$ in the catalyst support suppressed coke formation from the SBR reaction due to oxygen storage and ability to improve oxide reducibility.

4. Regardless of the $CeZrO_2$-Al_2O_3 composition of the catalyst support, all the metal-foam-coated Pd-Rh catalysts maintained catalytic stability for the SBR reaction steadily for 200 on-stream hours. Some catalyst sintering was observed without a clear correlation to the extent of $CeZrO_2$ modification of the Al_2O_3 support of the catalyst.

Acknowledgements

This work was supported by California Energy Commission through Energy Innovation Small Grant No. 57825A/13-08G. Kiseok Kim is grateful to Yeungnam University for the 2015 Research Abroad Grant. Authors are grateful to Kyle Hunter, Vincent Van, Sean Franco and the Central Facility for Advanced Microscopy and Microanalysis at the University of California, Riverside.

3.6 References

[1] P. Kolbitsch, C. Pfeifer, H. Hofbauer, Catalytic steam reforming of model biogas, Fuel 87 (2008) 701-706.

[2] P.S. Roy, M.S. Kang, K. Kim, Effects of Pd–Rh Composition and CeZrO2-Modification of Al2O3 on Performance of Metal-Foam-Coated Pd–Rh/Al2O3 Catalyst for Steam Reforming of Model Biogas, Catal. Letters 144 (2014) 2021-2032.

[3] I. Suelves, M.J. Lázaro, R. Moliner, B.M. Corbella, J.M. Palacios, Hydrogen production by thermo catalytic decomposition of methane on Ni-based catalysts: influence of operating conditions on catalyst deactivation and carbon characteristics, Int. J. Hydrogen Energy 30 (2005) 1555-1567.

[4] A.A. Iordanidis, P.N. Kechagiopoulos, S.S. Voutetakis, A.A. Lemonidou, I.A. Vasalos, Autothermal sorption-enhanced steam reforming of bio-oil/biogas mixture and energy generation by fuel cells: Concept analysis and process simulation, Int. J. Hydrogen Energy 31 (2006) 1058-1065.

[5] A. Galvagno, V. Chiodo, F. Urbani, F. Freni, Biogas as hydrogen source for fuel cell applications, Int. J. Hydrogen Energy 38 (2013) 3913-3920.

[6] L. Guczi, A. Erdôhelyi, Catalysis for Alternative Energy Generation, Springer, New York 2012.

[7] J.G. Jakobsen, T.L. Jørgensen, I. Chorkendorff, J. Sehested, Steam and CO2 reforming of methane over a Ru/ZrO2 catalyst, Appl. Catal. A Gen. 377 (2010) 158-166.

[8] J.P. Van Hook, Methane-steam reforming, Catal. Rev. 21 (1980) 1-51.

[9] P.S. Roy, C.S. Park, A.S.K. Raju, K. Kim, Steam-biogas reforming over a metal-foam-coated (Pd–Rh)/(CeZrO2–Al2O3) catalyst compared with pellet type alumina-supported Ru and Ni catalysts, J. CO2 Util. 12 (2015) 12-20.

[10] P.S. Roy, A.S.K. Raju, K. Kim, Influence of S/C ratio and temperature on steam reforming of model biogas over a metal-foam-coated Pd–Rh/(CeZrO2–Al2O3) catalyst, Fuel 139 (2015) 314-320.

[11] P.S. Roy, N-K. Park, K. Kim, Metal foam-supported Pd–Rh catalyst for steam methane reforming and its application to SOFC fuel processing, Int. J. Hydrogen Energy 39 (2014) 4299-4310.

[12] S.D. Angeli, L. Turchetti, G. Monteleone, A.A. Lemonidou, Catalyst development for steam reforming of methane and model biogas at low temperature, Appl. Catal. B Environ. 181 (2016) 34-46.

[13] W. Cho, H. Yu, W.S. Ahn, S.S. Kim, Synthesis gas production process for natural gas conversion over Ni–La2O3 catalyst, J. Ind. Eng. Chem. 28 (2015) 229-235.

[14] J. Károlyi, M. Németh, C. Evangelisti, G. Sáfrán, Z. Schay, A. Horváth, F. Somodi, Carbon dioxide reforming of methane over Ni–In/SiO2 catalyst without coke formation, J. Ind. Eng. Chem. 58 (2017) 189-201.

[15] F. Meshkani, M. Rezaei, M. Andache, Investigation of the catalytic performance of Ni/MgO catalysts in partial oxidation, dry reforming and combined reforming of methane, J. Ind. Eng. Chem. 20 (2014) 1251-1260.

[16] J.E. Min, Y.J. Lee, H.G. Park, C. Zhang, K.W. Jun, Carbon dioxide reforming of methane on Ni–MgO–Al2O3 catalysts prepared by sol–gel method: Effects of Mg/Al ratios, J. Ind. Eng. Chem. 26 (2015) 375-383.

[17] M. Khajenoori, M. Rezaei, F.J. Meshkani, Dry reforming over CeO2-promoted Ni/MgO nano-catalyst: Effect of Ni loading and CH4/CO2 molar ratio, Ind. Eng. Chem. 21 (2015) 717-722.

[18] F. Meshkani, M. Rezaei, High-temperature water-gas shift reaction over nanostructured Cr-free Fe2O3Al2O3CuOMO (M: Ba, Ca, Mg and Sr) catalysts for hydrogen production, J. Ind. Eng. Chem. 30 (2015) 353-358.

[19] D.W. Jeong, W.J. Jang, H.S. Na, J.O. Shim, A. Jha, H.S. Roh, Comparative study on cubic and tetragonal Cu–CeO2–ZrO2 catalysts for water gas shift reaction, J. Ind. Eng. Chem. 27 (2015) 35-39.

[20] F. Mirzaei, M. Rezaei, F. Meshkani, Z. Fattah, Carbon dioxide reforming of methane for syngas production over Co–MgO mixed oxide nanocatalysts, J. Ind. Eng. Chem. 21 (2015) 662-667.

[21] B.V. Ayodele, C.K. Cheng, Modelling and optimization of syngas production from methane dry reforming over ceria-supported cobalt catalyst using artificial neural networks and Box–Behnken design, J. Ind. Eng. Chem. 32 (2015) 246-258.

[22] H.R. Forutan, E. Karimi, A. Hafizi, M.R. Rahimpour, P. Keshavarz, Expert representation chemical looping reforming: A comparative study of Fe, Mn, Co and Cu as oxygen carriers supported on Al2O3, J. Ind. Eng. Chem. 21 (2015) 900-911.

[23] O.A. Bereketidou, M.A. Goula, Biogas reforming for syngas production over nickel supported on ceria–alumina catalysts, Catal. Today 195 (2012) 93-100.

[24] S. Ahmed, S.H.D. Lee, M.S. Ferrandon, Catalytic steam reforming of biogas–Effects of feed composition and operating conditions, Int. J. Hydrogen Energy 40 (2015) 1005-1015.

[25] P.K. Cheekatamarla, C.M. Finnerty, Reforming catalysts for hydrogen generation in fuel cell applications, J. Power Sources 160 (2006) 490-499.

[26] M.P. Kohn, M.J. Castaldi, R.J. Farrauto, Auto-thermal and dry reforming of landfill gas over a Rh/γAl2O3 monolith catalyst, Appl. Catal. B Environ. 94 (2010) 125-133.

[27] P.G. Schulz, M.G. Gonzalez, C.E. Quincoces, C.E. Gigola, Methane Reforming with Carbon Dioxide. The Behavior of Pd/α-Al2O3 and Pd−CeOx/α-Al2O3 Catalysts, Ind. Eng. Chem. Res. 44 (2005) 9020-9029.

[28] D. Li, Y. Nakagawa, K. Tomishige, Methane reforming to synthesis gas over Ni catalysts modified with noble metals, Appl. Catal. A Gen. 408 (2011) 1-24.

[29] V. Palma, A. Ricca, E. Meloni, M. Martino, M. Miccio, P. Ciambelli, Experimental and numerical investigations on structured catalysts for methane steam reforming intensification, J. Clean. Prod. 111 (2016) 217-230.

[30] A. Ricca, V. Palma, M. Martino, E. Meloni, Innovative catalyst design for methane steam reforming intensification, Fuel 198 (2017) 175-182.

[31] S. Cimino, L. Lisi, G. Russo, R. Torbati, Effect of partial substitution of Rh catalysts with Pt or Pd during the partial oxidation of methane in the presence of sulphur, Catal. Today 154 (2010) 283-292.

[32] D. Pakhare, J. Spivey, A review of dry (CO 2) reforming of methane over noble metal catalysts, Chem. Soc. Rev. 43 (2014) 7813-7837.

[33] V. Dal Santo, A. Gallo, A. Naldoni, M. Guidotti, R. Psaro, Bimetallic heterogeneous catalysts for hydrogen production, Catal. Today 197 (2012) 190-205.

[34] M.H. Halabi, M.H. De Croon, J. Van der Schaaf, P.D. Cobden, J.C. Schouten, Low temperature catalytic methane steam reforming over ceria–zirconia supported rhodium, Appl. Catal. A Gen. 389 (2010) 68-79.

[35] X. Wang, R.J. Gorte RJ, A study of steam reforming of hydrocarbon fuels on Pd/ceria, Appl. Catal. A Gen. 224 (2002) 209-218.

[36] J. Wei, E. Iglesia, Structural requirements and reaction pathways in methane activation and chemical conversion catalyzed by rhodium, J. Catal. 225 (2004) 116-127.

[37] F. Pompeo, D. Gazzoli, N.N. Nichio, Stability improvements of Ni/α-Al2O3

catalysts to obtain hydrogen from methane reforming, Int. J. Hydrogen Energy 34 (2009) 2260-2268.

[38] S.D. Angeli, G. Monteleone, A. Giaconia, A.A. Lemonidou, State-of-the-art catalysts for CH4 steam reforming at low temperature, Int. J. Hydrogen Energy 39 (2014) 1979-1997.

[39] M.A. Goula, N.D. Charisiou, G. Siakavelas, L. Tzounis, I. Tsiaoussis, P. Panagiotopoulou, G. Goula, I.V. Yentekakis, Syngas production via the biogas dry reforming reaction over Ni supported on zirconia modified with CeO2 or La2O3 catalysts, Int. J. Hydrogen Energy 42 (2017) 13724-13740.

[40] F. Pompeo, D. Gazzoli, N.N. Nichio, Characterization of α-Al2O3 supports modified with CeO2 and ZrO2, Mater. Letters 63 (2009) 477-479.

CHAPTER 4 TECHNO-ECONOMIC AND LIFE CYCLE ANALYSIS OF CO_2 CONVERSION TO METHANOL THROUGH BI-REFORMING

4.1 Abstract

Technology options to convert CO_2 into higher value fuels and chemicals are currently not commercially available. CO_2 conversion to chemicals or fuel can improve renewable and non-renewable carbon-based energy production economics while significantly decreasing the net CO_2 emissions. This study evaluates techno-economic and life cycle analysis of methanol production through the bi-reforming pathway. Bi-reforming is the reforming of methane with steam and CO_2 and has the potential to reduce greenhouse gas emissions compared to conventional process. The study was conducted in three different parts: material and energy balance of the process, process economics and the life cycle assessment of the process. An Aspen Plus based process model was developed to calculate the material and energy balances for the proposed pathway. The process simulation model estimates the process thermal efficiency for the bi-reforming process is 71.7%. Economic analysis conducted using a discounted cash flow model shows that the process has the potential to be commercially viable. The life cycle analysis was conducted using the GHGenius model for the proposed pathway and the conventional steam methane reforming based methanol production pathway. Greenhouse gas emissions from the conventional steam methane reforming based methanol production is 497 kilograms of CO_2e/tonne of methanol whereas the emissions from the proposed bi-reforming based process is 203 kilograms of CO_2e/tonne of methanol produced on an LHV basis. The proposed pathway

can potentially decrease the GHG emissions from an industrial methanol production process by one million tonnes per year through a single commercial scale plant.

4.2 Introduction

Methanol is an intermediate product that is commonly used to produce formaldehyde, dimethyl ether, esters, and other chemicals and used as a fuels, pesticides, and medicines and in various industrial processes [1]. The primary raw material for methanol production is natural gas although methanol can be produced from renewable biomass or even CO_2 in the atmosphere. Converting CO_2 into commercially valuable products can improve the economic viability of renewable and non-renewable carbon-based energy production by creating additional revenue streams while significantly decreasing net Greenhouse Gas (GHG) emissions [2–4]. Technology to convert CO_2 into higher value fuels and/or chemicals such as processes for methanol and dimethyl ether (DME) production are commercially feasible under very few circumstances and the search for improved technologies is ongoing.

Synthetic gas (syngas) is raw material for methanol synthesis and steam methane reforming (SMR) is the primary pathway for syngas production. The methanol synthesis process is energy intensive and production from fossil or renewable fuel contributes GHG emissions. There are a number of LCAs of methanol production using natural gas, and the majority have studied SMR. Avishai et. al., investigated the economics of methanol production process from natural gas and reported the production cost is around US $400/ton of methanol in Australia [5]. However, the study didn't perform GHG emission from the

production process. The simulation study performed by Bonfim-Rocha et. al., reports that production costs is in the range of 510-620 $/tonne methanol with a GHG consumption of 1105-1596 kg CO_2-e/tonne of methanol produced in a small process 1136-1988 tonnes of methanol per year [6] using CO_2 supplied from a fermentation process in ethanol production distilleries and hydrogen from electrolyzing treated water of the distilleries. The emission from hydrogen production is considered out of the system boundary in this study. The study compared the cost analysis with Pérez-Fortes et al., and reported that production cost is 620 $/tonne methanol with GHG emission of 1234 kg CO_2-e/tonne of methanol produced when emission from H_2 production process is considered [7]. The LCA and economic assessment study performed by Li et. al., reported that the methanol production cost from coke oven gas (consisting H_2, CO, CH_4, CO_2) lower than that of coal and natural gas routes by 25.1% and 19.8%, respectively [8]. Another study performed by Kim et. al., reported the methanol synthesis cost is around US $450/ton produced from CO_2 using solar-thermal energy [9]. Iaquaniello et. al., claimed that the alternative process for methanol production from waste has the potential to reduce the emission by 40% with respect to the production from natural gas and the production cost is less than the market price (with a return of investment 29%) [10].

Typically, GHG emissions from methanol production process range between 500 kg CO_2-eq/tonne methanol for steam reforming and 1400 kg CO_2-eq/tonne methanol for partial oxidation of residual oil which is about 760 kg CO_2-eq/tonne methanol in European plants [7]. Brynolf et. al., reported the emission of 1566 kg CO_2-e/tonne of methanol production from steam methane reforming based methanol production and biomass based methanol

production pathways [11]. In another study performed by Kim et. al., shows relatively small GHG emission of 670 kg CO_2-e/tonne of methanol produced by steam methane reforming pathways [12] whereas GHG emission is about 800 kg CO_2-e/tonne of methanol produced by similar pathway reported by Hoppe et. al., [13]. Reno et al., evaluated a case study of a 100,000 t/y methanol plant, using sugarcane bagasse as raw material and their study shows that every ton of methanol synthesis process generates about 1830 kg of CO_2 and 928 g NO_x, 524 g SO_2, 930 gm PM [14]. The coke oven gas route produces about 1200 kg GHG/tonne of methanol produced in WTT analysis. Li et. al., studied the coal based methanol synthesis in China: coal gasification technology, coal coking technology [15]; coal gasification based process emits about 17700 kg and coal coking technology emits about 2890 kg of CO_2-eq GWP per ton of methanol produced. Study performed by Yao et. al., considers 4 different methanol production pathways for the comparison [16]: coal based methanol production emits about 6356 kg CO_2-e/tonne of methanol whereas coke oven gas based, conventional natural gas based and shale gas based production pathways produces about 4313, 3360 and 4226 kg CO_2-e/tonne of methanol, respectively.

Michael et. al., presented the LCA study of methanol synthesis from renewable hydrogen and CO_2 where the hydrogen is collected from electrolysis of wind farm electricity and CO_2 is collected from biomass fermentation [17]. The study was performed for a 96.7 tonne MEOH/day plant using GREET model and showed about 82-86% reduction in Well to Tank GHG emission for methanol production. The study by Matzen et al., reports the CO_2 consumption is 1050 kg /tonne methanol produced by CO_2 hydrogenation when the electricity is used for hydrogen production obtained from wind energy [18].

Syngas produced via SMR has a H_2/CO ratio higher than three and requires conditioning to adjust the H_2/CO ratio essential for favorable methanol synthesis [19]. Dry reforming (DR), reforming of methane in the presence of CO_2 but without steam, is an alternative for syngas production. Although the dry reforming reaction consumes CO_2, the energy requirement for dry reforming is higher compared to conventional steam reforming. DR is prone to coke formation [20] and a small amount of steam addition improves the gasification of deposited carbon [21]. Bi-reforming, the idea of adding steam with dry reforming, is the reforming of methane in the presence of steam and CO_2. The major reactions involved in the bi-reforming process are listed below [22]:

SMR: $CH_4 + H_2O \rightarrow 3H_2 + CO$	$\Delta H^\theta = 206.1$ kJ/mol	eq 4-1
WGS: $CO + H_2O \rightarrow H_2 + CO_2$	$\Delta H^\theta = -41.2$ kJ/mol	eq 4-2
DR: $CH_4 + CO_2 \rightarrow 2H_2 + 2CO$	$\Delta H^\theta = 247.3$ kJ/mol	eq 4-3
CH_4 dehydrogenation: $CH_4 \rightarrow 2H_2 + C$	$\Delta H^\theta = 74.8$ kJ/mol	eq 4-4
Bi-reforming: $3CH_4 + 2H_2O + CO_2 \rightarrow 8H_2 + 8CO$	$\Delta H^\theta = 659.5$ kJ/mol	eq 4-5

Recent studies have shown that bi-reforming has the potential to convert CO_2 into higher value products, particularly methanol and it derivatives [23]. Traditionally methanol is produced from syngas obtained via the steam methane reforming of natural gas. The syngas is catalytically converted to methanol via an exothermic reaction at temperatures of 210-270˚C and pressures of 50-100 bar [24,25]:

$$CO + 2H_2 \rightarrow CH_3OH \qquad \Delta H^{\theta} = -49.2 \text{ kJ/mol} \qquad \text{eq 4-6}$$

The bi-reforming reaction has been experimentally studied over a number of catalysts. Olah et. al., used an input molar ratio 3/2.4/1.2 for $CH_4/H_2O/CO_2$ and observed stable activity over a NiO/MgO catalyst for 320 h with a product H_2/CO ratio of 2/1 [23]. An industrially significant result reported in this study was that the H_2/CO ratio in the product gas could be adjusted by changing the CO_2/H_2O ratio of the feed. Similar results have been reported by Choudhary et al. [26–29], where they studied the effect of reactant composition on the H_2/CO ratio for the oxy-CO_2 methane reforming process. For bi-reforming reactions carried out by the same group [30,31], the product H_2/CO ratio varied from 1.5 to 2.5 for varying concentrations of stream and CO_2 in the feed.

The overall reaction for the bi-reforming based methanol production pathway is:

$$3CH_4 + 2H_2O + CO_2 \rightarrow 8H_2 + 4CO \rightarrow 4CH_3OH \qquad \text{eq 4-7}$$

SMR based methanol synthesis is a well-established commercial process whereas the bi-reforming process is still under development and there is a need to carefully evaluate this approach. The study performed by Luu et. al., reported WTT GHG emission is about 1858 kg/ tonne of methanol produced from bi-reforming process combined with methanol synthesis process [32]. The study also compared the CO_2 emission process from steam methane reforming, dry reforming based methanol synthesis as 1909 and 1582 kg/ tonne of methanol.

Methanol is high volume and high demand chemicals as methanol is used as the feedstock for other chemicals or directly used for different purpose. Industrially methanol is produced from syngas which is a versatile chemical. Power or electricity generation process received a significant attention for low carbon intensity whereas most of the chemical synthesis process is lacking the production with low carbon footprint. In order to produce methanol or syngas with low carbon footprint the process either require CO_2 capture and sequestration (CCS) or producing from renewable resources or alternate pathways. Both CCS enhanced and renewable resource (i.e., biomass is a distributed resource) based process are location/resource limited due to the huge size of methanol production plant. To reduce GHG alternative pathways for methanol production is essential and steam reforming step of the methanol production replaced with bi-reforming step may be a viable alternative. The goal of this study is to evaluate carbon intensity and economic viability of bi-reforming based methanol synthesis pathway. The study used current conversion data from most up to date literature and state of the art industry data off the shelf technologies except for the bi-reforming stage. An Aspen Plus based process model was developed and used to evaluate the material and energy balances for a bi-reforming based methanol production plant. The process simulation results were used to perform economic analysis and life cycle analysis of the pathway. The results are compared to the SMR based pathway.

4.3 Materials and Methods

The methanol production economics and LCA by CO_2 and steam reforming of methane is conducted in several parts: 1. the methanol production process energy efficiency; 2. the

assumptions for economic analysis and using the excel-based Discounted Cash Flow (DCF) model; 3. GHGenius for estimating the CO_2 footprint for methanol production process.

4.3.1 Simulation model

The Aspen Plus simulation tool was used to calculate the material and energy balances by creating a process model for the pathway including all the major conversion steps. The bi-reforming and methanol synthesis reactors in the Aspen model are simulated using the built-in stoichiometric reactor modules. The model also consists of a number of process units including furnaces, heat exchangers, compressors, distillation columns, etc. Figure 4-1 shows the process flow diagram of the combined process. The CO_2 produced from the furnaces is released to the atmosphere. The syngas from the reformer is then sent to a methanol synthesis reactor to generate the final product. Bi-reforming process parameter inputs for the Aspen model, including CH_4 and CO_2 conversion at specific temperatures were taken from experimental data published by Kumar et. al., [33]. Input variables such as efficiencies and the production steps are based on literature values [33–39].

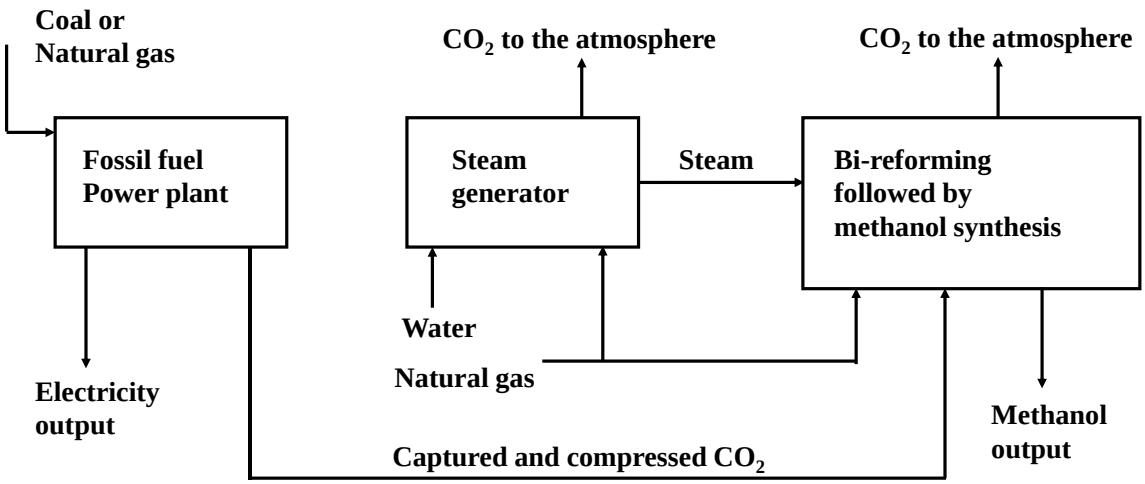

Figure 4-1: The bi-reforming reactor system coupled with methanol synthesis and carbon capture and compression.

The process conditions such as pressure & temperatures are based on thermodynamic analysis of the systems are listed below:

1. Bi-reformer is operated at 25 atmospheric pressure. Feed ratio used for the bi-reformer is $CH_4/CO_2/H_2O$ = 3/1/2. Depending on the operating temperature of the bi-reformer different conversion level is achieved: the conversion level is 86.7% at 850 ºC, 92.9% at 900 ºC and 96.6% at 950 ºC.

2. Methanol synthesis reactor is operated at 265 ºC and 45 atm pressure and feed inlets to the reactor is at the same condition. H_2/CO ratio at inlet is 2 & H_2/CO_2 is 3. Only 5% CO, 5% CO_2 inlet to reactor is converted to methanol.

3. Furnace for heat generation is operated either at 900 ºC or 950 ºC and 5 atm pressure. 100% of the combustible components burned inside the furnace in presence of 40% excess air.

Major assumptions are listed below and are based on standard practices of existing commercial syngas and hydrogen production facilities [35].

1. The model uses the Peng-Robinson equation of state for thermodynamic calculations.

2. The model uses the experimental data published by Kumar et. al., [33].

3. The energy required for CO_2 separation from a coal based power plant is assumed to be 4.32 GJ/tonne of CO_2 [38]. The CO_2 separation step is not simulated using Aspen Plus but the energy requirement is included in the process energy efficiency calculations.

4. Natural gas (CH_4) and CO_2 are assumed to be supplied to the plant at 13.8 atm pressure and 25 °C whereas water and air enter at ambient temperature and pressure.

5. Heat required for the bi-reforming reaction, steam generation etc. are supplied by combustion of CH_4 and recovered combustible gases in presence of 40% excess air.

6. The input gases are compressed using a multistage positive displacement compressor. The mechanical efficiency of the compressor is 70% and of the pump used for water supply is 65% [36,37].

7. The bi-reformer is operated at 25 atm pressure and 900 °C (other temperatures including 850 and 950 °C as part of the optimization process) [34]. The input CH_4/CO_2/steam ratio is maintained at 3/1/2.

8. Produced syngas goes through a separator before entering the methanol synthesis system. The syngas is mixed with unreacted CH_4, CO_2 and steam. The separator removes the CH_4, CO_2 and steam. The separation process also removes 25% CO and 20~25% H_2 from the syngas.

9. Methanol synthesis reactor operates at 265 °C, 45 bar and 5% of the CO is converted to CH_3OH per pass [40–45].

10. The methanol synthesis reaction is an exothermic reactor, and the product methanol is mixed with water at the reactor outlet which requires purification by distillation. Heat generated from the methanol synthesis reactor is utilized in the distillation column to improve the process efficiency.

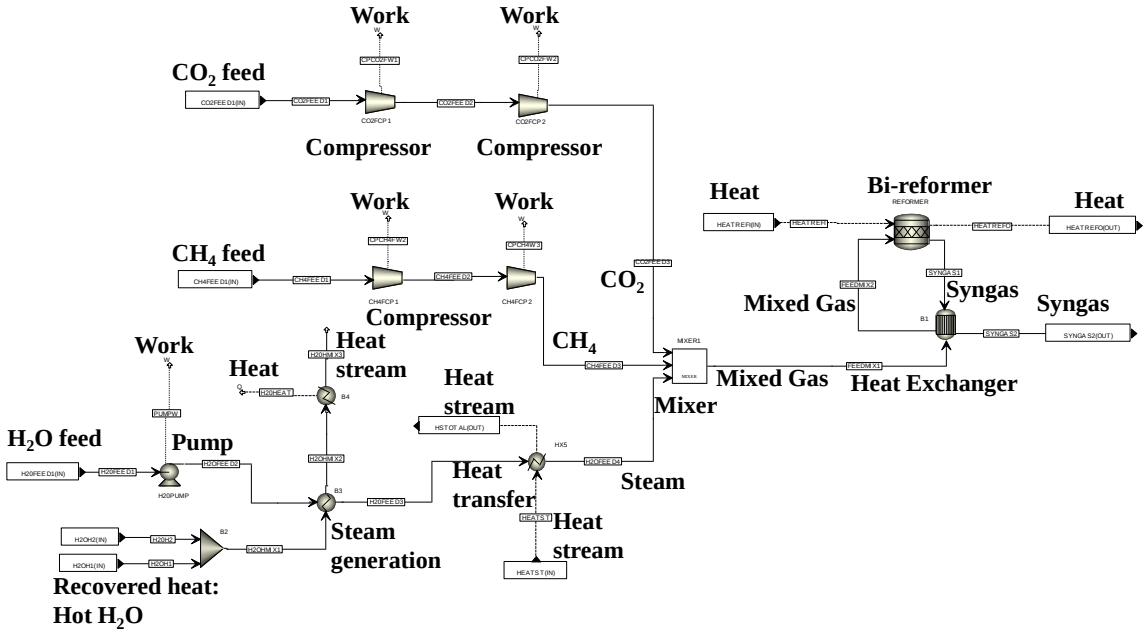

Figure 4-2: The bi-reforming reactor system for the combined process.

The bi-reforming section of the Aspen model is shown in Figure 4-2. This includes feed preparation, steam generation, the bi-reforming reactor, and auxiliary equipment. The syngas conditioning and methanol synthesis reactor system are shown in Figure 4-3. Process efficiency is defined as follows.

Overall process thermal efficiency =

$$\frac{MJ/s\ of\ the\ product\ MEOH + MJ/s\ of\ heat\ stream\ output}{MJ/s\ of\ CH_{4_{in}} + MJ/s\ of\ additional\ fuel_{in} + MW\ of\ the\ compressor\ and\ electrical\ system + MJ/s\ of\ CO_2\ spearation}$$

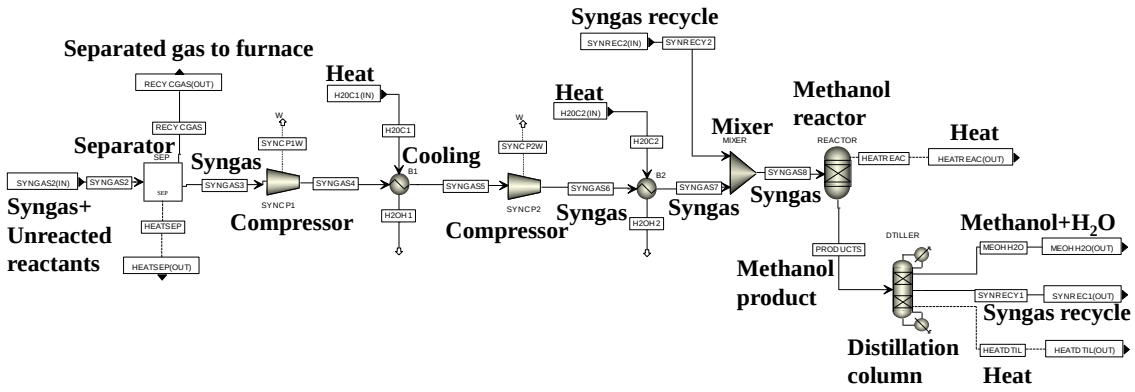

Figure 4-3: The methanol synthesis reactor system for the combined process.

4.3.2 Economic analysis

The economic analysis was conducted using an Excel-based Discounted Cash Flow (DCF) model. This model is a modified version of the Power Systems Financial Model (PSFM) developed by the National Energy Technology Laboratory of the US Department of Energy [46]. The PSFM model calculates the investment decision criteria used by energy project

developers to evaluate the financial performance of energy production systems. The key assumptions used in the economic analysis are:

- Plant Capacity: 10,000 metric tonnes per day (TPD) of methanol produced
- Plant on-stream percentage: 91.3% (8,000 hours of operation per year)
- Location: Alberta, Canada
- Capital cost for the plant: $1.26 billion
- Debt/Equity: 70/30 % (loan period - 15 years)
- Plant life: 30 years
- Loan interest rate: 10%
- Inflation rate: 3%
- Construction and startup: 4 years
- Operating & maintenance costs: 5% of EPC costs (Fixed O&M + Variable O&M: Fixed O&M costs: 3.5% of EPC costs. Variable O&M costs: 1.5% of EPC costs)
- Process thermal efficiency: 71.7% (includes the energy needed to capture, concentrate, and compress the CO_2 from the point source)
- Carbon capture and sequestration (CCS) percentage: none
- Natural gas prices: $3.50 to $6.00 per GJ (Natural gas prices are based on past and projected prices for Alberta, Canada)
- Methanol sales price: $400 to $500 $/metric tonne (Methanol prices are based on past and projected prices for Canada)

- CO_2 cost: the cost associated with CO_2 capture, conditioning, compression and delivery is assumed to be $40 per metric tonne of CO_2.
- All monetary values are in Canadian dollars unless otherwise specified.

4.3.3 Life cycle analysis model

LCA models iteratively calculate the energy use and emissions associated with specific pathways using large databases consisting information on various stages of the pathways and some user-specified input values. The LCA was conducted using the GHGenius model (Version 4.03). GHGenius is an LCA tool developed for Natural Resources Canada over the past decade [47]. The model can evaluate a number of conventional and alternative fuels and production pathways. The GHGenius model was chosen since it has the best database of Canadian information for all the pathways and provides the option to perform the calculations for specific provinces such as Alberta. This study was aimed at evaluating GHG reductions from implementing the proposed approach in Alberta. The process efficiency for LCA is calculated using the Aspen Plus process model as described earlier. Only the GHG emissions are considered in the LCA and the criteria pollutant emissions are not discussed. WTW studies are typically conducted as "Well to Tank" and "Tank to Wheel" calculations for fuels. The final product in this study is methanol and end use of the methanol depends on a number of factors. Therefore, the calculations presented here are only on a "Well to Tank" basis, although the term LCA is used to refer to the calculations. The LCA conducted for "baseline" pathway involves the steam reforming of natural gas followed by methanol synthesis and study of the proposed "bi-reforming"

pathway involves syngas production using the bi-reforming reaction followed by methanol synthesis. The analysis year for this study is 2013.

4.3.3.1 Baseline Case Pathway: The baseline case considers the synthesis of methanol using conventional steam reforming technology as currently practiced in Alberta, Canada. The efficiency of the methanol conversion process has a large impact on the GHG emissions produced. Existing SMR methanol plants consume about 35.8 GJ/t of methanol produced, at a HHV efficiency of 63.3%. New combined reforming facilities can reduce gas consumption to 30.0-31.2 GJ/t (72.5-75% energy efficiency HHV). The basis for the modeling is 31.8 GJ/t in the year 2000, improving at the rate of 0.2% per year to the year 2010. The gas requirement in 2010 is 31.2 GJ/t. This amounts to a thermal efficiency of 73.42%. The plant is assumed to produce its own electricity and the energy for that is included in the gas consumption.

The plant produces its own electricity and the energy for that is included in the gas consumption. The average natural gas transportation distance in pipeline is 373 km. The distribution of methanol may involve water transport, depending on where the plant is built, as well as rail and truck transport. The base case modeled here assumes that the methanol transportation involves 1700 miles by rail and 75 miles by truck. The 1700 miles is the current weighted average rail distance that product methanol moves from the Methanex plant in Medicine Hat, Alberta to Canadian customers. The model assumes that the methanol plant is close to the source of gas and it is assumed that the relative distance for the transport of the feedstock is 12% of the average transport distance for other gas uses such as hydrogen plants, and commercial and residential applications. With a large enough

demand for methanol it is possible that it could be moved by pipeline, which is more energy efficient than rail transport.

4.3.3.2 Bi-reforming Pathway: The bi-reforming pathway option considers the synthesis of methanol through the proposed new bi-reforming technology option as it would be implemented in commercial scales in Alberta, Canada. This pathway uses all the assumptions and data from the Baseline Case pathway except for the methanol plant thermal efficiency, the CO_2 feed stream and related aspects. The thermal efficiency of the bi-reforming based methanol plant is calculated using the Aspen Plus process simulation tool.

The bi-reforming reactor is simulated using a built in stoichiometric reactor module in Aspen Plus. The heat necessary for the reforming process is assumed to be supplied by a natural gas-fired furnace similar to the furnaces used in the steam reforming process. The thermal efficiency of the furnace is assumed to be 90% [48]. The fuel input to the reformer furnace is calculated to be twice the energy required based on the heat of reaction of the bi-reformer. Thermal efficiency of bi-reforming step is 71.7%. The excess heat generated by the furnace is recovered and used for operating the auxiliary systems in the plant. These assumptions are based on standard practices of existing commercial syngas and hydrogen production facilities [35,48].

Since the baseline and the proposed pathway both produce an identical product (industrial quality methanol), the emissions during the 'Tank to Wheels' portion will also be identical for both options.

4.4 Results and discussion

4.4.1 Aspen plus process simulation

The bi-reforming reactor is simulated using a built in stoichiometric reactor module in Aspen Plus simulation model. The bi-reformer is heated using gas-fired furnaces and efficiency of these furnaces approaches 90% [48]. The excess heat generated by the furnace is recovered and used for operating the auxiliary systems in the plant.

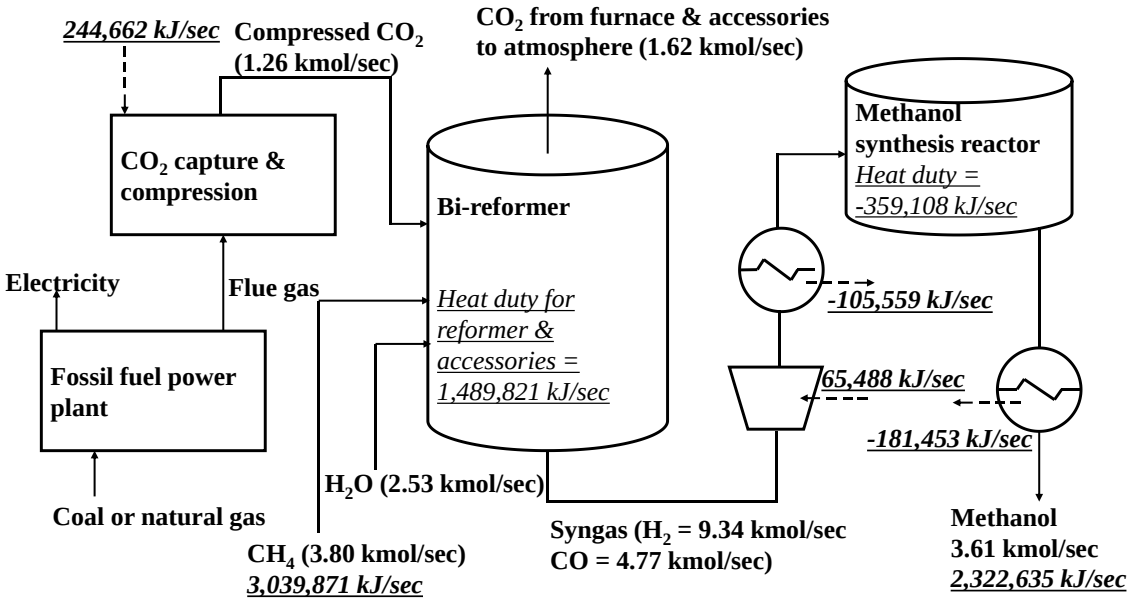

Figure 4-4: Mass and energy flow of bi-reforming process coupled with methanol synthesis (bi-reformer operates at 900 °C).

A block flow diagram of the material and energy balance with relevant stream flow rates of the proposed system is shown in Figure 4-4. The produced syngas has syngas ratio very close to 2 (1.96). In bi-reforming process (Figure 4-1), CO_2 is captured from a large point

source such as a fossil fuel power plant and used as feedstock for the bi-reforming reactor, in which CO_2 reacts with CH_4 and steam to produce syngas. The energy required for the capture, conditioning of the CO_2 is estimated to be 4.32 GJ per metric tonne of CO_2. The process efficiency of the complete process is dependent on the bi-reforming reactor operating temperature. Bi-reformer operating at 800 ºC leads to an overall process efficiency of 58%. The increase in temperature leads to increase in the process thermal efficiency which attenuated to about 65% at temperature in between 850 and 900 °C. The process that runs with conventional steam methane reforming process (CH_4/steam ratio is 1/2.7) operating at 900° C shows overall process thermal efficiency of 67.6%.

4.4.2 Economic analysis

The capital cost for the proposed plant is estimated to be $1.26 billion. The capital cost information for the proposed process is estimated using two different sources. Methanex Corporation, Canada based methanol production company, announced in April 2013 that a planned 1 million tonnes per year methanol plant in Louisiana, USA will cost an estimated US$550 million [46,49]. An independent report by HPI Project Managers Inc. provides estimated capital costs for various sized steam reforming based methanol plants, including a value of US$90,000/ton for a 12,000 TPD plant [50]. These capital cost values are consistent with each other and have been extrapolated using the “six-tenths” rule to estimate the capital cost for the 10,000 TPD plant. The estimated capital cost ($1.05 billion) was then increased by 20% to account for the risks associated with the new technology

option (bi-reforming instead of conventional steam reforming) and the potential complexities associated with the CO_2 supply.

The plant is assumed to be located close to the CO_2 point source so that CO_2 transportation costs are minimized. Alternatively, the plant could be located adjacent to a CO_2 pipeline associated with a carbon capture project. Methanol sales price of $400 to $500 $/metric tonne is based on past and projected prices for Canada.

The economic analysis demonstrates that the proposed pathway has high potential to be profitable even after including additional costs related to the new technology and the CO_2 feed stream. The results for the four scenarios analyzed are presented in Table 4-1.

Table 4-1: Economic analysis of methanol production plant in terms of IRR and NPV at different conditions*.

NG price ($/GJ)	Methanol market price ($/tonne)	Internal Rate of Return (%)	Net Present Value ($, in thousand dollars)
3.50	400	57	3,497,110
6.00	400	39	990,667
3.50	500	71	5,737,839
6.00	500	59	3,231,396

*The payback year on equity is 5 years from the start of the project. NPV is calculated at a 10% discount rate

4.4.3 Life cycle analysis

4.4.3.1 Baseline case pathway

The GHG emissions in CO_2e values for the baseline pathway and bi-reforming pathway stages are shown in Figure 4-5. Land use and cultivation includes emissions of N_2O, NOx, and CH_4 associated with cultivation and the use of fertilizer. Gas leaks and flare includes emissions of H_2S from crude oil tanks. Assumes that flared gas is burned completely to CO_2 and H_2O, with no residual CH_4, NMOC, CO, NOx, N_2O. CO2, H_2S removed from NG includes SO_2 emissions from the incineration of H_2S. Very little H_2S is incinerated; most is recovered as a source of sulfur or sulfuric acid. The emissions displaced are based on the quantity of CO_2 consumed by the plant minus the energy required for the capture, compression and supply of the CO_2. The total GHG emissions from the baseline pathway is 24,745 grams of CO_2e GHGs per GJ of methanol produced (LHV basis). This value is equivalent to 497 kilograms of CO_2e GHGs per metric tonne of methanol produced. The results show that CO_2 constitutes the bulk of the emissions. The “end use” energy values, for example, miles driven for transportation fuels, are not included in these results since the calculations are conducted on a Well to Tank basis.

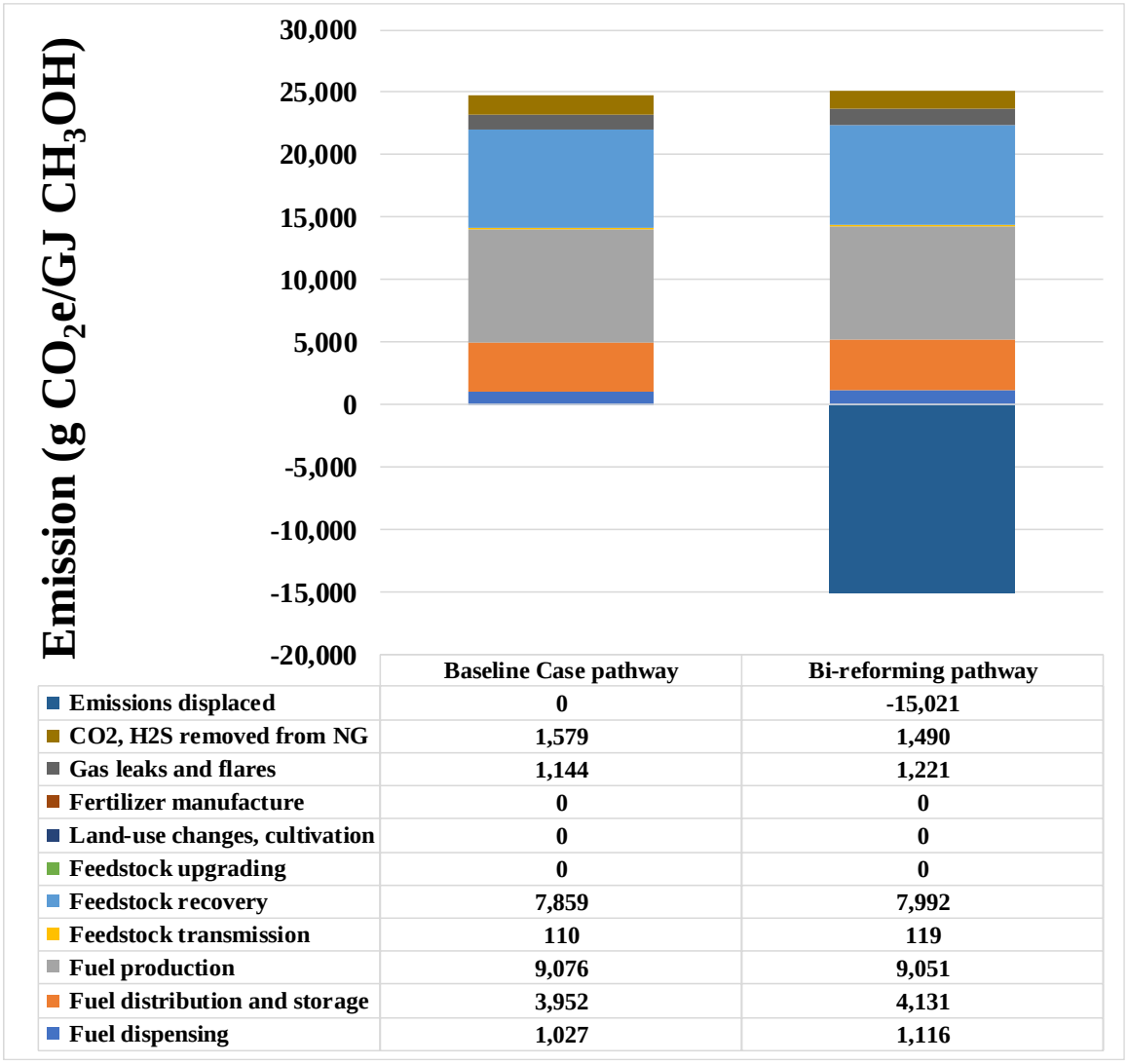

	Baseline Case pathway	Bi-reforming pathway
Emissions displaced	0	-15,021
CO2, H2S removed from NG	1,579	1,490
Gas leaks and flares	1,144	1,221
Fertilizer manufacture	0	0
Land-use changes, cultivation	0	0
Feedstock upgrading	0	0
Feedstock recovery	7,859	7,992
Feedstock transmission	110	119
Fuel production	9,076	9,051
Fuel distribution and storage	3,952	4,131
Fuel dispensing	1,027	1,116
Total, g/GJ	**24,745**	**10,098**
Total, kg CO2e/tonne CH3OH	**497**	**203**

Figure 4-5: The emission analysis compared for baseline case pathway and proposed bi-reforming pathway.

4.4.3.2 Bi-reforming Pathway

The total GHG emissions from the baseline pathway is 10,098 grams of CO_2e GHGs per GJ of methanol produced (LHV basis). This value is equivalent to 203 kilograms of CO_2e GHGs per metric tonne of methanol produced.

The GHG emission reductions achieved through the proposed bi-reforming pathway is calculated directly from the results for the two pathways. GHG emissions based on the Baseline Case pathway is 497 kg CO_2e/tonne of CH_3OH. Therefore, total GHG emissions from the 10,000 TPD plant = 1,723,348 tonnes CO2e/year. The number reduced to 203 kg CO_2e/tonne of CH_3OH and 703,903 tonnes CO_2e/year, respectively. Net reduction in GHG emissions achieved by replacing conventional technology with the proposed bi-reforming pathway in a 10,000 TPD plant is 1,019,445 tonnes CO_2e/year.

Aresta et al. conducted an LCA of methanol synthesis using several pathways, including the options listed below [51].

- Syngas from NG steam reforming
- Syngas from NG steam reforming with limited CO_2 addition
- Syngas from bi-reforming of methane
- CO_2 hydrogenation using hydrogen from water electrolysis

The analysis was conducted using a European plant as the basis for calculations. The study estimates that the CO_2 reduction achieved through the bi-reforming pathway is 0.36 kg CO_2e/kg of CH_3OH. Although this value is slightly higher than the reductions estimated by us (0.29 kg CO_2e/kg of CH_3OH), the values are comparable given the differences in

location and related assumptions. Aresta et al. also conclude that the bi-reforming pathway, if feasible, is the best option from an energetic and GHG emissions perspective, unless renewable electricity is available for water electrolysis resulting in renewable hydrogen production [51].

4.4.4 Uncertainties/Alternate Pathways

The major uncertainties in the analysis are related to the net thermal efficiency of the proposed bi-reforming pathway. To minimize the risk of potential overestimation of GHG emission reductions, a conservative approach was used in determining the process material and energy balances for the bi-reforming pathway. Also, it should be noted that the bi-reforming option includes the energy needed for CO_2 capture, conditioning and compression from the point source as one of the energy inputs to the process. The energy penalty assumed for CO_2 supply is at the higher end of the reported values [52]. If CO_2 is available from an existing capture project or can be captured with a reduced energy penalty (for ex., in a brand new facility), then the thermal efficiency will be further improved.

Data from well-established commercial plants are used for all the steps in the Life Cycle Analysis except for the bi-reformer, and the use of 'advanced state of the art' or 'in the pipeline' types of technology improvements are avoided. As an example, the furnace efficiency of the reformer is assumed to be 90%, although current efficiencies of many such furnaces are around 93% and efficiencies as high as 96% have been reported [53,54]. The uncertainties and the risk of overestimation of GHG benefits are minimized through this conservative approach. On the other hand, the SMR and tri-reforming pathways are

assumed to have higher efficiencies (attributed to future plants) compared to existing facilities [54,55]. The relatively similar GHG benefit results from our calculations compared with the Aresta et al. study mentioned above also indicates that the estimates are sound.

The baseline scenario considered here is the steam reforming based syngas production pathway. This option was chosen because it is the most widely practiced industrial process today. Alternate options include partial oxidation reforming and auto-thermal reforming. These options offer an efficiency improvement of 3-10% over the steam reforming process.

Shale gas based methanol production is another important alternative considering the emergence of shale as a major factor in the North American natural gas market and the resources available in Alberta. Preliminary estimates show that GHG benefits of magnitudes similar to the values reported here can be achieved if the conventional and the bi-reforming process use shale gas resources.

4.5 Conclusions

Chemical/fuel production using CO_2 is essential for future energy as an alternative to current transportation fuel. Methanol is industrially produced from syngas produced via steam reforming of methane. Commercial viability of low carbon intensity methanol production pathway has not received significant focus of improvement. Methanol or syngas production with low carbon footprint is possible to achieve via CCS or using renewable resources or alternate pathways. CCS enhanced and renewable resource are

resource/location limited. Alternative pathways of methanol production involve modifying the existing commercial pathways: the proposed idea is replacing steam methane reforming step with bi-reforming of methane. The study evaluates the economic viability of the proposed low carbon intensity process. The study uses current conversion data from most up to date literature and state of the art industry data off the shelf technologies except for the bi-reforming stage. The reforming of methane with CO_2 (from a fossil fuel based power plant) and steam with controlled reactant ratio produces the syngas with certain H_2/CO ratio required for the methanol production in this study. An Aspen plus process simulation model for a bi-reforming based methanol production process was developed. The process thermal efficiency calculated from the simulation model is used for economic analysis and LCA of the proposed pathway as well as methanol production technology. The LCA is conducted using the 'GHGenius' LCA model. Existing production pathway considers the synthesis of methanol using conventional steam reforming technology as currently practiced in Alberta, Canada whereas proposed bi-reforming pathway considers the synthesis of methanol through the proposed new bi-reforming technology. The major outcomes of this study are:

1. The economic analysis shows that at the methanol sales price of $400/tonne and natural gas price $3.5/GJ the IRR is 57% which drops down to 39% with the change in gas price to $6.0/GJ for the proposed bi-reforming pathway combined with methanol production.

2. The total GHG emissions from the baseline case pathway are estimated to be 497 kilograms of CO_2e GHGs/ tonne of methanol produced on an LHV basis.

The total GHG emissions from the bi-reforming are estimated to be 203 kilograms of CO_2e GHGs/metric tonne of methanol produced on an LHV basis.

3. CO_2 reduction through the proposed bi-reforming pathway is about 0.29 kg CO_2e/kg of CH_3OH.

4. The results show that the proposed pathway can decrease the net GHG emissions from an industrial methanol production process by one million tonnes per year.

Acknowledgements

This work was supported by the Climate Change and Emissions Management Corporation (CCEMC) through a CCEMC Grand Challenge grant. Authors are grateful to Prof. Jerry Spivey at Louisiana State University, Kyle Hunter, Vincent Van and Sean Franco.

4.6 References

[1] C.-J. Yang, R.B. Jackson, China's growing methanol economy and its implications for energy and the environment, Energy Policy 41 (2012) 878-884.

[2] T.H. Gardner, J.J. Spivey, E.L. Kugler, D. Pakhare, CH4-CO2 reforming over Ni-substituted barium hexaaluminate catalysts, Appl. Catal. A Gen. 455 (2013) 129-136.

[3] J. Kothandaraman, A. Goeppert, M. Czaun, G.A. Olah, G.K.S. Prakash, Conversion of CO2 from air into methanol using a polyamine and a homogeneous ruthenium catalyst, J. Am. Chem. Soc. 138 (2016) 778-781.

[4] B. Li, X. Xu, S. Zhang, Synthesis gas production in the combined CO2 reforming with partial oxidation of methane over Ce-promoted Ni/SiO2 catalysts, Int. J. Hydrogen Energy 38 (2013) 890-900.

[5] A. Lerner, M.J. Brear, J.S. Lacey, R.L. Gordon, P.A. Webley, Life cycle analysis (LCA) of low emission methanol and di-methyl ether (DME) derived from natural

gas, Fuel 220 (2018) 871-878.

[6] L. Bonfim-Rocha, M.L. Gimenes, S.H. Bernardo de Faria, R.O. Silva, L.J. Esteller, Multi-objective design of a new sustainable scenario for bio-methanol production in Brazil, J. Clean. Prod. 187 (2018) 1043-1056.

[7] M. Pérez-Fortes, J.C. Schöneberger, A. Boulamanti, E. Tzimas, Methanol synthesis using captured CO2 as raw material: Techno-economic and environmental assessment, Appl. Energy 161 (2016) 718-732.

[8] J. Li, X. Ma, H. Liu, X. Zhang, Life cycle assessment and economic analysis of methanol production from coke oven gas compared with coal and natural gas routes, J. Clean. Prod. 185 (2018) 299-308.

[9] J. Kim, C.A. Henao, T.A. Johnson, D.E. Dedrick, J.E. Miller, E.B. Stechel, C.T. Maravelias, Methanol production from CO2 using solar-thermal energy: process development and techno-economic analysis, Energy Environ. Sci. 4 (2011) 3122-3132.

[10] G. Iaquaniello, G. Centi, A. Salladini, E. Palo, S. Perathoner, L. Spadaccini, Waste-to-methanol: Process and economics assessment, Bioresour. Technol. 243 (2017) 611-619.

[11] S. Brynolf, E. Fridell, K. Andersson, Environmental assessment of marine fuels: liquefied natural gas, liquefied biogas, methanol and bio-methanol, J. Clean. Prod. 74 (2014) 86-95.

[12] J. Kim, C.A. Henao, T.A. Johnson, D.E. Dedrick, J.E. Miller, E.B. Stechel, C.T. Maravelias, Methanol production from CO2 using solar-thermal energy: process development and techno-economic analysis, Energy Environ. Sci. 4 (2011) 3122-3132.

[13] W. Hoppe, N. Thonemann, S. Bringezu, Life cycle assessment of carbon dioxide-based production of methane and methanol and derived polymers, J. Ind. Ecol. 22 (2018) 327-340.

[14] M.L.G. Renó, E.E.S. Lora, J.C.E. Palacio, O.J. Venturini, J. Buchgeister, O. Almazan, A LCA (life cycle assessment) of the methanol production from sugarcane bagasse, Energy 36 (2011) 3716-3726.

[15] C. Li, H. Bai, Y. Lu, J. Bian, Y. Dong, H. Xu, Life-cycle assessment for coal-based methanol production in China, J. Clean. Prod. 188 (2018) 1004-1017.

[16] Y. Yao, Y. Chang, R. Huang, L. Zhang, E. Masanet, Environmental implications of the methanol economy in China: well-to-wheel comparison of energy and environmental emissions for different methanol fuel production pathways, J. Clean. Prod. 172 (2018) 1381-1390.

[17] M. Matzen, Y. Demirel, Methanol and dimethyl ether from renewable hydrogen and carbon dioxide: Alternative fuels production and life-cycle assessment, J. Clean. Prod. 139 (2016) 1068-1077.

[18] M. Matzen, M. Alhajji, Y. Demirel, Chemical storage of wind energy by renewable methanol production: Feasibility analysis using a multi-criteria decision matrix, Energy 93 (2015) 343-353.

[19] G.A. Olah, A. Goeppert, M. Czaun, T. Mathew, R.B. May, G.S. Prakash, Single step bi-reforming and oxidative bi-reforming of methane (natural gas) with steam and carbon dioxide to metgas (CO-2H2) for methanol synthesis: self-sufficient effective and exclusive oxygenation of methane to methanol with oxygen, J. Am. Chem. Soc. 137(2015) 8720-8729.

[20] D. Pakhare, J. Spivey, A review of dry (CO2) reforming of methane over noble metal catalysts, Chem. Soc. Rev. 43 (2014) 7813-7837.

[21] M. García-Diéguez, I.S. Pieta, M.C. Herrera, M.A. Larrubia, L.J. Alemany, RhNi nanocatalysts for the CO2 and CO2 + H2O reforming of methane, Catal. Today 172 (2011) 136-142.

[22] J. Xu, G.F. Froment, Methane steam reforming, methanation and water-gas shift: I. Intrinsic kinetics, AIChE J. 35 (1989) 88-96.

[23] G.A. Olah, A. Goeppert, M. Czaun, G.K.S Prakash, Bi-reforming of methane from any source with steam and carbon dioxide exclusively to metgas (CO-2H2) for methanol and hydrocarbon synthesis, J. Am. Chem. Soc. 135 (2013) 648-650.

[24] H.H. Kung, Methanol Synthesis, Catal. Rev. 22 (1980) 235-259.

[25] C.W. Nian, F. You, Design of methanol plant (2013).

[26] V.R. Choudhary, K.C. Mondal, T.V. Choudhary, Oxy-CO2 reforming of methane to syngas over CoOx/MgO/SA-5205 catalyst, Fuel 85(2006) 2484-2488.

[27] V. Choudhary, B. Uphade, A. Mamman, Simultaneous steam and CO2 reforming of methane to syngas over NiO/MgO/SA-5205 in presence and absence of oxygen, Appl. Catal. A Gen. 168 (1998) 33-46.

[28] V.R. Choudhary, K.C. Mondal, CO2 reforming of methane combined with steam reforming or partial oxidation of methane to syngas over NdCoO3 perovskite-type mixed metal-oxide catalyst, Appl. Energy 83 (2006) 1024-1032.

[29] V.R. Choudhary, K.C. Mondal T.V. Choudhary, Oxy-CO2 reforming of methane to syngas over CoOx/CeO2/SA-5205 catalyst, Energy Fuels 20 (2006) 1753-1756.

[30] V.R. Choudhary, A.M. Rajput, Simultaneous carbon dioxide and steam reforming of methane to syngas over NiO−CaO catalyst, Ind. Eng. Chem. Res. 35(1996) 3934-3939.

[31] T.V. Choudhary, V.R. Choudhary, Energy-efficient syngas production through catalytic oxy-methane reforming reactions, Angew. Chemie. Int. Ed. 47 (2008) 1828-1847.

[32] M.T. Luu, D. Milani, A. Bahadori, A. Abbas, A comparative study of CO2 utilization in methanol synthesis with various syngas production technologies, J. CO2 Util, 12 (2015) 62-76.

[33] N. Kumar, A. Roy, Z. Wang, E.M. L'Abbate, D. Haynes, D. Shekhawat, J.J. Spivey, Bi-reforming of methane on Ni-based pyrochlore catalyst, Appl. Catal. A Gen. 517 (2016) 211-216.

[34] J.C. Molburg, R.D. Doctor, Hydrogen from steam-methane reforming with CO2 capture, In 20th annual International Pittsburgh Coal Conference (September 2003) p. 20.

[35] S. Patel, Simplify your thermal efficiency calculation, Hydrocarb. Process. 84 (2005) 63-63.

[36] Foray J. Energy efficiency considerations in pumps and pump stations, http://www.energy.wsu.edu/LinkClick.aspx?fileticket=t3ubiA8D8A4%3D&tabid=692&mid=1345, 2014 [accessed 19 October 2018].

[37] B.P. Meherwan, Principles of operation and performance estimation of centrifugal compressors, In Proceedings of the 22nd Turbomachinery Symposium. Texas A&M University. Turbomachinery Laboratories (1993).

[38] H. Herzog, J. Meldon, A. Hatton, Advanced post-combustion CO2 capture, Clean Air Task Force 1 (2009) 39.

[39] W. Budzianowski, Assessment of thermodynamic efficiency of carbon dioxide separation in capture plants by using gas-liquid absorption, In Energy Effic. Solvents

CO2 Capture by Gas, Springer (2017) 13-26.

[40] National Energy Technology Laboratory. Syngas conversion to methanol, http://www.netl.doe.gov/research/coal/energy-systems/gasification/gasifipedia/methanol [accessed 19 October 2018].

[41] National Energy Technology Laboratory. Methanol plant process configuration, http://www.netl.doe.gov/research/Coal/energy-systems/gasification/gasifipedia/process-configurations [accessed 19 October 2018].

[42] Products from Syngas—Methanol (Catalyst),

http://bioweb.sungrant.org/Technical/Bioproducts/Bioproducts+from+Syngas/Methanol/Default.htm [accessed 2014].

[43] Y. Kansha, M. Ishizuka, A. Tsutsumi, Development of innovative methanol synthesis process based on self-heat recuperation, Chem. Eng. Transactions 35 (2013) 37-42.

[44] R.A. Dagle, V. Lebarbier, J.A. Lizarazo Adarme, D.L. King, Y. Zhu, M.J. Gray, S.B. Jones, M.J. Biddy, R.T. Hallen, Y. Wang, J.F. White, Single-step syngas-to-distillates (S2D) synthesis via methanol and dimethyl ether intermediates, No. PNNL-22984. Pacific Northwest National Lab.(PNNL), Richland, WA (United States), 2016.

[45] T.D. Matson, K. Barta, A.V. Iretskii, P.C. Ford, One-pot catalytic conversion of cellulose and of woody biomass solids to liquid fuels, J. Am. Chem. Soc. 133 (2011) 14090-14097.

[46] Power Systems Financial Model Version 6.6 User's Guide, No. DOE/NETL-2011/1492. National Energy Technology Laboratory (NETL), 2011.

[47] GHGenius. A model for lifecycle assessment of transportation fuels,

https://www.ghgenius.ca/ [accessed July 18, 2017].

[48] P. Mullinger, B. Jenkins, Industrial and process furnaces principles, design and operation, Elsevier 2011.

[49] Methanex Corporation. 2012 Annual Report,

https://www.methanex.com/sites/default/files/investor/annual-reports/Methanex-

2012-Annual-Report.pdf [accessed October 19, 2017].

[50] HPI Project Managers Inc. Methanol Prospects and Outlook. 2008.

[51] M. Aresta, A. Caroppo, A. Dibenedetto, M. Narracci, Life Cycle Assessment (LCA) applied to the synthesis of methanol. Comparison of the use of syngas with the use of CO2 and dihydrogen produced from renewables, Environ. Challenges Greenh. Gas Control Foss. Fuel Util. 21st Century, Boston, MA: Springer US; 2002, p. 331-347.

[52] C.E. Daza, S. Moreno, R. Molina, Ce - promoted catalyst from hydrotalcites for CO2 reforming of methane: calcination temperature effect. Quim. Nova 35 (2012) 1325-1328.

[53] M.H. Amin, K. Mantri, J. Newnham, J. Tardio, S.K. Bhargava, Highly stable ytterbium promoted Ni/γ-Al2O3 catalysts for carbon dioxide reforming of methane, Appl. Catal. B Environ. 119 (2012) 217-216.

[54] C.S.V. Ramachandran, V. Balasubramanian, P.V. Ananthapadmanabhan, Thermal cycling behaviour of plasma sprayed lanthanum zirconate based coatings under concurrent infiltration by a molten glass concoction, Ceram. Int. 39 (2013) 1413-1431.

[55] G.T. Rochelle, Amine Scrubbing for CO2 Capture, Science 325 (2009) 1652-1654.

CHAPTER 5 PREDICTING WOBBE INDEX AND METHANE NUMBER OF A RENEWABLE NATURAL GAS BY THE MEASUREMENT OF SIMPLE PHYSICAL PROPERTIES

5.1 Abstract

This study describes a fuel quality prediction strategy that predicts the fuel quality parameter and component composition of Renewable Natural Gas (RNG) containing CH_4, C_2H_6 and CO_2. Onsite measurement of the gas properties in a renewable natural gas (RNG) fuel is necessary to ensure an expected level of quality, which must be maintained for better combustion efficiency. The Wobbe index (WI) and methane number (MN) are the natural gas quality indicators used. To predict the WI, MN, and component composition, a data set that consists of WI, MN, thermal conductivity and sound velocity of the gaseous fuel mixture as a function of its temperature, pressure and composition, was created. Through a regression analysis of the data set, a model that estimates the WI, MN and composition of the gaseous fuel mixture from its physical properties (temperature, pressure, thermal conductivity and sound velocity), was developed. The results of the study including the data set and the prediction model that can accurately estimate the WI, MN, and gas composition, is presented in this paper.

5.2 Introduction

Renewable Natural Gas (RNG), i.e., natural gas produced from renewable feedstocks (e.g., landfill gas, anaerobic digestion gas, etc.) is an important alternative fuel that can aid in

achieving goals set by the local and federal governments related to fossil fuel replacement and greenhouse gas (GHG) emissions reduction. Most RNG production projects are small to medium scale by nature, and comprehensive gas cleanup/upgrading to meet the fuel specifications of pipeline natural gas is often not feasible from an economical perspective. This results in most RNG resources being wasted (e.g., flaring) or being left unused.

The RNG from landfills or anaerobic digestion comes with a significant amount of CO_2: the CH_4 concentration varies from 50 to 70% whereas CO_2 composition varies from 25 to 45% [1, 2]. Upgrading RNG to the quality of a pipeline natural gas requires removal of CO_2 from the biogas as well as purification, drying, and compression. Among these processes, CO_2 removal is the most expensive. It can cost more than $2/mcf [2] which is almost 50% of total upgrading cost.

Typical calorific value of RNG without CO_2 removal is around 50–60% of an equal volume of fossil natural gas and varies significantly by project site and season. Accurate fuel quality predictions can enable a more economic use of RNG without removing CO_2 since the CO_2 separation cost can be avoided. Furthermore, adjustment of the air/fuel ratio and optimization of combustion inside an engine or boiler becomes easy with fuel quality information.

The two most important parameters for the natural gas quality are Wobbe Index (WI) and Methane Number (MN). WI is the ratio of the fuel's calorific value to the square root of its specific gravity or relative density [3]. WI is a critical factor in evaluating the interchangeability of fuel gases, such as natural gas and liquefied petroleum gas (LPG), by

comparing the combustion energy output between the different compositions of fuel gases [4]. Two fuels having identical WI have the identical energy output under the same operating conditions. Therefore, WI is used in a wide variety of equipment and processes that require a specific NG combustion energy output. However, WI is typically measured using bulky and expensive analyzers. These devices measure the energy value of the fuel via direct calorimetry followed by a separate measurement of density using an optical method. The complexity of the existing WI measurement systems prevents its off-site application.

The MN of a gaseous fuel is defined as the methane composition (vol%) combined with hydrogen that makes the same knocking of the gas fuel under specified operating conditions in a knock testing engine [5]. A different engine has a different MN range for suitable working conditions. MN is an important parameter in measuring engine performance, especially when the fuel is from a renewable source with a high possibility of MN variation. Traditionally, MN is calculated from the gas composition. The gas composition can be measured by gas chromatography (GC) or residual gas analyzer (RGA), which is time consuming and requires a laboratory environment.

There are methods and apparatuses available for measuring the calorific value of a gas by measuring the thermal conductivity of a gas [6]. Lotters et al., proposed an on-chip system that measures the energy content of fuel gases such as natural gas, biogas and hydrogen [7]. A thermal conductivity microsensor system proposed and developed by Puente et al., shows that the device is able to detect the thermal conductivity of the gaseous fuel mixture with minimal error, but the effect of temperature variation was not studied [8]. Rahmouni

et al., proposed an approach to measure the MN and lower the heating value of a gas for certain temperatures and thermal conductivities [9]. A wide variation or range of temperature and pressure were not available in the study.

Several other previous studies attempt to determine the composition, energy content, or thermal conductivity of a gas [10-12]. Gutierrez proposed using a thermal conductivity microsensor to measure the MN [13], but no practical application or implementation of the idea was shown in the study. Another study, Lotters et al. designed and implemented an analytical calculation model to determine the composition of gaseous fuel mixtures in real-time. However, they did not report the effects caused by the compressibility of the gaseous fuel mixture and temperature in their model [14].

The gas components used here are CH_4, C_2H_6 and CO_2. The thermal conductivity of methane is about twice of the thermal conductivity of CO_2 makes it easily distinguishable to detect the difference as shown in Table 5-1. Whereas the thermal conductivity of C_2H_6 is 25% more than the thermal conductivity of CO_2.

Table 5-1: The thermal conductivity of the CH_4, C_2H_6 and CO_2 gases [15].

Gases	**Thermal Conductivity, mW/mK @ RT**
CH_4	34.4
C_2H_6	21.2
CO_2	16.8

The sound velocity of methane is about 67% more than the sound velocity of CO_2 as shown in Table 5-2. The sound velocity of C_2H_6 is 18% more than the sound velocity of CO_2.

Table 5-2: The sound velocity of the CH_4, C_2H_6 and CO_2 gases.

Gases	**Sound velocity, m/s @ RT**
CH_4	453
C_2H_6	318
CO_2	270

The thermal conductivity of the ideal gas mixture is calculated using the simple relationship in between pure component thermal conductivity and the gas composition. The sound velocity of the gas mixture is complex and calculated using complex relation of molecular weight and the ratio of specific heats of the gas mixture. Both thermal conductivity and sound velocity varies over a wide range of more than 65% from the lowest value.

There are sensors available in market for CO_2 concentration measurement in the environmental (atmospheric air) condition not all of them are working in natural gas condition. Thermal conductivity and sound velocity shows good selectivity between major components in RNG. The thermal conductivity and sound velocity measuring sensors are proved technology, economic, readily available, ruggedness, reliability, and potential to integrate such as Micro-Electro-Mechanical Systems (MEMS) makes it attractive to select as the physical parameter for the gas mixture composition estimation.

As discussed above, results from previous research show that the WI, MN, thermal conductivity (k), and sound velocity (v) are dependent on the temperature, pressure, density, and composition of the gaseous fuel mixture. Limited research also indicates the possibility of estimating MN and gas composition using thermal conductivity and sound velocity instead of using GC or RGA.

In this paper, a predictive model is proposed. The proposed predictive model can accurately and efficiently estimate the WI, MN, and composition of the gaseous fuel mixture based solely on the values of easily measured physical properties (thermal conductivity, sound velocity, temperature, and pressure of the gas) without using an approach such as GC or RGA. The proposed model can accurately predict the quality and composition of gas in real-time. The implementation of the proposed model, equipped with a sensor technology that measures the physical properties, can promote the use of RNG with wide fuel quality variation. It makes easy to adjust air/fuel ratio as well as optimizing combustion inside an engine.

5.3 Development of a Predictive Model

A sizable data set is first required for a statistical data analysis to develop the relevant predictive model. In this study, the collected data set consists of the following attributes: thermal conductivity, sound velocity, temperature, pressure, gas composition, WI, and MN. Attributes in this data set - such as thermal conductivity, sound velocity, temperature, and pressure - are physical properties that depend on the gas composition and can be easily measured using widely available sensors or calculated using software tools against the

gaseous fuel mixture. The other attributes, WI and MN, also depend on the gas composition. Traditional approaches to measuring the gas composition, as well as calculating the WI and MN from these measurements, are time-consuming and expensive. In contrast, the proposed model in this paper accurately estimates in real-time the WI, MN, and composition of the gaseous fuel mixture based on its physical properties (such as thermal conductivity, sound velocity, temperature, and pressure). Since the physical properties can be measured directly within the gas using sensors currently available in the market, the proposed approach therefore saves a significant amount of time and effort and lowers the cost without analyzing gas composition via the traditional methods. This section will discuss in detail the process of preparing the data set and developing the predictive model to estimate the WI, MN, and gas composition.

5.3.1 Creating a data set

Table 5-3: Percent of Volumes of Components in Gases.

Component of gaseous fuel mixture	Fossil gas [16]	Anaerobic digester gas [17]	Landfill gas [16]
Methane (mol %)	97	68	60
Carbon Dioxide (mol %)	0	26	33
Water (mol %)	0	5	6.5
Ethane (mol %)	2	0	0
Other (N_2, O_2) (mol %)	1	1	0.5
Percent of volumes of components in normalized gases			
Methane (mol %)	98	72.3	64.5
Carbon Dioxide (mol %)	0	27.7	35.5
Ethane (mol %)	2	0	0

Fossil gas, anaerobic digester gas, and landfill gas were mixed together to get the various combinations of gaseous fuel mixture, which contains components of CH_4, CO_2 and C_2H_6 from 0% to 100% in 10% increments.

Table 5-4: Combination of the gaseous fuel mixture.

Gaseous fuel mixture composition (%)			Composition (%)		
Fossil Natural Gas	Anaerobic Disaster Gas	Landfill Gas	CH_4	C_2H_6	CO_2
100	0	0	94	6	0
90	10	0	91.83	5.4	2.77
80	0	20	88.1	4.8	7.1
70	20	10	86.71	4.2	9.09
60	30	10	84.54	3.6	11.86
50	30	20	81.59	3	15.41
40	40	20	79.42	2.4	18.18
30	20	50	74.91	1.8	23.29
20	50	30	74.3	1.2	24.5
10	60	30	72.13	0.6	27.27
10	20	70	69.01	0.6	30.39
0	100	0	72.3	0	27.7
0	0	100	64.5	0	35.5

Table 5-3 illustrates the composition in fossil natural gas, anaerobic digester gas, and landfill gas. For example, a mixture of 40% fossil gas, 30% anaerobic digester gas and 30% landfill gas contains 78.64% CH_4, 18.96% CO_2, and 2.4% C_2H_6. Using this approach, 66 different combinations of the gaseous fuel mixture were created as shown in Table 5-4.

Pressure and temperature are related to the thermal conductivity, sound velocity, WI, and MN of the gaseous fuel mixture. This indicates that the inverse can be found: the thermal conductivity, sound velocity, WI, and MN may be estimated by temperature, pressure, and gas composition. The combinations of temperature and pressure with a pressure range of 3447 kPa - 20684 kPa with 3447 kPa intervals and a temperature range of 253 K ~ 353 K with 20 K intervals were created. From 6 different temperature intervals and 6 different pressure intervals, 36 possible combinations were used. With these 36 temperature-pressure combinations along with 66 gaseous fuel mixture combinations, a total of 2376 possible combination were created.

Then, specific gas properties such as thermal conductivity and sound velocity were calculated. Thermal conductivity of the gaseous fuel mixture was calculated by $k = \Sigma\, x_i k_i$ where k_i is the thermal conductivity of a pure gas component and x_i is its percent in the mixture [18]. The thermal conductivity data for each pure gas component at a specific T and P was taken from [19,20]. The thermal conductivity of a pure gas component in the mixture was calculated by equations, eq 5-1 and eq 5-2 [21]. The equations are valid for methane when the reduced temperature is above 1 and valid for other hydrocarbons at any temperature.

$$k_i = 10^{-7}\,(14.52\,T_r - 5.14)^{2/3}\,\frac{C_p}{\lambda} \qquad \text{eq 5-1}$$

$$\lambda = T_c^{1/6}\,M^{1/2}\left(\frac{101.325}{p_c}\right)^{2/3} \qquad \text{eq 5-2}$$

where k_i = vapor thermal conductivity of pure components, W/m K; T_r = reduced temperature, T/T_c; T = temperature, K; T_c = critical temperature, K; C_p = heat capacity at constant pressure, J/kmol K; M = molecular weight and p_c = critical pressure, kPa.

Sound velocity of the gaseous fuel mixture is calculated by the following equation:

$$\text{Sound velocity } v = \sqrt{\frac{\gamma Z R_u T}{M_g}} \qquad \text{eq 5-3}$$

where $\gamma = \frac{C_p}{C_v}$; Z = compressibility factor; R_u = universal gas constant; constant pressure specific heat $C_p = \Sigma(x_i C_{pi}(T_j))$ [J/mol.K].

The compressibility factor, Z, is calculated by using eq 5-4 as described below [22]:

$$Z = 1 + (A_1 + \frac{A_2}{T_{pr}} + \frac{A_3}{T_{pr}^3} + \frac{A_4}{T_{pr}^4} + \frac{A_5}{T_{pr}^5})\rho_{pr} + (A_6 + \frac{A_7}{T_{pr}} + \frac{A_8}{T_{pr}^2})\rho_{pr}^2 - A_9 (\frac{A_7}{T_{pr}} + \frac{A_8}{T_{pr}^2})\rho_{pr}^5 - A_{10}(1 + A_{11}\rho_{pr}^2)\frac{\rho_{pr}^2}{T_{pr}^3} \exp(-A_{11}\rho_{pr}^2) \qquad \text{eq 5-4}$$

While ρ_{pr} is described as following equation [22]:

$$\rho_{pr} = 0.27 \frac{P_{pr}}{Z T_{pr}} \qquad \text{eq 5-5}$$

The value of the constants A1~A11 is described by Dranchuk et. al., [22].

Temperature-based constant pressure heat capacity of a pure component was calculated for ideal gas law conditions [23] by the equation:

Constant volume specific heat $C_v = C_p - R$ [J/mol.K] eq 5-6

where the compressibility factor is a function of pseudo reduced pressure and temperature [24,25]. The pseudo reduced pressure and temperature are calculated by using the Suttons gas gravity method [26]:

$p_{pc} = 756.8 - 131.07\,\gamma_g - 3.6\,\gamma_g^2$ eq 5-7

$T_{pc} = 169.2 + 349.5\,\gamma_g - 74.0\,\gamma_g^2$ eq 5-8

$p_{pr} = \frac{p}{p_{pc}}$ eq 5-9

$T_{pr} = \frac{T}{T_{pc}}$ eq 5-10

where relative density/Specific gravity (γ_g) = $\frac{Molecular\ weight\ of\ the\ gas\ (M_g)}{Molecular\ weight\ of\ air\ (M_a)}$

Molecular weight of the gaseous fuel mixture is calculated by $M_g = \Sigma M_i x_i$ where M_i is the molecular weight of the component and x_i is the composition of the component.

WI for the gaseous fuel mixture is calculated by the following equation:

$WI = \frac{H_c}{\sqrt{\gamma_g}}$ eq 5-11

where H_c is the heating value of the gaseous fuel mixture at a specific temperature and pressure and γ_g is the relative density/specific gravity of the gaseous fuel mixture.

Aspen Plus, a simulator tool, is used to calculate the heating value of the combustible components [27]. The model developed by Aspen Plus is shown in Figure 5-1. In the model, the combustible components CH_4 and C_2H_6 are burned at a stoichiometric air ratio, and the product leaves the reactor at a temperature and pressure that is used to calculate WI. CO_2 also affects WI by changing the volume, not by changing the total heat content.

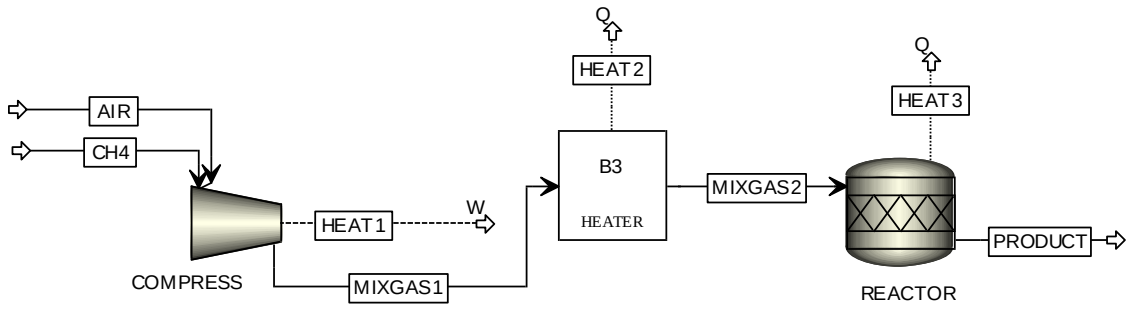

Figure 5-1: Aspen Plus setup for heating value calculation.

The methane number of each gaseous fuel mixture was obtained from the Cummins Westport's (CWI) website, which uses a Cummins Proprietary calculation and provides a more accurate representation of the true MN of the fuel [28]. Table 5-5 illustrates a portion of the data set that includes the physical properties, WI, MN, and gas composition.

Table 5-5: A portion of the data set including the physical properties, WI, MI, and gas composition.

Temperature, T	Pressure, P	Composition			Thermal Conductivity, k × 10^3	Sound Velocity, v	Wobbe Index	Methane number
		CH_4	C_2H_6	CO_2				
K	kPa	%	%	%	W/(m.K)	m/s	MJ/Nm^3	MN
253.15	3447	94.00	6.00	0.00	27.36	350.86	54.90	84.5
253.15	3447	91.83	5.40	2.77	27.02	343.90	52.16	88.8
253.15	3447	89.66	4.80	5.54	26.68	336.48	49.53	93.2
253.15	3447	87.49	4.20	8.31	26.33	330.29	47.03	97.6
253.15	3447	85.32	3.60	11.08	25.99	324.43	44.62	102.0
253.15	3447	83.15	3.00	13.85	25.64	318.88	42.32	106.4
253.15	3447	80.98	2.40	16.62	25.30	313.60	40.10	110.7
253.15	3447	78.81	1.80	19.39	24.95	307.78	37.97	115.0
253.15	3447	76.64	1.20	22.16	24.61	303.00	35.91	119.2
253.15	3447	74.47	0.60	24.93	24.26	298.44	33.92	123.3
253.15	3447	72.3	0.00	27.7	23.92	294.08	32.00	127.3
253.15	3447	71.52	0.00	28.48	23.80	292.74	31.51	128.1
253.15	3447	73.69	0.60	25.71	24.14	297.04	33.41	124.2
253.15	3447	70.74	0.00	29.26	23.68	291.42	31.03	129.0
253.15	3447	75.86	1.20	22.94	24.49	301.54	35.38	120.1
253.15	3447	72.91	0.60	26.49	24.03	295.66	32.91	125.0
253.15	3447	69.96	0.00	30.04	23.56	290.11	30.55	129.8
253.15	3447	78.03	1.80	20.17	24.83	306.24	37.42	115.9
253.15	3447	75.08	1.20	23.72	24.37	300.09	34.86	121.0
253.15	3447	72.13	0.60	27.27	23.91	294.30	32.41	125.9
253.15	3447	69.18	0.00	30.82	23.45	288.83	30.07	130.7
253.15	3447	80.2	2.40	17.4	25.18	311.98	39.53	111.6

The data that will be used for our modeling, was obtained using Aspen Plus simulation tool for calculating the necessary values and from the CWI website without actual measurements.

5.3.2 Constructing a predictive model

In statistical modeling, regression analysis is commonly used for estimating the relationships among variables in a data set. Multiple regression was used to build a predictive model that estimates the WI, MN, and gas composition.

The general multiple regression equation for a dependent variable, y_i is

$$y_i = \beta_0 + \beta_1 x_{1i} + \cdots + \beta_m x_{mi} + \varepsilon_i \text{ for } i = 1..n \qquad \text{eq 5-12}$$

where x represents independent variables; β represents the unknown coefficients that are to be found; ε represents the error; n represents the number of samples; m represents the number of independent variables. Based on this, a multiple regression model is typically presented in the following form:

$$Y = X\beta + \varepsilon \qquad \text{eq 5-13}$$

where Y is a vector representing the values of dependant variables; X is a matrix representing the values of independent variables. In regression analysis, the value of ε is assumed to be randomly distributed [29]. From this equation, a regression model approximates Y to a function of X and β, that is, $Y \approx f(X, \beta)$. To find a functional relational relationship between X and Y, a data set with appropriate number of samples were chosen

as shown below (eq 5-14) where n is number of samples and m is the number of variables. The sample data set used in this modelling was collected through the method previously described in this paper.

$$Y = \begin{bmatrix} y_1 \\ y_2 \\ \vdots \\ y_n \end{bmatrix}, X = \begin{bmatrix} 1 & x_{11} & x_{21} & \cdots & x_{m1} \\ 1 & x_{12} & x_{22} & \ldots & x_{m2} \\ \vdots & \vdots & \vdots & \ddots & \vdots \\ 1 & x_{1n} & x_{2n} & \cdots & x_{mn} \end{bmatrix}, \beta = \begin{bmatrix} \beta_0 \\ \beta_2 \\ \vdots \\ \beta_m \end{bmatrix}, \varepsilon = \begin{bmatrix} \varepsilon_1 \\ \varepsilon_2 \\ \vdots \\ \varepsilon_n \end{bmatrix} \quad \text{eq 5-14}$$

In this paper, Y represents a vector consisting of WI, MN, or gas composition for dependent variables. X is a matrix representing values from the 2376 samples for all the physical properties for independent variables. Our goal is to find a vector $\tilde{\beta}$ of coefficients for the model that minimizes the square sum of the error. That is $\tilde{\beta} = argmin_{\beta} \sum_{i=1}^{n} (y_i - \beta^T x_i)^2$. The coefficients ($\beta$-vector) are calculated using the *Least Squares Equation* [13]:

$$\tilde{\beta} = (X^T X)^{-1} X^T Y \quad \text{eq 5-15}$$

With the calculated coefficients $\tilde{\beta}$, the estimated Y, or $\hat{Y}$, is calculated by $\hat{Y} = X\tilde{\beta}$. Furthermore, the average error of the model is calculated by the root mean square (rms) between the actual value in the data set and the predicted value by the model as shown by the formula below:

$$\text{error}_{\text{rms}} = \sqrt{\frac{\sum error^2}{2376}} \quad \text{eq 5-16}$$

5.4 Results from the Proposed Model

The proposed model to predict the WI, MN, and gas composition from its physical properties was developed based on multiple regression analysis using MATLAB. The unit used is K for temperature, kPa for pressure, W/(m.K) for thermal conductivity, m/s for sound velocity in the prediction model. The unit obtained for WI is MJ/Nm^3 from the model equation, and % for CH_4, CO_2 and C_2H_6 composition.

5.4.1 Wobbe Index prediction model

The model was created based on 4 different variables: constant (1); temperature (T), X_1; pressure (P), X_2; thermal conductivity (k), X_3; sound velocity (v), X_4. The coefficients for the model are:

$$\beta = \begin{bmatrix} 70.76 \\ -0.55 \\ 0.000225 \\ 3635.79 \\ 0.05 \end{bmatrix}$$

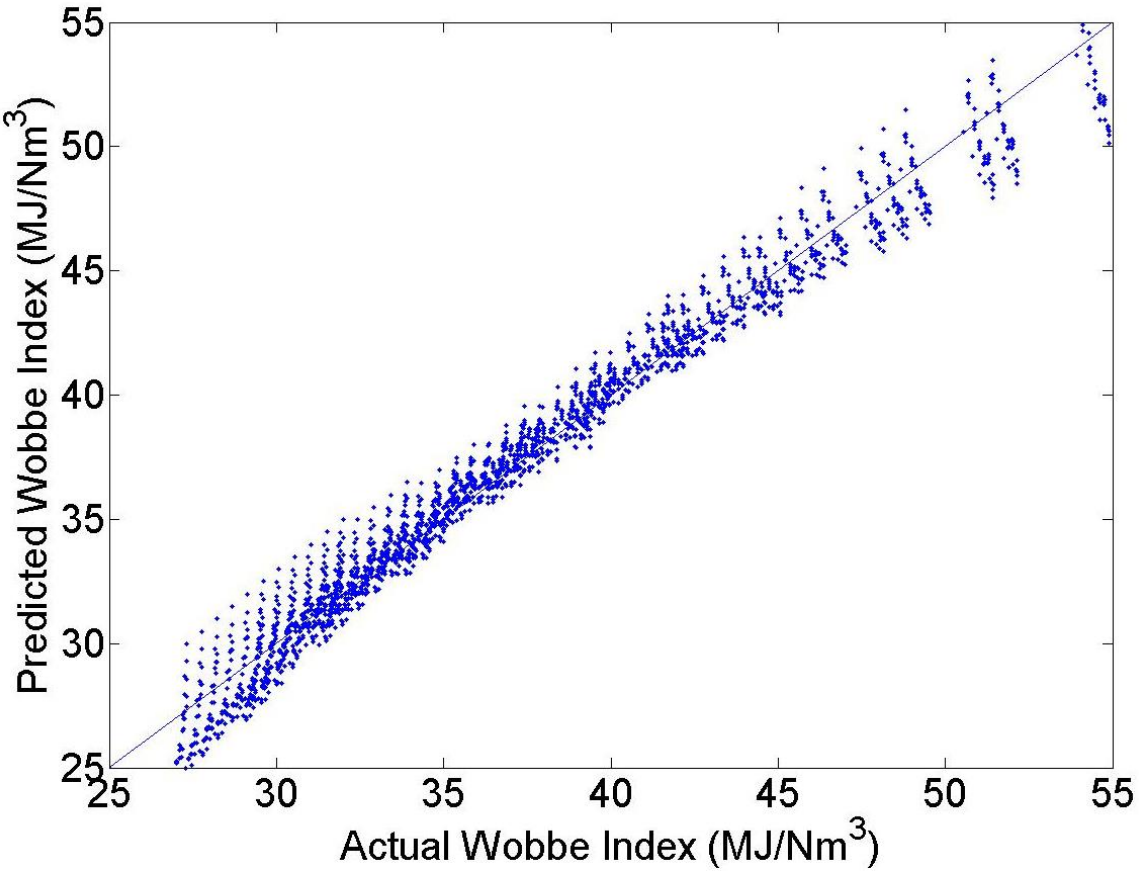

Figure 5-2: Predicted Wobbe Index vs Actual Wobbe Index.

Figure 5-2 shows a comparison of the actual value and the predicted value of WI. The trend line is desirable. Accuracy of predicted WIs in the range of 30 - 40 was very high but suffered a slight reduction when WIs were outside of the range.

The $error_{rms}$ was 1.02 and the average percentage of error calculated between the actual value and predicted value was 2.76%. For additional statistics that support the accuracy of the proposed model for WI, R^2 value and variance of the prediction was 0.98 and 0.94, respectively. The values of t-statistic for all the coefficients were greater or less than 2. The p-values for all the coefficients were 0.0. The detailed regression statistics for the WI

prediction model is shown in Table 5-6. All these statistics strongly support the significance and accuracy of the model for WI.

Table 5-6: Regression statistics of WI prediction.

R Square	0.98		
Standard Error	0.94		
	Standard Error	t Stat	P-value
Intercept (constant)	0.48	238.35	0.00
Variable 1 (Temperature, T)	0.00	-171.64	0.00
Variable 2 (Pressure, P)	0.00	-22.29	0.00
Variable 3 (Thermal conductivity, k)	37.38	112.05	0.00
Variable 4 (Sound velocity, v)	0.00	24.07	0.00

5.4.2 Methane number prediction model

The model for MN prediction was developed using 4 different variables: constant (1); temperature (T), X_1; pressure (P), X_2; thermal conductivity (k), X_3; sound velocity (v), X_4. Y is the matrix representing the methane number for all the samples.

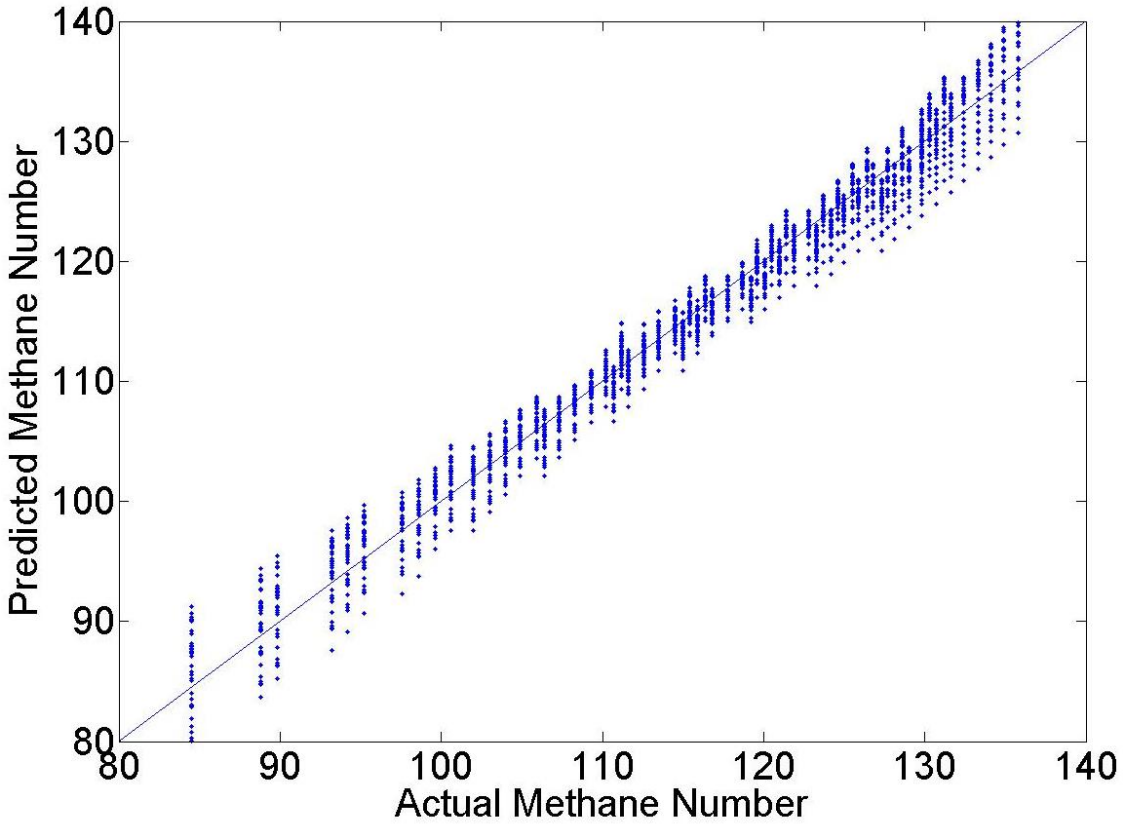

Figure 5-3: Predicted methane number vs Actual methane number.

The coefficients for the model are:

$$\beta = \begin{bmatrix} 51.71 \\ 1.06 \\ 0.000402 \\ -7240.22 \\ -0.10 \end{bmatrix}$$

Figure 5-3 shows the accuracy of the methane number predictions. As illustrated in the figure, the accuracy of the predicted MNs was much higher than the predicted WIs. The $error_{rms}$ was 1.92 and the average percentage of error was 1.65%. R^2 value and variance of the MN prediction was 0.98 and 1.92, respectively. The t-statistics, p value for the MN prediction model is shown in Table 5-7.

Table 5-7: Regression statistics of MN prediction.

R Square	0.98		
Standard Error	1.92		
	Standard Error	t Stat	P-value
Intercept (constant)	0.98	52.67	0.00
Variable 1 (Temperature, T)	0.01	-147.54	0.00
Variable 2 (Pressure, P)	0.00	-22.66	0.00
Variable 3 (Thermal conductivity, k)	76.20	95.01	0.00
Variable 4 (Sound velocity, v)	0.00	24.47	0.00

5.4.3 Gas composition prediction model

The model for the gas composition prediction was developed using 4 different variables: constant (1); temperature (T), X_1; pressure (P), X_2; thermal conductivity (k), X_3; sound velocity (v), X_4. Table 5-8 shows the vector β for predicting the gas composition.

Table 5-8: Model parameters for the gas composition prediction

Components	CH_4	C_2H_6	CO_2
β_0	9.59	114.78	-24.37
β_1	-0.13	-0.61	0.74
β_2	-0.000100	-0.000194	0.000250
β_3	861.54	4187.91	-5049.45
β_4	0.01	0.05	-0.06
$Error_{rms}$	0.94	0.43	1.16
Average % of error	1.22	21.59	5.51

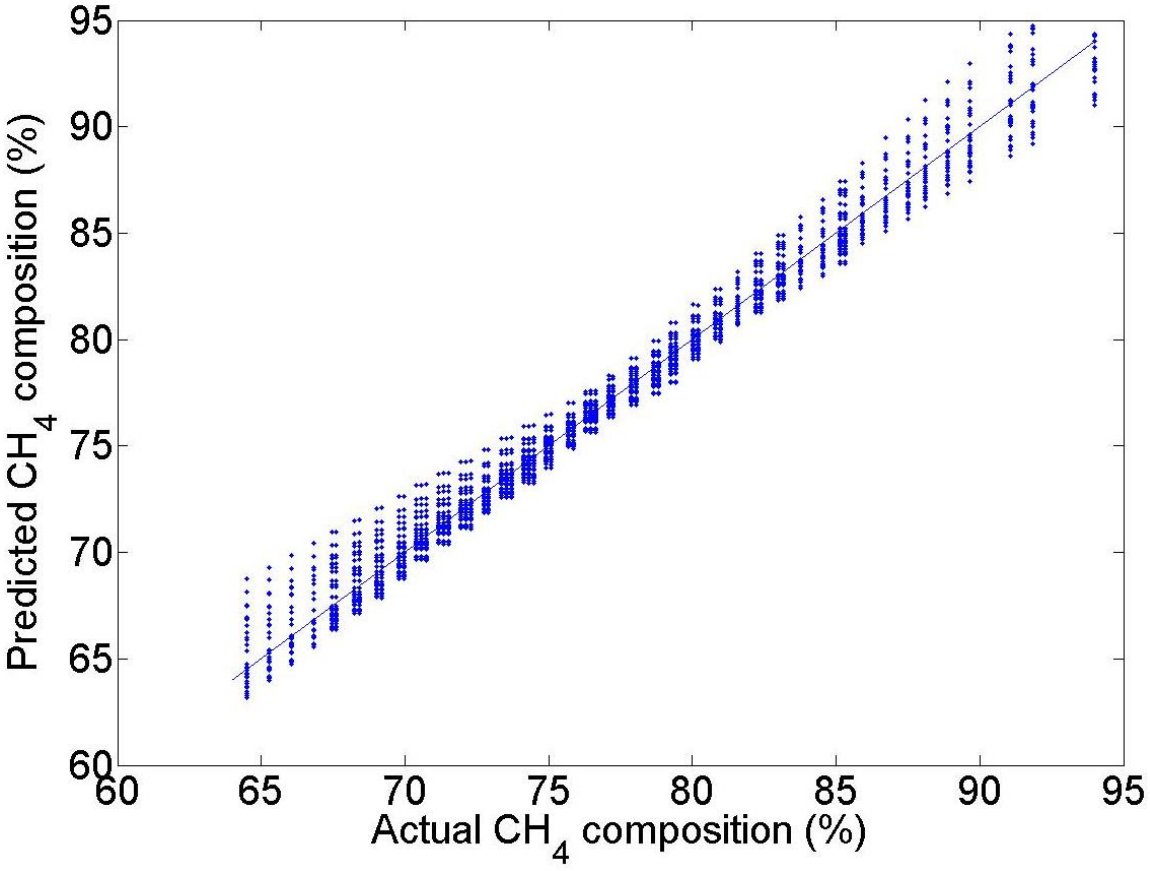

Figure 5-4: Predicted CH_4 composition vs Actual CH_4 composition.

The predicted data versus the actual data plot for CH_4, C_2H_6, and CO_2 are presented in Figure 5-4, Figure 5-5, and Figure 5-6, respectively. The predicted methane composition in Figure 5-4 showed negligible error for a methane composition in the range of 70 - 85%. Predicted data out of this range had the largest fluctuation. The prediction of methane composition is closely connected with WI prediction since WI is mostly influenced by the combustible components, methane and ethane. As the ethane concentration is negligible, the predicted methane composition and WI in the range can be considered accurate. The

$error_{rms}$ for the methane composition prediction model was 0.94 and the average percentage of error was 1.22%.

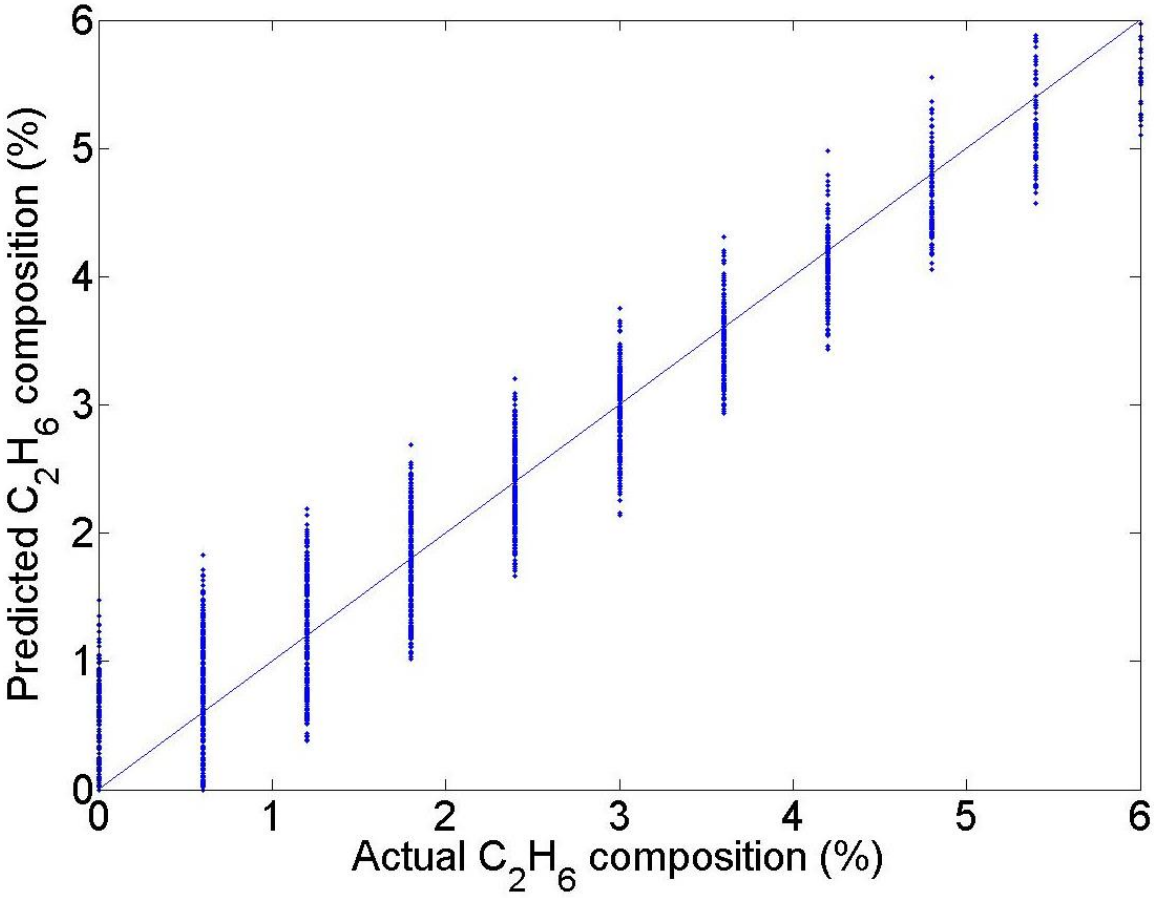

Figure 5-5: Predicted C_2H_6 composition vs Actual C_2H_6 composition.

Figure 5-5 shows the predicted and actual ethane composition. As illustrated in the figure, with limited number of data points, the prediction of ethane composition was relatively inaccurate. The $error_{rms}$ for this prediction was 0.43 and the average percentage of error was 5.51%.

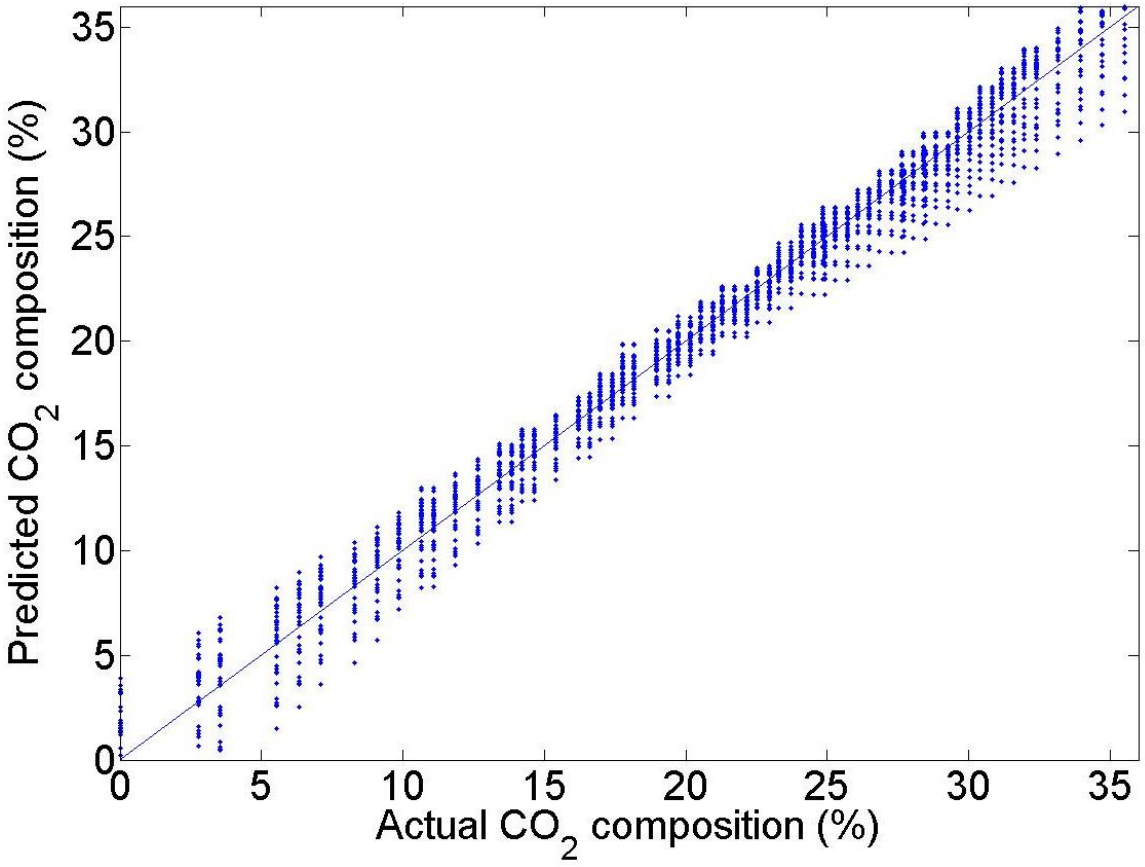

Figure 5-6: Predicted CO_2 composition vs Actual CO_2 composition.

Figure 5-6 shows the predicted CO_2 composition versus actual CO_2 composition. Accuracy of the prediction was very high where CO_2 composition was above 10%. The $error_{rms}$ for CO_2 composition prediction model was 1.16 and the average percentage of error was 21.59%. The R^2 value and variance, t-statistics, p value for the component composition prediction model is shown in Table 5-9.

.

Table 5-9: Regression statistics of component composition prediction.

R Square	CH_4 – 0.98 C_2H_6 – 0.93 CO_2 – 0.98								
Standard Error	CH_4 – 0.94 C_2H_6 – 0.43 CO_2 – 1.16								
	Standard Error			t Stat			P-value		
	CH_4	C_2H_6	CO_2	CH_4	C_2H_6	CO_2	CH_4	C_2H_6	CO_2
Intercept (constant)	0.48	0.22	0.59	238.35	43.39	40.99	0.00	0.00	0.00
Variable 1 (Temperature, T)	0.00	0.00	0.00	-171.64	-79.11	168.40	0.00	0.00	0.00
Variable 2 (Pressure, P)	0.00	0.00	0.00	-22.29	14.13	23.30	0.00	0.00	0.00
Variable 3 (Thermal conductivity, k)	37.38	17.16	46.15	112.05	50.21	-109.40	0.00	0.00	0.00
Variable 4 (Sound velocity, v)	00000.00	0.00	0.00	24.07	15.26	-25.17	0.00	0.00	0.00

5.5 Conclusion

Since transportation and other combustion devices constitute the largest portion of overall gas use, an extensive worldwide use of RNG significantly depends on an efficient combustion compatibility of this fuel in engines and other gas-powered devices. WI and MN are the fuel quality indicators. An efficient way to correctly estimate the fuel quality of a RNG can promote more use of RNG as opposed to fossil gas. This can ultimately aid in reducing the net GHG emission.

This study presents a predictive model that can estimate WI, MN, and gas composition from the values of easily measured physical properties such as temperature, pressure, thermal conductivity, and sound velocity without going through the long and expensive process of GC or RGA. From the results of our modeling, temperature and thermal conductivity are significant in estimating all the parameters. The proposed model can efficiently predict the WI of the gaseous fuel mixture with an average error of 1.02 and MN with an average error of 1.92. The model can also predict the composition of methane, ethane and CO_2 in the gaseous fuel mixture with the error of 0.94, 0.43, and 1.16, respectively. The proposed model, coupled with sensor technology, has the potential to predict the fuel quality of both renewable natural gas and fossil natural gas.

Acknowledgements

This work was supported by Proof of Concept grant from UCR's Office of Research and Economic Development. Authors are also grateful to partial support from the Department

of Transportation through National Center for Sustainable Research Grant No UCR-DOT-306.

5.6 References

[1] M. Feroskhan, S. Ismail, Investigation of the effects of biogas composition on the performance of a biogas–diesel dual fuel CI engine, Biofuels 7 (2016) 593-601.

[2] J.C. Lackey, B. Peppley, P. Champagne, A. Maier, Composition and uses of anaerobic digestion derived biogas from wastewater treatment facilities in North America, Waste Manag. Res. 33 (2015) 767-771.

[3] O. Florisson, P.H. Burrie, Rapid determination of the Wobbe index of natural gas, J. Phys. E Sci. Instrum. 22 (1989) 123-128.

[4] T. Lieuwen, V. McDonell, E. Petersen, D. Santavicca, Fuel flexibility influences on premixed combustor blowout, flashback, autoignition, and stability, J. Eng. Gas Turbines Power 130 (2008) 011506-011510.

[5] C.S. Park, A.S. Raju, S.A. Franco, P.S. Roy, H.S. Jung, Development of a fuel sensor technology for a Variable-blend Natural Gas Vehicle, J. Nat. Gas. Sci. Eng. 31 (2016) 149-155.

[6] R.R. Thurston, P.S. Hammond, B.L. Price, Method and apparatus for measuring the calorific value of a gas, U.S. Patent 6,442,996 (2002).

[7] J.C. Lötters, T.S. Lammerink, M.G. Pap, R.G. Sanders, M.J. de Boer, A.J. Mouris, R.J. Wiegerink, Integrated micro Wobbe index meter towards on-chip energy content measurement, In Micro Electro Mechanical Systems (MEMS), IEEE (January 2013) 965-968.

[8] D. Puente, F.J. Gracia, I. Ayerdi, Thermal conductivity microsensor for determining the Methane Number of natural gas, Sens. Actuators B Chem. 110 (2005) 181-189.

[9] C. Rahmouni, O. Le Corre, Tazerout, Online determination of natural gas properties, Comptes. Rendus. Mecanique. 331 (2003) 545-550.

[10] S. Udina, M. Carmona, G. Carles, J. Santander, L. Fonseca, S. Marco, A micromachined thermoelectric sensor for natural gas analysis: Thermal model and

experimental results, Sens. Actuators B Chem. 134 (2008) 551-558.

[11] S. Udina, M. Carmona, A. Pardo, C. Calaza, J. Santander, L. Fonseca, S. Marco, A micromachined thermoelectric sensor for natural gas analysis: Multivariate calibration results, Sens. Actuators B Chem. 166 (2012) 338-348.

[12] S. Narayanan, G. Rice, M. Agah, A micro-discharge photoionization detector for micro-gas chromatography, Microchim. Acta. 181 (2014) 493-499.

[13] A. Gutierrez, D. Puente, D. Toro, E. Pérez, I. Ayerdi, J. Gracia, J. Sabin, New thermal conductivity microsensor to measure the methane number of natural gas, In 23rd World Gas Conference, Ámsterdam (Holanda) (June 2006).

[14] J.C. Lötters, E.J. van der Wouden, J. Groenesteijn, W. Sparreboom, T.S. Lammerink, R.J. Wiegerink, Real-time composition determination of gas mixtures, In SENSORS, IEEE (November 2014) 1640-1643.

[15] M.L. Huber, A.H. Harvey, Thermal conductivity of gases. CRC Handbook of Chemistry and Physics, (2011) 92 (CRC Handbook of Chemistry and Physics).

[16] S.C Eichmann, J. Kiefer, J. Benz, T. Kempf, A. Leipertz, T. Seeger, Determination of gas composition in a biogas plant using a Raman-based sensor system, Meas. Sci. Technol. 25 (2014) 075503.

[17] URS. Digester gas energy recovery alternatives,

http://www.ohiowea.org/docs/202%20DigesterGasEnergy_Krinks.pdf; 2017 [accessed 5 December 2017]. [18] A.L. Lindsay, L.A. Bromley, Thermal conductivity of gas mixtures, Ind. Eng. Chem. 42 (1950) 1508-1511.

[19] F.J. Uribe, E.A. Mason, J. Kestin, Thermal conductivity of nine polyatomic gases at low density, J. Phys. Chem. Ref. Data 19 (1990) 1123-1136.

[20] B.A. Younglove, J.F. Ely, Thermophysical properties of fluids. II. Methane, ethane, propane, isobutane, and normal butane, J. Phys. Chem. Ref. Data 16 (1987) 577-798.

[21] R.H. Perry, D.W. Green, J.O. Maloney, Perry's Chemical Engineer's Handbook. McGraw-Hill (1984).

[22] P.M. Dranchuk, H. Abou-Kassem, Calculation of Z factors for natural gases using equations of state, J. Can. Pet. Technol. 14 (1975) 34-36.

[23] M.M. Abbott, J.M. Smith, H.C. Van Ness, Introduction to Chemical Engineering Thermodynamics, McGraw-Hill (2001).

[24] D.L.V. Katz (ed.), Handbook of natural gas engineering, McGraw-Hill (1959).

[25] PETE, http://www.pe.tamu.edu/barrufet/public_html/PETE310/pdf/L10-Real%20Gases.pdf; 2017 [accessed 5 December 2017].

[26] R.P. Sutton, Compressibility factors for high-molecular-weight reservoir gases, In SPE Annual Technical Conference and Exhibition, Society of Petroleum Engineers (January 1985).

[27] AspenPlus, http://home.aspentech.com/products/engineering/aspen-plus; 2017 [accessed 6 November 2017].

[28] Cummins Westport. Fuel Quality Calculator,

http://www.cumminswestport.com/fuel-quality-calculator; 2017 [accessed 27 July 2017].

[29] J.J. Kinney, Statistics for science and engineering. Vol. 172. New York: Pearson Education, Inc. (2002).

CHAPTER 6 CONCLUSIONS AND RECOMMENDATIONS

This section summarizes the conclusions derived from the experimental, modeling and simulation work performed as part of this thesis.

1. A process model using the Aspen Plus simulation tool has been developed for steam biogas reforming process. This model estimates the equilibrium conversion of biogas reacting with methane to produce syngas using built-in process units (an equilibrium reactor) and physical/chemical property databases. The produced syngas is used as the fuel for SOFC (a stochiometric combustor). The SOFC exhaust is inside a combustor and the produced heat is supplied to the endothermic reforming reaction. The simulation results have been used to calculate the CH_4 conversion, CO_2 conversion, process thermal efficiency over the temperature range of 873 to 1123 K. The system performance was evaluated using the Aspen Plus process simulation tool and through SBR experiments over a metal-foam-coated 1.31 wt% [Pd(7)-Rh(1)]/[CeZrO2(25)-Al2O3(75)] catalyst. CH_4 conversion over the catalyst at 973 K was comparable with the equilibrium and experimentally positive CO_2 conversion was achieved at 1073 K and above. H_2/CO ratio of the product syngas was greater than the equilibrium with a coke formation of 1.05~2.88% of the carbon input to the system. The biogas reforming coupled with a combustor and SOFC integrated system can achieve energy efficiency values of 40% or higher at reformer temperatures of 948 K and above.

Experimental work has been performed on the selecting the suitable catalyst composite support composition of the metal-foam-coated 1.31 wt% [Pd(7)-Rh(1) catalyst for steam

biogas reforming process inside the HEP reactor. Increasing the $CeZrO_2$ content from 0 to 100% of the support material resulted in CH_4 and CO_2 conversion improvements and were accompanied by increased H_2/CH_4 yield, reduced H_2/CO ratio of the product syngas and reduced coke formation. The metal-foam-coated Pd-Rh catalysts steady catalytic performance during a 200 on-stream hour stability test.

CO_2 can be converted to the catalytically valuable chemicals. CO_2 and CH_4 with controlled amount of water (steam) can produce syngas with a specific H_2/CO ratio. For the methanol synthesis, precise control of syngas ratio to 2 is required. In industry, methanol is produced from syngas produced via steam reforming of methane whereas proposed bi-reforming pathway considers the synthesis of methanol through the proposed new bi-reforming technology. This study evaluates the LCA of methanol production process where the steam methane reforming step is replaced by bi-reforming of methane. The reforming of methane with CO_2 (from a fossil fuel based power plant) and steam with controlled reactant ratio produces the syngas with certain H_2/CO ratio required for the methanol production in this study. An Aspen plus process simulation model for a bi-reforming based methanol production process was developed. The process thermal efficiency calculated from the simulation model is used for economic analysis and LCA of the proposed pathway as well as methanol production technology. The LCA is conducted using the 'GHGenius' LCA model. The economic analysis shows that at the methanol sales price of $400/tonne and natural gas price $3.5/GJ the IRR is 57% which drops down to 39% with the change in gas price to $6.0/GJ for the proposed bi-reforming pathway combined with methanol production. The total GHG emissions from the baseline case pathway are estimated to be

497 kilograms of CO_2e GHGs/ tonne of methanol produced on an LHV basis. The total GHG emissions from the bi-reforming are estimated to be 203 kilograms of CO_2e GHGs/metric tonne of methanol produced on an LHV basis. CO_2 reduction through the proposed bi-reforming pathway is about 0.29 kg CO_2e/kg of CH_3OH.

Transportation sector and other combustion devices are the largest natural gas user globally. The use of RNG as a fuel in engines and other gas-powered devices substantially depend on the efficient combustion compatibility of this fuel. Wobbe Index and Methane Number are the indicators for fuel quality. The RNG composition varies significantly and the fuel quality estimation of RNG is necessary to promote the use as opposed to fossil gas. This can eventually help in reducing the net GHG emission.

A database is developed for WI, MN using a mixture of biogas, anaerobic digester gas and natural gas at different temperature and pressure. A predictive model using the database is established that can estimate WI, MN, and gas composition from the values of easily measured physical properties such as temperature, pressure, thermal conductivity, and sound velocity without going through the long and expensive process of GC or RGA. Temperature and thermal conductivity are significant parameter for predicting the WI, MN and composition. The proposed model can efficiently predict the WI of the gaseous fuel mixture with an average error of 1.02 and MN with an average error of 1.92. The model can also predict the composition of methane, ethane and CO_2 in the gaseous fuel mixture with the error of 0.94, 0.43, and 1.16, respectively. The proposed model, coupled with sensor technology, has the potential to predict the fuel quality of both renewable natural gas and fossil natural gas.

Overall, metal foam supported Pd-Rh/(metal oxide) catalyst is developed and tested for reforming of methane with CO_2 and steam (bi-reforming) in a compact HEP reactor system. A life cycle assessment is studied for methanol synthesis process using CO_2 raw material instead of treating CO_2 as a waste stream (ex: CCS). A predictive model is developed that can estimate Wobbe Index and Methane Number by using temperature, pressure, thermal conductivity and sound velocity of a gas mixture.

Future Work

Some potential future research directions are listed below.

First, the dissertation is focused on experimental study of the steam biogas reforming process and simulation of the reforming process with the integrated SOFC process for better efficiency. In order to improve the biogas utilization a SOFC system other end user is needed to combine and study experimentally. The concept of the heat exchanger platform type reactor can be further improved from the lab scale process to pilot plant scale.

Second, the methanol synthesis process in this dissertation is studied with bi-reforming of methane with CO_2 and steam. The methane and CO_2 was obtained from fossil sources. The study is require further estimation where the methane and CO_2 is from the renewable sources to check the GHG footprint of the methanol synthesis process.

Third, the prediction strategy of RNG quality sensor is developed and the physical sensor is still under development. The next step would be to develop the physical sensor and check the performance of the sensor in the real world.